

Establishment of a modified imperfection factor for cold-formed hollow sections

Auteur : Duchene, Louis

Promoteur(s) : Demonceau, Jean-François; Saufnay, Loris

Faculté : Faculté des Sciences appliquées

Diplôme : Master en ingénieur civil des constructions, à finalité spécialisée en "civil engineering"

Année académique : 2024-2025

URI/URL : <http://hdl.handle.net/2268.2/23214>

Avertissement à l'attention des usagers :

Tous les documents placés en accès ouvert sur le site le site MatheO sont protégés par le droit d'auteur. Conformément aux principes énoncés par la "Budapest Open Access Initiative"(BOAI, 2002), l'utilisateur du site peut lire, télécharger, copier, transmettre, imprimer, chercher ou faire un lien vers le texte intégral de ces documents, les disséquer pour les indexer, s'en servir de données pour un logiciel, ou s'en servir à toute autre fin légale (ou prévue par la réglementation relative au droit d'auteur). Toute utilisation du document à des fins commerciales est strictement interdite.

Par ailleurs, l'utilisateur s'engage à respecter les droits moraux de l'auteur, principalement le droit à l'intégrité de l'oeuvre et le droit de paternité et ce dans toute utilisation que l'utilisateur entreprend. Ainsi, à titre d'exemple, lorsqu'il reproduira un document par extrait ou dans son intégralité, l'utilisateur citera de manière complète les sources telles que mentionnées ci-dessus. Toute utilisation non explicitement autorisée ci-avant (telle que par exemple, la modification du document ou son résumé) nécessite l'autorisation préalable et expresse des auteurs ou de leurs ayants droit.

Establishment of a modified imperfection factor for cold-formed hollow sections

Duchêne Louis

Thesis presented to obtain the degree of :
Master of Science in Civil Engineering

Thesis supervisor :
Demonceau Jean-François

Guidance :
Saufnay Loris

Members of the jury :
Bezas Marios-Zois
Bijelic Nenad

Academic year: **2024 - 2025**

Acknowledgments - Remerciements

Je tiens tout d'abord à remercier chaleureusement Monsieur Jean-François Demonceau, mon promoteur, ainsi que Monsieur Loris Saufnay, pour leur disponibilité, leur écoute et les nombreux éclairages qu'ils m'ont apportés avec patience et pertinence. Leur accompagnement rigoureux et bienveillant a grandement contribué à la complétion de ce travail.

Je souhaite également à exprimer ma profonde gratitude à mes parents, pour leur soutien indéfectible tout au long de ce travail. Leur présence, leurs nombreux conseils avisés et leurs relectures attentives m'ont été d'une aide précieuse à chaque étape de ce projet.

Enfin, je remercie mes amis, qui ont, comme moi, traversé cette aventure du travail de fin d'études. Les échanges que nous avons partagés m'ont apporté un soutien constant et une motivation précieuse

Abstract

This master's thesis evaluates the possibilities for improving the current European standards (FprEN1993-1-1:2022) for the buckling design of cold-formed steel tubular sections, particularly for high-strength steels ($f_y > 460$ MPa).

High-strength steels (HSS) offer a high strength-to-weight ratio, allowing for the design of more slender members for a same load-bearing capacity. Their use thus leads to lighter structures and reduced consumption of raw materials, offering numerous economic and environmental benefits. Moreover, many studies have shown that HSS members exhibit a higher normalised buckling resistance compared to normal-strength steels (NSS). These findings have led to partial modifications of the Eurocodes for buckling design, which until then showed increasing conservatism with rising yield strength. These changes have allowed the use of a more favorable buckling curve for hot-formed steels from grade S460 up to grade S700. However, this modification has not been introduced for cold-formed (CF) steels, even though HSS coils are already commercially available for cold-forming, whereas hot-formed members are not produced beyond grade S460.

The objective of this work is therefore to improve the design standards for CF steels by accounting for the standardised increase in buckling resistance associated with higher steel grades. This study focuses particularly on cold-formed hollow sections. The methodology follows a classical scientific approach, based on experimental tests from the literature, which are used to develop and validate a numerical model capable of reproducing the experimental results. This model is then used to conduct a parametric study on various steel grades and column lengths in order to assess the performance of the European design standards as well as modification proposals from the literature based on them. At the conclusion of this analysis, a proposal for improving the standards for cold-formed hollow sections is presented.

Résumé

Ce travail de fin d'études évalue les possibilités d'amélioration des normes européennes actuelles (FprEN1993-1-1:2022) pour le dimensionnement au flambement des profilés tubulaires en acier formés à froid, en particulier pour les aciers à haute résistance ($f_y > 460$ MPa).

Les aciers à haute résistance (HSS) présentent en effet, un rapport résistance/poids élevé permettant de concevoir des éléments plus élancés pour une même capacité portante. Leur utilisation se traduit donc par un allègement des structures et une réduction de la consommation en matières premières offrant de nombreux avantages tant économiques qu'environnementaux. En outre, de nombreuses études ont mis en évidence que les éléments HSS disposent d'une résistance normalisée au flambement supérieure à celle des aciers de résistance normale (NSS). Ces découvertes ont permis de partiellement modifier les Eurocodes de dimensionnement au flambement qui, jusque là, présentaient un conservatisme croissant avec l'augmentation de la limite élastique. Ces modifications ont permis l'utilisation d'une courbe de flambement plus favorable pour les aciers formés à chaud à partir de la nuance S460 jusqu'à la nuance S700. Pourtant, cette modification n'a pas été introduite pour les aciers formés à froid (CF) alors que les bobines de HSS sont déjà commercialisées pour cette filière tandis que les éléments formés à chaud ne sont pas produit au-delà de la nuance S460.

L'objectif de ce travail est donc d'améliorer les normes de dimensionnement des aciers CF en prenant en compte l'augmentation normalisée de la résistance au flambement associée à l'élévation de la nuance d'acier. Cette étude se concentre plus particulièrement sur les profilés creux CF. La méthodologie adoptée suit une approche scientifique classique, fondée sur des essais expérimentaux issus de la littérature, utilisés pour développer et valider un modèle numérique capable de reproduire les résultats expérimentaux. Ce modèle doit permettre de mener une étude paramétrique sur différentes nuances d'acier et longueurs de colonnes en vue d'évaluer les normes de dimensionnement européennes ainsi que des propositions de modifications de la littérature basées sur celles-ci. Au terme de cette analyse, une proposition d'amélioration des normes pour les profilés creux formés à froid est proposée.

Contents

1	Introduction	1
1.1	High-strength steels, uses and advantages in the construction sector	1
1.2	Advantages of cold-forming over hot-forming	2
1.3	Use of cold-forming in the construction sector	2
1.4	European standards and standards improvement	3
1.5	Research objectives and outline	3
2	Research context and objectives	5
2.1	Existing norms	5
2.2	State of the art	8
2.3	Research questions and objectives	12
2.4	Methodology	13
3	Modelling assumptions	14
3.1	Numerical model description	14
3.2	Material law	14
3.3	Geometrical and material imperfections	15
3.4	Scope	15
3.5	Validation process	15
4	Validation	17
4.1	Material laws	17
4.2	Numerical model meshing	22
4.3	Residual stresses	22
4.4	Numerical model validation	26
4.5	Discussion on Ramberg-Osgood law parameters	33
5	Parametric study and developments	36
5.1	Numerical parametric study	36
5.2	Assessment of EC3 design rules	37
5.3	Assessment of modified EC3 design rules	41
5.4	Developement of a modified imperfection factor	44
6	Conclusions and perspectives	46
	Appendices	48
	Bibliography	56

List of Figures

2.1	Maximum width-to-thickness ratios - (FrpEN1993-1-1, 2022)	6
2.2	Imperfection factors α for buckling curves - (FrpEN1993-1-1, 2022)	8
2.3	Idealised residual stresses distributions for cold-formed SHS150x150x4.9 (Key and Hancock, 1993)	9
3.1		
	Column model	14
3.2	Reference cross-sections	16
4.1	Typical stress-strain curves from hot-formed sections and cold-formed SHS steel sections (Meng, Whitfield, et al., 2024)	18
4.2	elastic-perfectly plastic	19
4.3	elastic-plastic with linear hardening	19
4.4	Bilinear behaviour laws	19
4.5	single-phase Ramberg-Osgood	20
4.6	two-phase Ramberg-Osgood	20
4.7	Ramberg-Osgood behaviour laws	20
4.8	Theoretical material laws and coupon test from S275 SHS100x8 (Poursadrollah, D'Aniello, and Landolfo, 2022)	20
4.9	Theoretical material laws and coupon test from S355 SHS300x9 (Satou, 2015)	20
4.10	Theoretical material laws and coupon test from S700 CHS139.7x5 (Meng and Leroy Gardner, 2021)	21
4.11	Theoretical material laws and coupon test from S1100 CHS89x4 (Ma, 2016)	21
4.12	Ramberg-Osgood behaviour laws	21
4.13	Theoretical material laws and coupon test from S355-S420 SHS100x8 (Meng, Whitfield, et al., 2024)	21
4.14	Residual stresses for CHS and RHS hot rolled-cold finished sections - (FrpEN1993-1-14, 2025)	22
4.15	Longitudinal residual stresses in press-braked SHS sections (W. M. Quach, 2005)	23
4.16	Indirect cold-rolling of CHS (W. M. Quach, 2005)	24
4.17	air bending	25
4.18	bottom bending	25
4.19	coining	25
4.20	Types of press and die for press-braking (Meng Xiao et al., 2022)	25
4.21	Deformed strips cut from SHS S900 (Ma, 2016)	25
4.22	Deformed strips cut from CHS S1100 (Ma, 2016)	25
4.23	Coupon test and theoretical laws for S355/S420 serie from Meng, Whitfield, et al. (2024)	27
4.24	Load-deflection curves for S355-S420 SHS100x8 column with $\bar{\lambda} = 0.26$ (Meng, Whitfield, et al., 2024)	28

4.25	Load-deflection curves for S355-S420 SHS100x8 column with $\bar{\lambda} = 1.33$ (Meng, Whitfield, et al., 2024)	28
4.26	Ultimates loads for S355-S420 SHS100x8 serie of Meng, Whitfield, et al. (2024)	29
4.27	Ultimate loads for S700 CHS139.7x5 column (Meng and Leroy Gardner, 2021)	29
4.28	Load-deflection curves for S700 CHS139.7x5 column with $\bar{\lambda} = 1.15$ (Meng and Leroy Gardner, 2021)	29
4.29	Theoretical material laws and coupon test from S700 CHS139.7x5 (Meng and Leroy Gardner, 2021)	30
4.30	Load-deflection curves for S355-S420 SHS100x8 column with $\bar{\lambda} = 0.26$ (Meng, Whitfield, et al., 2024)	30
4.31	Load-deflection curves for S355-S420 SHS100x8 column with $\bar{\lambda} = 0.53$ (Meng, Whitfield, et al., 2024)	30
4.32	Load-deflection curves for S700 CHS139.7x5 column with $\bar{\lambda} = 0.37$ (Meng and Leroy Gardner, 2020)	31
4.33	Load-deflection curves for S700 CHS139.7x5 column with $\bar{\lambda} = 1.00$ (Meng and Leroy Gardner, 2020)	31
4.34	Load-deflection curves for S700 CHS139.7x5 column with $\bar{\lambda} = 0.37$ (Meng and Leroy Gardner, 2020)	32
4.35	Load-deflection curves for S700 CHS139.7x5 column with $\bar{\lambda} = 1.15$ (Meng and Leroy Gardner, 2020)	32
4.36	Assessment of ultimate strain ϵ_u for colf-formed steels (Leroy Gardner and Yun, 2018)	33
4.37	Evaluation of predictive expression for strain-hardening exponent m for cold-formed steels with measured f_y/f_u ratios (Leroy Gardner and Yun, 2018)	34
4.38	Evaluation for predictive expressions for strain hardening exponent n for cold-formed steels with measured $\sigma_{0.01\%}$ and $\sigma_{0.05\%}$ (Leroy Gardner and Yun, 2018)	35
5.1	CHS 178x10 - Buckling curves for S235, S460 and S690	37
5.2	CHS 813x30 - Buckling curves for S235, S460 and S690	37
5.3	SHS 180x10 - Buckling curves for S235, S460 and S690	37
5.4	SHS 350x16 - Buckling curves for S235, S460 and S690	37
5.5	Comparisons of numerical data with unfactored EC3 resistance predictions for cold-formed tubular columns	38
5.6	Comparisons of test and numerical data with unfactored EC3 resistance predictions for cold-formed CHS columns (Meng and Leroy Gardner, 2021)	38
5.7	Comparison of simulation results to european buckling curve b for cold-formed SHS 120x120x6 (Somodi and Kövesdi, 2017)	39
5.8	Optimised values of the imperfection factor α	40
5.9	S355 numerical data with EC3 buckling curve c and Somodi and Kövesdi (2017) modified buckling curve	41
5.10	S690 numerical data with EC3 buckling curve c and Somodi and Kövesdi (2017) modified buckling curve	41
5.11	Comparison of Somodi and Kövesdi (2017) modified imperfection factor $\alpha_{S\&K}$ and the numerical α_{opt}	41
5.12	S460 numerical data with EC3 buckling curve c and Fang, T.-M. Chan, and Ben Young (2018) modified buckling curve	42
5.13	S690 numerical data with EC3 buckling curve c and Fang, T.-M. Chan, and Ben Young (2018) modified buckling curve	42
5.14	Optimised imperfection factor α_{opt} for the modified generalised imperfection factor η as proposed by Fang, T.-M. Chan, and Ben Young (2018)	43
5.15	S235 numerical data with EC3 buckling curve c and Meng and Leroy Gardner (2020) modified buckling curve	43

5.16	S235 numerical data with EC3 buckling curve c and Meng and Leroy Gardner (2020) modified buckling curve	43
5.17	Comparison of Meng and Leroy Gardner (2020) modified imperfection factor $\alpha_{Gardner}$ and the numerical α_{opt} with the modified plateau $\bar{\lambda} = 0.1$ of η	44
5.18	Correlation between the optimised imperfection factor α_{opt} and the formulations by Maquoi, considering $n = 0.68$ (left) and $n = 0.7$ (right) with the 0.1 plateau introduced by Meng and Leroy Gardner (2020)	44
5.19	S235 numerical data with EC3 buckling curve c and the modified buckling curve with 0.1 plateau for η and Saufnay (2025) modified α^*	45
5.20	S355 numerical data with EC3 buckling curve c and the modified buckling curve with 0.1 plateau for η and Saufnay (2025) modified α^*	45
5.21	S460 numerical data with EC3 buckling curve c and the modified buckling curve with 0.1 plateau for η and Saufnay (2025) modified α^*	45
5.22	S690 numerical data with EC3 buckling curve c and the modified buckling curve with 0.1 plateau for η and Saufnay (2025) modified α^*	45
6.1	S235 numerical data with EC3 buckling curve c and Somodi and Kövesdi (2017) modified buckling curve	48
6.2	S275 numerical data with EC3 buckling curve c and Somodi and Kövesdi (2017) modified buckling curve	48
6.3	S355 numerical data with EC3 buckling curve c and Somodi and Kövesdi (2017) modified buckling curve	48
6.4	S420 numerical data with EC3 buckling curve c and Somodi and Kövesdi (2017) modified buckling curve	48
6.5	S460 numerical data with EC3 buckling curve c and Somodi and Kövesdi (2017) modified buckling curve	49
6.6	S500 numerical data with EC3 buckling curve c and Somodi and Kövesdi (2017) modified buckling curve	49
6.7	S550 numerical data with EC3 buckling curve c and Somodi and Kövesdi (2017) modified buckling curve	49
6.8	S620 numerical data with EC3 buckling curve c and Somodi and Kövesdi (2017) modified buckling curve	49
6.9	S690 numerical data with EC3 buckling curve c and Somodi and Kövesdi (2017) modified buckling curve	49
6.10	Comparison of Somodi and Kövesdi (2017) modified imperfection factor $\alpha_{S\&K}$ and the numerical α_{opt}	49
6.11	S235 numerical data with EC3 buckling curve c and Fang, T.-M. Chan, and Ben Young (2018) modified buckling curve	50
6.12	S275 numerical data with EC3 buckling curve c and Fang, T.-M. Chan, and Ben Young (2018) modified buckling curve	50
6.13	S355 numerical data with EC3 buckling curve c and Fang, T.-M. Chan, and Ben Young (2018) modified buckling curve	50
6.14	S420 numerical data with EC3 buckling curve c and Fang, T.-M. Chan, and Ben Young (2018) modified buckling curve	50
6.15	S460 numerical data with EC3 buckling curve c and Fang, T.-M. Chan, and Ben Young (2018) modified buckling curve	50
6.16	S500 numerical data with EC3 buckling curve c and Fang, T.-M. Chan, and Ben Young (2018) modified buckling curve	50
6.17	S550 numerical data with EC3 buckling curve c and Fang, T.-M. Chan, and Ben Young (2018) modified buckling curve	51

6.18	S620 numerical data with EC3 buckling curve c and Fang, T.-M. Chan, and Ben Young (2018) modified buckling curve	51
6.19	S690 numerical data with EC3 buckling curve c and Fang, T.-M. Chan, and Ben Young (2018) modified buckling curve	51
6.20	Optimised imperfection factor α_{opt} for the modified generalised imperfection factor η as proposed by Fang, T.-M. Chan, and Ben Young (2018)	51
6.21	S235 numerical data with EC3 buckling curve c and Meng and Leroy Gardner (2020) modified buckling curve	52
6.22	S275 numerical data with EC3 buckling curve c and Meng and Leroy Gardner (2020) modified buckling curve	52
6.23	S355 numerical data with EC3 buckling curve c and Meng and Leroy Gardner (2020) modified buckling curve	52
6.24	S420 numerical data with EC3 buckling curve c and Meng and Leroy Gardner (2020) modified buckling curve	52
6.25	S460 numerical data with EC3 buckling curve c and Meng and Leroy Gardner (2020) modified buckling curve	52
6.26	S500 numerical data with EC3 buckling curve c and Meng and Leroy Gardner (2020) modified buckling curve	52
6.27	S550 numerical data with EC3 buckling curve c and Meng and Leroy Gardner (2020) modified buckling curve	53
6.28	S620 numerical data with EC3 buckling curve c and Meng and Leroy Gardner (2020) modified buckling curve	53
6.29	S690 numerical data with EC3 buckling curve c and Meng and Leroy Gardner (2020) modified buckling curve	53
6.30	Comparison of Meng and Leroy Gardner (2020) modified imperfection factor $\alpha_{Gardner}$ and the numerical α_{opt} with the modified plateau $\bar{\lambda} = 0.1$ of η	53
6.31	S235 numerical data with EC3 buckling curve c and the modified buckling curve with 0.1 plateau for η and Saufnay (2025) modified α^*	54
6.32	S275 numerical data with EC3 buckling curve c and the modified buckling curve with 0.1 plateau for η and Saufnay (2025) modified α^*	54
6.33	S355 numerical data with EC3 buckling curve c and the modified buckling curve with 0.1 plateau for η and Saufnay (2025) modified α^*	54
6.34	S420 numerical data with EC3 buckling curve c and the modified buckling curve with 0.1 plateau for η and Saufnay (2025) modified α^*	54
6.35	S460 numerical data with EC3 buckling curve c and the modified buckling curve with 0.1 plateau for η and Saufnay (2025) modified α^*	54
6.36	S500 numerical data with EC3 buckling curve c and the modified buckling curve with 0.1 plateau for η and Saufnay (2025) modified α^*	54
6.37	S550 numerical data with EC3 buckling curve c and the modified buckling curve with 0.1 plateau for η and Saufnay (2025) modified α^*	55
6.38	S620 numerical data with EC3 buckling curve c and the modified buckling curve with 0.1 plateau for η and Saufnay (2025) modified α^*	55
6.39	S690 numerical data with EC3 buckling curve c and the modified buckling curve with 0.1 plateau for η and Saufnay (2025) modified α^*	55
6.40	Comparison of Saufnay (2025) modified imperfection factor $\alpha_{Saufnay}$ and the numerical α_{opt} with the modified plateau $\bar{\lambda} = 0.1$ of η	55

Chapter 1

Introduction

1.1 High-strength steels, uses and advantages in the construction sector

Aesthetic considerations are driving architects and engineers to design more slender structures. This pursuit of visual lightness is made possible by advances in the steel industry, particularly in the development of new steel grades with ever-increasing strength. Over the last twenty years, markets have seen the arrival of 'high strength' steels. Although there is no universal consensus on the definition of these steels, since a steel grade can be classified as 'standard' or 'high-strength' depending on its application, the new general design standard FprEN1993-1-1:2022 characterises high-strength steels (HSS) as having a yield strength of at least 460 MPa (S460). Grades with a yield strength of 550 MPa or more are referred to as ultra-high strength steels (UHSS) and cover steels from grade S550 to grade S1100 and above. Today, these high-strength steels are produced in many modern steelworks worldwide.

Although HSS see their ultimate-to-yield strength ratio, f_u/f_y , and strain at failure, ϵ_u , reduce as their yield strength increases, the benefit of their excellent strength-to-weight ratio implies that slender elements can be considered for the same loading, thus increasing the usable space within the structure. However, for some applications, this reduction is limited by the sensitivity of slender elements to vibration and deflection.

Beside these technical limitations, the unitary cost of high-strength steels is higher than the one of standard steels. Therefore, HSS are nowadays limited to specific uses such as columns in the base of high-rise buildings or bridge structures and have yet to be widely adopted in the other construction sectors. However, it is expected that their structural efficiency in construction will become economically more attractive with the economies of scale made possible by growing demand. Indeed, a greater strength-to-weight ratio means that structures are lighter, and this goes hand in hand with a reduction in the importance of foundations, which in turn translates into a reduction in the quantity of materials consumed and the associated costs.

In parallel with the economic and technical advantages, the use of HSS also offers environmental benefits, in particular, by reducing the demand for raw materials. This reduction in consumption is accompanied by a reduction in the carbon footprint, not only during transport and installation but also during the production of the elements themselves, since less material is used and the increase in the elastic limit of the steels is achieved without any significant rise in CO_2 emissions (Saufnay, 2025; Baddoo and Chen, 2020).

1.2 Advantages of cold-forming over hot-forming

Today, these environmental considerations are more important than ever, given the reality of climate change. It is now more necessary than ever to review the production and consumption methods employed in the various sectors of human activity. Among these, the construction industry plays a major role in the disruption affecting our ecosystems. In fact, the building sector, with its energy supply, is responsible for 37% to 42% of global emissions of CO₂ (Intergovernmental Panel on Climate Change (IPCC), 2023; UN Environment Programme (UNEP) and Global Alliance for Buildings and Construction (GlobalABC), 2025). Almost a quarter of these emissions are attributed to building materials and their supply chain. While the use of components with greater load-bearing capacity per unit of weight makes it possible to rationalise the sector's consumption, it is also necessary to act directly on the production methods of these components.

In this context, cold forming of steel offers a good alternative to the hot-rolling process historically used in the steel industry. Unlike hot rolling, cold forming processes the steel at ambient temperature, and therefore enables direct energy savings by avoiding element heating. In addition, cold-working steel avoids the formation of a surface layer of iron oxide, known as mill scales, and the subsequent loss of raw material through scaling. The absence of thermal shrinkage also provides greater dimensional accuracy, reducing the need for extra thickness. This improved dimensional control is combined with a better surface finish of the components produced through the cold-forming process, thereby reducing energy requirements and material losses during post-processing. Cold forming therefore benefits from reduced energy consumption and a higher raw material yield than hot forming, helping to reduce the carbon footprint of finished products (Dawson Shanahan, 2021).

In addition, these environmental considerations are backed up by substantial economic and strategic advantages in a context of rising energy costs and increasingly stringent environmental requirements. Cold forming enables complex sections to be produced rapidly by bending/profiling and welding, without the need for heavy tooling. As a result, this form of production has proved to be highly versatile and cost-effective, particularly for cold-formed tubes produced in small or medium quantities and with non-standard cross-sectional dimensions. Finally, cold forming stands out for its rapid implementation and excellent material yield, contributing to efficient industrial production at lower cost. These qualities make it a strategic choice for meeting the challenges of competitiveness, sustainability and the demand for customised steel components in the construction sector (Raksha Sharma, 2021).

1.3 Use of cold-forming in the construction sector

Cold forming allows the creation of thin-walled elements with optimised shapes, designed to withstand loading with minimal material use. The logistics sector in particular uses cold-formed elements for racking structures, where the search for lighter structures is driving extreme optimisation of the elements. Today, this method is no longer reserved for thin sections, as it can produce sections with thicknesses of up to 12 mm, or even 30 mm in some cases. Cold forming is therefore able to compete with hot forming, although the latter is still preferred for the production of solid steel elements and large parts, as well as for applications requiring high ductility. Indeed, the significant plastic deformations undergone during the cold-work result in a consequent strain-hardening of the steel. As a result, the material has higher post-forming strength and lower ductility than the parent strip. However, the work-hardening of cold-formed sections has the advantage of making finished products more efficient in terms of strength per unit weight than hot-rolled products of the same grade. In the construction sector, this process is experiencing significant growth, fuelled by the need for lightness and rapid installation, as well as by the demand for modularity and durability.

1.4 European standards and standards improvement

For both cold-formed members and high-strength steels, effective and reliable design methods are needed to exploit their full potential. The scope of the current FprEN1993-1-1:2022 for buckling of cold-formed steel columns covers grades S235 to S700 and is supplemented by FrpEN1993-1-1 (2022) for higher grades. This standard adopts the same rules as for grade S700, specifying the particular features of higher grades up to grade S960. However, for cold-formed elements, the dimensioning rules for higher grades are the same as those defined in the standards for normal-strength steels. There is therefore no distinction between the S235 grade and the S700 grade for the dimensioning rules of cold-formed columns.

Yet, several previous research results prove that the buckling resistance of HSS structures is superior to that of structures with normal strength steels (NSS) on a non-dimensional basis. Current standards therefore leave room for improvement in terms of accuracy and consistency. Numerous previous studies and residual stress measurements show that the ratio between residual stress and yield strength is lower for HSS than for NSS, which can translate into a significant advantage in terms of buckling resistance. Indeed, buckling behaviour is governed by the ratio of residual stress to yield strength, rather than by the magnitude of the residual stress itself. In addition, high-strength steels have been shown to be less sensitive to geometric imperfections. As a result, The Eurocodes have been updated in a step-wise manner to permit the use of a higher buckling curve for steel grades starting from S460. However, this modification has only been introduced for hot-rolled steels. Yet, high yield strength steels are already commercially available in coil form for cold-forming applications whereas, for hot-rolled sections, production does not yet extend beyond grade S460.

1.5 Research objectives and outline

The aim of this work is therefore to determine the potential for improving European standards for the buckling dimensioning of cold-formed tubular columns, with a view to developing an modified version of these standards. The current standards will therefore be compared with experimental tests available in the literature and with proposals for modified standards that already exist.

This optimisation will focus on cold-formed hollow sections which are widely used in a variety of structural applications, including low-to-medium-rise buildings as well as bridges, walkways and trusses. Their effective structural shape offers improved torsional rigidity along with excellent resistance to bending under different axes, thus contributing to superior performances with respect to buckling and lateral-torsional buckling. In addition to their stability under transverse loading and, above all, axial loading, tubular elements have a reduced exposure surface area, which is advantageous with regard to corrosion and maintenance aspects. Their aesthetic appeal also makes them popular with architects, further reinforcing their interest in construction.

This topic has already been addressed for hot-formed tubular columns as part of Loris Saufnay's PhD on the use of high-strength steels and the development of innovative and sustainable design approaches for steel structures at the University of Liège. This research work forms the starting point for the present document. The approach followed is a conventional scientific method, based on experimental data from the literature, a numerical model capable of reproducing test results is developed to allow the performance of a parametric study assessing the effect of steel grades over the buckling of columns.

The following chapters of this thesis are organised as follows:

Research context and objectives: this first chapter starts by presenting the content of current European standards. This is followed by a review of the literature on the buckling behavior of high-strength steels and cold-formed elements, and a summary of proposed modifications to existing buckling design rules. The research objectives and questions addressed by this work are then highlighted. Finally, the methodology followed in this work is presented.

Modelling assumptions: This second chapter describes the finite element model used and the assumptions considered in the numerical simulations. The domain considered in terms of grades, reduced slenderness and cross-sections is then detailed, before presenting the experimental test profiles used as a reference for the model's validation.

Validation: The choice and verification of the hypotheses mentioned in the previous chapter are first detailed in this third chapter. The numerical simulations are then compared with the reference experimental tests to assess their reliability. Finally, on the basis of these comparisons, several possible solutions are proposed to improve the reliability of the model based on the behaviour law.

Parametric study and developments: This chapter first describes the numerical study carried out to complement the experimental data. Next, numerical and experimental tests are used to assess the reliability of the European standards, as well as that of the modified standards proposed in the literature, by means of a parametric study. On this basis, a modified proposal for buckling design rules is put forward for cold-formed tubular columns.

Conclusion: this final chapter draws together the contributions of this paper, providing recommendations and further research questions for future work.

Chapter 2

Research context and objectives

This work focuses on the potential optimisation of the European recommendations for the design of cold-formed steel tubular members under buckling. It is therefore appropriate to first recall the nature of these recommendations as defined in standard FprEN1993:2022, as well as previous studies related to this topic.

2.1 Existing norms

European standards define two types of resistance for a member, on the one hand, its cross-sectional resistance, and on the other hand, its global resistance, the latter being defined based on the cross-sectional resistance, modified to account for the mechanisms and instabilities governing global behaviour.

The section resistance depends directly on the cross-sectional area and the intrinsic yield strength of the material. It therefore increases proportionally with the steel grade or with larger profile sizes. However, beyond the cross-sectional area, the geometry of the section is also a decisive factor. Indeed, excessive slenderness of part of the section under compression can lead to a risk of local buckling, independently of the member's overall dimensions. The Eurocodes thus introduce the concept of cross-section classification by distinguishing four classes to categorise the different constituent plates of a section: 'Class 1: plastic', 'Class 2: compact', 'Class 3: semi-compact' and 'Class 4: slender.' The class of the section is then determined by the most critical of its component plates.

As exposed in Figure 2.1 This classification assesses the width-to-thickness ratio by distinguishing between outstand elements and internal elements, thereby reflecting the influence of geometry and support conditions. The classification criteria depend on the coefficient ϵ and thus take into account the yield strength. As a result, the recommendations become more restrictive as the yield strength of the steel increases.

Eurocode 3 evaluates the cross-sectional resistance of compressed profiles, denoted $N_{c,Rd}$, based on their class, using the relationships 2.1 and 2.2 below. $N_{c,Rk}$ represents the un-factored compressive resistance of the section, and $\gamma_{M0} = 1$ is the partial safety factor applied to it. A is the gross cross-sectional area, and f_y is the yield strength of the steel.

$$N_{c,Rd} = \frac{N_{c,R}}{\gamma_{M0}} = \frac{A \cdot f_y}{\gamma_{M0}} \quad \text{for Class 1-3 cross-sections} \quad (2.1)$$

$$N_{c,Rd} = \frac{N_{c,R}}{\gamma_{M0}} = \frac{A_{eff} \cdot f_y}{\gamma_{M0}} \quad \text{for Class 4 cross-sections} \quad (2.2)$$

In the case of a Class 4 cross-section, accounting for local buckling requires a notional reduction of the gross cross-sectional area, as local buckling limits the maximum attainable resistance. The resulting effective section A_{eff} is defined by the effective width of the constituent parts of the section, which

decreases with increasing width-to-thickness ratio. The load-bearing capacity of these Class 4 sections is therefore governed primarily by local elastic buckling rather than by the yield strength f_y .

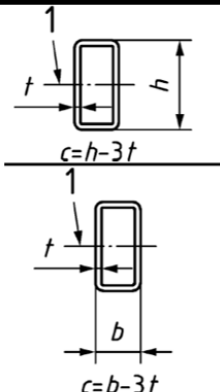
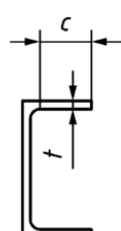
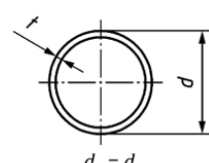
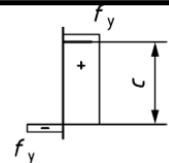
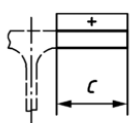
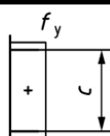
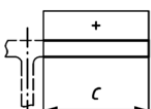
	Internal parts	Outstand flanges	Circular and elliptical hollow sections			
Key 1 Axis of bending						
Class	Part subject to compression	Part subject to compression	Section in compression			
Stress distribution in parts (compression positive)						
Class 1	$c/t \leq 28 \varepsilon$	$c/t \leq 9 \varepsilon$	$d_e/t \leq 50 \varepsilon^2$			
Class 2	$c/t \leq 34 \varepsilon$	$c/t \leq 10 \varepsilon$	$d_e/t \leq 70 \varepsilon^2$			
Stress distribution in parts (compression positive)						
Class 3	$c/t \leq 38 \varepsilon$	$c/t \leq 14 \varepsilon$	$d_e/t \leq 90 \varepsilon^2$			
$\varepsilon = \sqrt{\frac{235}{f_y}}$	f_y	235	275	355	420	460
	ε	1.00	0.92	0.81	0.75	0.71

Figure 2.1: Maximum width-to-thickness ratios - (FrpEN1993-1-1, 2022)

However, the support and loading conditions of compressed members may lead to failure by lateral instability before the load reaches $N_{c,Rd}$. This phenomenon, known as global buckling, occurs in slender steel columns and may develop sooner or later depending on the geometry of the member.

Hence, Eurocode 3 introduces the concept of reduced slenderness, $\bar{\lambda}$, to characterise the behaviour of a cross-section with respect to stability issues. This parameter provides an indication of the extent to which the resistance of a member is governed by instability or by plasticity, as reflected in its expression 2.3. A reduced slenderness value of 0.2 is adopted as the threshold below which buckling no longer affects the pure cross-sectional resistance, elements are then referred to as 'stub' columns ($\bar{\lambda} \leq 0.2$) as opposed to 'slender' columns ($\bar{\lambda} > 0.2$)

$$\text{Relative slenderness} = \sqrt{\frac{\text{Characteristic resistance}}{\text{Resistance to elastic buckling}}} \quad (2.3)$$

For compressed members, it becomes :

$$\bar{\lambda} = \sqrt{\frac{N_{c,R}}{N_{cr}}} = \sqrt{\frac{A \cdot f_y}{N_{cr}}} \quad \text{for Class 1-3 cross-sections} \quad (2.4)$$

$$\bar{\lambda} = \sqrt{\frac{N_{c,R}}{N_{cr}}} = \sqrt{\frac{A_{eff} \cdot f_y}{N_{cr}}} \quad \text{for Class 4 cross-sections} \quad (2.5)$$

Where N_{cr} is Euler's critical load representing the buckling resistance of an axially loaded column with no initial imperfections and composed of an indefinitely elastic material.

$$N_{cr} = \frac{\pi^2 \cdot E \cdot I}{L_{cr}^2} \quad (2.6)$$

According to this evolving dynamic of the partial influence of plasticity and instability, buckling-induced failure of slender elements may occur (1) through full plastic deformation in the case of short columns, (2) through partial plastic deformation for intermediate-length columns, and (3) through elastic buckling for long columns.

In standard EN 1993-1-1:2022, the global axial buckling of steel columns is treated as a penalty and is thus accounted for by a reduction of the cross-sectional resistance via the χ coefficient.

$$N_{b,Rd} = \frac{\chi \cdot N_{c,R}}{\gamma_{M1}} \quad (2.7)$$

This buckling reduction factor is determined based on the Ayrton-Perry formula (1886), whose current formulation 2.8 was developed by Maquoi and Rondal.

$$\chi = \frac{1}{\phi - \sqrt{\phi^2 - \bar{\lambda}^2}} \quad (2.8) \quad \text{with} \quad \phi = 0.5 \cdot (1 + \eta + \bar{\lambda}^2) \quad (2.9)$$

$$\eta = \alpha \cdot (\bar{\lambda} - 0.2) \quad (2.10)$$

This expression for the reduction factor χ makes it possible to assess the effect of global axial buckling as a function of the column's reduced slenderness. In this expression, the generalised initial imperfection factor η is used to account for the combined effects of initial out-of-straightness and residual stresses. In the formulation of the latter, α is the imperfection factor defined according to the type and dimensions of the section, the buckling axis, and the manufacturing process of the member. This factor therefore incorporates the detrimental effect of geometric imperfections and residual stresses on the behaviour of

compressed columns.

To develop a practical design tool based on the buckling curves $\chi = f(\bar{\lambda})$, Eurocode 3 defines five distinct curves, each characterised by a specific imperfection factor α 2.2. These five curves were calibrated against a wide range of experimental and numerical data for various types of cross-sections. These various experimental and numerical test campaigns also validated the half-sine out-of-straightness imperfection with an amplitude of $L/1000$, which was first proposed by the ECCS (1976) and forms the basis for defining the α factor.

Buckling curve	a_0	a	b	c	d
Imperfection factor α	0,13	0,21	0,34	0,49	0,76

Figure 2.2: Imperfection factors α for buckling curves - (FrpEN1993-1-1, 2022)

For cold-formed hollow sections, Eurocode 3 prescribes the use of buckling curve *c* with its imperfection factor $\alpha = 0.49$, regardless of the steel grade considered.

2.2 State of the art

Many researchers have investigated the economic potential of high-strength steels (HSS) as a new construction material. The properties of these steels, along with the geometric imperfections of elements fabricated from them, their residual stresses, and their resistance, have been the subject of numerous studies and analyses. Early research on high-strength steel focused on the structural behavior of welded sections made from high-strength steel plates, as most HSS products available at the time were supplied in plate form. In this context, extensive research was conducted on welded box and I-sections. Various experimental programs examined residual stress distributions, global imperfections, plate slenderness limits, and buckling behaviour. Studies on high-strength steel elements (HSS) with a nominal yield strength exceeding 690 MPa were initiated during the seventies with Nishino, Ueda, and Tall (1966), highlighting that it is the ratio between yield strength and residual stress, rather than the magnitude of the residual stresses themselves, that governs the buckling behaviour of columns. The same results were observed by in following publications Nishino and Tall (1970). Subsequently, it was found that HSS columns exhibited better structural performance than their counterparts made from conventional steel when experimental buckling reduction factors were compared.

It has indeed been demonstrated that residual stresses remain approximately constant regardless of the steel grade (ECCS, 1976), and therefore decrease proportionally with increasing yield strength for higher-grade steels. A number of experimental studies on the axial compression behaviour of SHS and RHS members have supported these findings. Several research projects initiated by the Comity for International Development and Education on Construction of Tubular Structures (CIDECT) investigated the buckling behaviour of SHS and RHS columns notably the works of Guiaux (1972), Salvarinas, Barber, and Birke-moe (1978), Braham, Grimault, and J. Rondal (1979), Sedlacek, J. Rondal, et al. (1996) and Sedlacek, Kuhn, et al. (1999), which reported a large number of buckling tests on hot-rolled columns. Laboratory tests on hot-rolled SHS and RHS columns were also conducted by Jean Rondal (1984) and Wang and Leroy Gardner (2017), in which high-strength steel elements once again demonstrated higher load-carrying capacities than their mild steel counterparts when compared based on the buckling reduction factor.

For cold-formed members, it is widely recognised that the stress-strain response of the steel exhibits a gradual transition from elastic to plastic behaviour due to manufacturing-induced strain hardening, and

therefore lacks a clearly defined yield point. Previous studies on cold-formed sections have also shown that cold working increases both the yield strength and the ultimate strength (f_y and f_u , respectively), while reducing ductility, particularly when the internal radius-to-thickness ratio decreases. Several studies have focused on developing material models capable of simulating such a stress-strain response. The Ramberg-Osgood model (Ramberg and Osgood, 1943) is the most widely used, and many recent models are derived from it. Mirambell and Real (2000) proposed a two-phase stress-strain model for round-house-type steels, based on the conventional Ramberg-Osgood formulation. Leroy Gardner and Yun (2018) adopted the model developed by Mirambell and Real to propose predictive equations and calibrated parameters relevant to cold-formed steels, covering a wide range of steel grades through a comprehensive analysis of literature data.

In contrast, research on the distribution of residual stresses in cold-formed elements has led to less clear results. Key and Hancock (1993) investigated cold-formed *SHS* 152x152x4.9 sections with a yield strength of $f_y = 350 \text{ MPa}$, manufactured using the 'direct cold rolling' method. Their residual stress measurements revealed two main components of longitudinal stress, a membrane component and a bending component. The membrane stress distribution consisted of tensile stresses at the mid-width of the flat faces and compressive stresses in the corner regions. In both regions, the membrane stresses showed relatively low amplitudes, with extreme values mostly ranging between $\pm 40 \text{ MPa}$. Conversely, the measured bending residual stresses were found to be much higher, with tensile stresses on the outer surfaces and compressive stresses on the inner surfaces of the hollow sections. The maximum bending residual stress reached approximately 300 MPa in the central part of the flat faces. However, significantly lower values were observed in the corner regions. The transition zones between high and low bending residual stresses were found to be rather narrow, resulting in an almost uniform bending stress distribution across the main flat portion of the plates. Variations in longitudinal residual stresses across the thickness are difficult to assess experimentally for thin-walled sections, but they were measured in thick plates by Key and Hancock (1993), who proposed idealised distributions for both longitudinal and transverse residual stresses in cold-formed sections. Due to the greater plate thickness in these SHS sections, their measurements were able to capture complex through-thickness variation of residual stresses. They concluded that the longitudinal and transverse residual stresses in SHS sections consist of three components: (a) membrane stresses, (b) bending stresses and (c) layering stresses.

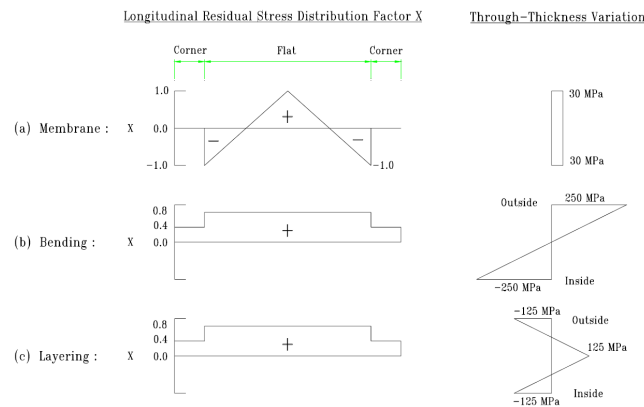


Figure 2.3: Idealised residual stresses distributions for cold-formed *SHS*150x150x4.9 (Key and Hancock, 1993)

Abdel-Rahman and Sivakumaran (1997) suggested that transverse residual stresses could be neglected due to their low amplitudes, and that only longitudinal residual stresses should be considered significant. Consequently, most existing studies on residual stress modelling in cold-formed sections have focused on characterising longitudinal residual stresses.

Experimental studies later confirmed that residual stresses in cold-formed sections originate from the cold-working of the steel. Residual stress measurements in cold-formed sections have often been idealised to define residual stress models. However, large variations in the amplitude of the measured residual stresses have been reported. For example, in lipped channel sections, Kwon and Hancock (1992) as well as B. Young and Rasmussen (1995) measured negligible residual stresses in the flat regions, whereas Weng and Peköz (1990) found residual stresses reaching up to approximately 40% of the yield strength. This discrepancy in flat-region residual stresses was suggested to be due to variable cold-forming parameters depending on the manufacturing process. Batista and Rodrigues (1992) measured the longitudinal residual stress distributions in U-sections formed by both cold-rolling and press-braking, using identical cross-sectional geometry. They concluded that the residual stresses in roll-formed sections were higher than in press-braked sections, indicating that the magnitude of residual stresses depends on the degree of cold work and, hence, on the manufacturing method. Li et al. (2009) measured residual stresses in seven cold-rolled square hollow sections produced by direct cold-rolling and in three hollow square sections produced by indirect cold-rolling, using steel grades ranging from S235 to S355. The X-ray diffraction method was used to enable through-thickness measurements, and showed that the residual stress distribution across the plate thickness is approximately bilinear, as shown by Key and Hancock (1993). The study confirmed that bending stresses are predominant in cold-formed profiles and that the manufacturing process significantly influences the residual stress distribution. Residual stresses measured in samples produced by the indirect cold-rolling method were higher than those from the direct method, with the average longitudinal residual stress being $0.46 f_y$ for the direct method and reaching $0.64 - 0.7 f_y$ for the indirect method.

In general, research on the buckling behaviour of cold-formed tubular HSS members remains relatively limited compared to the research conducted on welded high-strength steel columns. Buckling tests on cold-formed SHS and RHS members have been carried out and reported by Bjorhovde (1977), Jean Rondal (1984), Key, Hasan, and Hancock (1988), and Sully and Hancock (1996), while cold-formed high-strength CHS columns have been investigated by Kato et al. (1984), Zhao et al. (2004), Ma, T. M. Chan, and Ben Young (2021) and Zhao (2000), who notably studied the behaviour of cold-formed high-strength circular hollow sections with a yield strength of 1350 MPa. Cold-formed columns were also tested by Pavlovčič et al. (2012), SSAB (2014), and SSAB (2014). A comprehensive experimental programme on cold-rolled RHS members made of S700 to S1100 steel was conducted by Ma (2016). This PhD thesis analysed the material properties and residual stress patterns through compression tests on both stub and slender columns under axial load, bending, and combined bending-compression. The results of these experimental and numerical investigations concluded that residual stresses have a significant impact on the buckling resistance of columns. Furthermore, many square and rectangular hollow section columns (SHS and RHS) with higher yield strengths than standard steels were found to exhibit better experimental buckling reduction coefficient when compared to the same sections made from conventional grades. As with hot-rolled steels, increasing the steel grade in cold-formed sections leads to a reduced influence of residual stresses and global imperfections on the overall buckling behaviour. Based on this, Somodi and Kövesdi (2017) and Meng and Leroy Gardner (2020) carried out further experimental and numerical studies on the buckling behaviour of cold-rolled high-strength RHS profiles and proposed that a steel-grade-dependent imperfection factor α could be incorporated into the calculation of the reduction factor to account for the effects of different material properties. More recently, Poursadrollah, D'Aniello, and Landolfo (2022) evaluated the mean partial safety factor in accordance with Annex D of EN 1990 for buckling curve *c* of the standard EN1993:2009, and showed that the current code formulation may on average underestimate the buckling resistance of cold-formed hollow sections. D'Aniello concluded that the current buckling curves have a non-uniform safety margin and may lead to uneconomical designs within the slenderness range typically used for columns in medium and high-rise steel structures.

Indeed, the buckling curves defined by FrpEN1993-1-1 (2022) were established based on a fictitious material with a yield strength of $f_y = 255 \text{ MPa}$, under the assumption that yield strength had little influence on the dimensionless buckling curves. However, subsequent studies have contradicted this assumption by demonstrating that the structural performance of high-strength steel members is less affected by residual stresses, due to the lower ratio between residual stress and yield strength (σ_{res}/f_y). Furthermore, in the original Ayrton-Perry formulation, on which the European buckling curves are based, the generalised global imperfection η can be rearranged to highlight its proportionality to the product of the non-dimensional slenderness $\bar{\lambda}$ and $1/\sqrt{f_y}$ for a given cross-sectional profile. As exposed by Meng and Leroy Gardner (2020), when considering a simply supported compressed member with an initial imperfection of amplitude $e_0 = L/1000$ and no residual stresses, expression 2.11 can be derived by rewriting the length L using the expression of the reduced slenderness $\bar{\lambda}$.

$$\eta = \frac{e_0 \cdot A}{W_{el}} = \frac{L}{1000} \cdot \frac{A}{W_{el}} = \bar{\lambda} \cdot \pi \cdot \sqrt{\frac{E \cdot I}{A \cdot f_y}} \cdot \frac{A}{1000 W_{el}} = \left(\frac{\pi}{1000} \frac{\sqrt{EIA}}{W_{el}} \right) \cdot \frac{\bar{\lambda}}{\sqrt{f_y}} \quad (2.11)$$

Expression 2.11 thus highlights the reduction of the generalised imperfection factor with the increase of the elastic limit. This less detrimental effect of global imperfections on the buckling behaviour of high-strength steels has been confirmed in several previous studies for cold-formed and hot-rolled hollow sections (Leroy Gardner and Yun, 2018; Fang, T.-M. Chan, and Ben Young, 2018; Poursadrollah, D'Aniello, and Landolfo, 2022; Saufnay, 2025). The reduction in the generalised imperfection factor with increasing yield strength for a given level of reduced slenderness therefore adds to the reduction in the influence of residual stresses.

In light of these positive effects on the buckling behaviour of higher steel grades, it could have been decided to define the generalised imperfection factor η as a function of the yield strength. Accordingly, various design rule proposals have been developed in this direction. Among these, Saufnay, Jaspart, and Demonceau (2024) distinguished three general approaches:

1. The first approach multiplies the expression of the generalised imperfection factor by a power of ε . This additional term is combined with the imperfection factor α in the form of a modified imperfection factor α^* .

$$\eta = \alpha^* \cdot (\bar{\lambda} - 0.2) \quad \text{with} \quad \alpha^* = \alpha \cdot \varepsilon^{2n}$$

This method is the most commonly used in research studies and has led to different proposed values for the parameter n . For example, Maquoi (1982) recommends a value of $n = 0.8$, whereas Johansson (2005) suggests $n = 1$ up to grade S400. Other studies indicate, however, that n may depend on the section type. Thus, for welded I-sections and hot-rolled hollow sections, Somodi and Kövesdi (2017) suggest $n = 0.6$, while for cold-formed hollow sections, they recommend $n = 0.5$. More recently, Saufnay, Jaspart, and Demonceau (2024) recommends $n = 0.7$ for both hot-formed I-sections and hot-rolled hollow sections.

2. The second approach proposes modifying the generalised imperfection factor by multiplying the reduced slenderness by ε . This method was developed by Jönsson and Stan (2017) for major-axis buckling of hot-formed sections and has also been proposed for both axis buckling by Fang, T.-M. Chan, and Ben Young (2018) for cold-formed hollow sections. The ε parameter is typically used to account for yield strength. In the current context, it implies the assumption of an increasing plastic plateau length with increasing yield strength.

$$\eta^* = \alpha \cdot (\varepsilon \cdot \bar{\lambda} - 0.2)$$

3. The third approach departs entirely from the conventional buckling curves and the α -values currently used in European standards by redefining the imperfection factor α as a function of ε . This modified approach was introduced by Meng and Leroy Gardner (2020), who developed for cold-formed hollow sections a linear function of ε with a value set at 0,56 for S235-grade steel. A reduction of the extent of the plastic plateau to a relative slenderness of 0.1 instead of 0.2 was introduced along this formulation in the expression of η .

$$\eta = \alpha^* \cdot (\bar{\lambda} - 0.1) \quad \text{with} \quad \alpha^* = 0.56 \cdot \varepsilon$$

2.3 Research questions and objectives

To address the shortcomings of the Eurocode 3 (EC3) in the design of cold-formed steel members under buckling and to allow for a better optimisation of structures using such profiles, it is necessary to improve the current buckling design rules so that it fully accounts for the influence of steel grade on the structural behaviour of cold-formed elements. Given the lack of experimental data available in the literature, the present work first aims to expand the existing database on buckling tests of cold-formed tubular columns. A finite element model (FEM) is therefore developed and validated in order to generate additional numerical data. The study then evaluates the reliability of both current FrpEN1993-1-1 (2022) design approaches and modified EC3-based formulations for cold-formed columns. The conclusions of this analysis are intended to support the development of an improved EC3-based design method, by defining the imperfection factor as a continuous function of the yield strength, with the objective of increasing the accuracy and consistency of European recommendations.

To achieve these objectives, the study addresses the following research questions:

1. Which material model, as defined in the draft standard FrpEN1993-1-14 (2025), best represents the stress-strain behaviour of cold-formed steel profiles?
2. What residual stresses are present in cold-formed hollow sections and how can they be incorporated into a finite element model?
3. What level of safety do the design provisions of FrpEN1993-1-1 (2022) offer for the buckling resistance of cold-formed columns?
4. How can the recommendations of FrpEN1993-1-1 (2022) be adapted to optimise the buckling design of cold-formed tubular columns?

2.4 Methodology

The first part of this work focuses on the development of a numerical model capable of simulating the buckling response of cold-formed tubular columns made of various steel grades. Once validated, this model is intended to complement experimental data through a series of numerical simulations, thereby enabling a parametric study covering a broad scope. The development of the numerical model builds upon the model proposed by Saufnay (2025) for simulating the buckling behavior of hot-formed tubular columns, while re-evaluating the assumptions made in the original model in light of the specific characteristics of cold-formed elements. The main material laws and residual stress models commonly used in the literature for cold-formed hollow sections are therefore assessed and their applicability validated against existing experimental measurements.

The second part of this work consists in conducting a parametric study involving various cross-section types, steel grades, and non-dimensional slenderness values. This study draws on experimental results from the literature as well as numerical data obtained using the developed model. The outcomes are then compared with current European design recommendations and with existing proposals for modified design rules. Based on this analysis, a revised expression for the imperfection factor α is developed, following the formulation initially proposed by Maquoi (1982).

Chapter 3

Modelling assumptions

This work follows the approach developed by Loris Saufnay in his doctoral thesis on high-strength steels (HSS), particularly the section addressing the development of a modified imperfection factor for hot-formed high-strength steel tubular columns. Accordingly, all the numerical models presented in this study were developed using the finite element software *Finelg*, jointly developed by the Bureau Greisch and the University of Liège. This software has been used and validated in numerous studies focused on modelling instability phenomena.

3.1 Numerical model description

The finite element model used to replicate the buckling behaviour of the members is discretised using a mesh of ten beam-type finite elements, all of equal length. A mesh sensitivity analysis carried out to validate the results confirmed that ten beam elements are sufficient. The simulated behaviour is restricted to a two-dimensional plane, thus excluding out-of-plane displacements.

Numerical simulations are conducted by applying a load without eccentricity at the top of the modelled column. The column is simply supported, with its base restrained both horizontally and vertically, while its top is restrained only in the horizontal direction.

Buckling resistance is evaluated using a geometrically and materially nonlinear analysis including imperfections (GMNIA). The nonlinear problem is solved using the arc-length method to accurately capture the post-peak load reduction behaviour.

3.2 Material law

The two-phase Ramberg-Osgood material model, as defined in FrpEN1993-1-14 (2025), is adopted to describe the stress-strain relationship. The description and choice of this model is discussed in further detail in Section 4.1. A uniform material law is applied across the entire cross-section. For the parametric study, the yield and ultimate strengths are taken as those prescribed by FrpEN1993-1-1 (2022) for the parent steel plate, thereby neglecting the strength enhancement resulting from strain hardening effects induced by cold-forming.

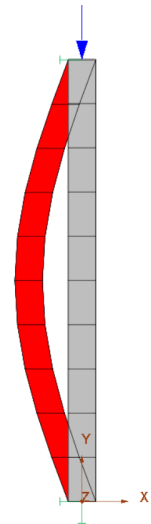


Figure 3.1:
Column model

3.3 Geometrical and material imperfections

The initial imperfection is modelled based on the first buckling mode shape (red in Figure 3.1) obtained from a linear buckling analysis (LBA) performed prior to the non-linear buckling analysis. This mode shape is introduced as a global geometric imperfection with a mid-height amplitude of $L/1000$, a value that was used in the derivation of the buckling curves and is still widely recommended in the literature. In contrast, no local imperfection is considered, as previous studies have shown that buckling resistance is relatively insensitive to the amplitude of local imperfections ω_l for non-slender cross-sections falling within classes 1 to 3 (Meng, Whitfield, et al., 2024).

Material imperfections, specifically residual stresses, are not explicitly modelled, but are implicitly accounted for through the use of the two-phase Ramberg-Osgood material law, as detailed in Section 4.3. The ultimate buckling load is therefore determined through a geometrically and materially non-linear analysis with both geometric and material imperfections (GMNIA).

3.4 Scope

The hollow sections considered are of circular and square types, due to the symmetry of these sections, only one buckling axis is thus investigated. The numerical investigations, which complement physical tests from the literature, cover a range of nine steel grades from S235 to S690, in order to encompass both standard and high-strength grades.

The reduction in effective cross-section with increasing steel grade, introduced to account for local buckling in class 4 sections, prevents the full exploitation of high-strength steels for such profiles. Therefore, the scope of the investigation is limited to class 1 to 3 sections, for which the use of a shell model is not required.

3.5 Validation process

To ensure the validity and accuracy of the developed finite element model, both the theoretical stress-strain curves and the numerical predictions were compared with experimental results reported in various published studies, covering different steel grades, sections types and column lengths. The validation of the numerical load-displacement curves presented in this work was carried out based on the experimental tests conducted by (1) Poursadrollah, D'Aniello, and Landolfo (2022), (2) Meng, Whitfield, et al. (2024), and (3) Meng and Leroy Gardner (2021). Their main characteristics are summarised in Figure 3.2.

Source	Section Type	Steel grade	f_y [MPa]	f_u [MPa]	E [MPa]	ϵ_u [%]	$\bar{\lambda}$ [–]	$N_{u,test}$ [kN]
(1)	SHS 100x8	S275	454.1	509.3	210,000*	11.8	0.21	1245.84
							0.43	1072.85
							0.51	1095.09
	SHS 200x8	S355	463.8	554.9	210,000	8.28	0.21	2692.2
(2)	SHS100x8	S355-S420	473	561.7	201000	7.2	0.26	1421.4
							0.52	1227.43
							0.79	973.94
							1.05	720.44
							1.33	507.27
(3)	CHS139.7x5	S700	729.7	843.3	212500	4.7	0.37	1524.96
							0.53	1424.59
							0.68	1288.08
							0.84	1141.53
							1.00	1015.06
							1.15	862.48

Figure 3.2: Reference cross-sections

*NB : As the value is not available in the source study, the recommendations of EC3 are applied.

Chapter 4

Validation

The development of the finite element model used to replicate the structural buckling response of compressed members required several modelling assumptions, including the choice of the theoretical material law, the implicit treatment of residual stresses, and the number of finite elements used for discretisation. The justification and validation of these assumptions are presented in this Chapter.

4.1 Material laws

Cold-formed steels, and particularly those classified as high-strength steels (HSS), are relatively recent materials in the field of structural engineering compared to conventional hot-rolled steels. In fact, structural elements made of cold-formed carbon steel were not widely used in buildings until the publication of the first design standard introduced by the American Iron and Steel Institute (AISI) (1946). Moreover, several important distinctions set them apart from conventional steels. It is therefore necessary to investigate their material properties and to question the applicability of numerical models traditionally used for hot-rolled steels when applied to cold-formed steel sections.

Numerous studies have addressed this issue by conducting coupon tests to determine yield strength, Young's modulus, and elongation at failure, as well as to assess the effects of cold-forming on the material. (W. M. Quach, 2005; Ma, 2016; Somodi and Kövesdi, 2017; Meng and Leroy Gardner, 2020; Poursadrollah, D'Aniello, and Landolfo, 2022; Meng, Whitfield, et al., 2024)

Whereas hot-finished hollow sections exhibit nearly homogeneous mechanical properties, cold-formed sections display greater variability due to welding and differing levels of strain hardening. Additionally, the stress-strain curves of standard hot-rolled steel profiles typically show a well-defined yield point followed by a plastic plateau and subsequent strain hardening. In contrast, cold-formed profiles tend to exhibit a rounded stress-strain response and relatively lower ductility, with no distinct yield plateau. Strain-hardening begins immediately after yielding, making the elastic limit harder to identify. As a result, the stress generating a residual strain of 0.2%, referred to as 0.2% proof stress, is commonly used as the yield strength for cold-formed steels. Typical stress-strain curves measured for hot-finished and cold-formed sections are shown in Figure 4.1.

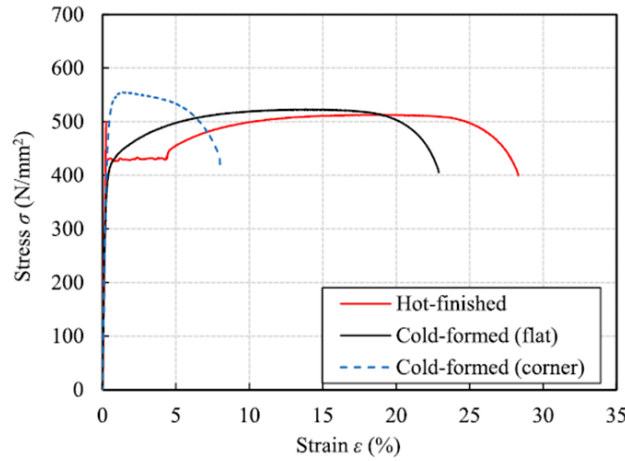


Figure 4.1: Typical stress-strain curves from hot-formed sections and cold-formed SHS steel sections (Meng, Whitfield, et al., 2024)

It is worth noting that the higher strain hardening observed in the corner regions of SHS profiles leads to a significant increase in corner strength, accompanied by a substantial reduction in ductility, as also illustrated by the blue dashed line in Figure 4.1.

In addition to the effects of cold-forming, several studies have highlighted that increasing the yield strength of steel generally results in a reduced plastic plateau and a more gradual transition around the yielding point, even for hot-rolled steels.

In light of these observations, the use of a bilinear elastic-perfectly plastic material law, commonly adopted for standard hot-rolled steels, must be reassessed. Accordingly, the development of the numerical model first required the selection of a suitable material law to represent the stress-strain behaviour of cold-formed steels.

Since cold-formed steels exhibit strain hardening from the onset of yielding, one initial alternative to the elastic-perfectly plastic law is to account for post-yield strengthening by shifting the ultimate state point from f_y to f_u . The idealised plastic plateau in the second phase of the material response is thus replaced by linear strain-hardening, allowing the section to retain some stiffness up to failure.

Moreover, unlike numerical modelling studies on hot-rolled steels, which typically employ a bilinear material law, research simulating the stress-strain behaviour of cold-formed steels most often uses the Ramberg-Osgood (Ramberg and Osgood, 1943) model, for which Hill (1944) proposed the adapted expression 4.1 based on the 0.2% proof stress. This law allows for an accurate representation of the gradual curvature observed around the yielding point in coupon tests of cold-formed steels.

$$\varepsilon = \frac{\sigma}{E} + 0.002 \left(\frac{\sigma}{\sigma_{0.2\%}} \right)^n \quad (4.1)$$

However, in its original form, the Ramberg-Osgood model does not differentiate between the pre-yield and post-yield behaviour. As a single-phase formulation, it thus fails to capture the stress state corresponding to the ultimate load-bearing capacity. Additionally, several studies have shown that this law tends to significantly overestimate stress levels beyond the yield point.

This lack of accuracy in capturing the post-yield behaviour has led to various investigations into the development of a two-phase Ramberg-Osgood model, notably by Mirambell and Real (2000) and later

Rasmussen (2003). The modified formulation 4.2 currently included in the European design recommendations FrpEN1993-1-14 (2025) was proposed and validated by L. Gardner and Nethercot (2004) and then by W. Quach and J. Huang (2011).

$$\varepsilon = \begin{cases} \frac{\sigma}{E} + 0.002 \left(\frac{\sigma}{\sigma_{0.2\%}} \right)^n & \text{pour } \sigma \leq \sigma_{0.2\%} \\ \frac{\sigma - \sigma_{0.2\%}}{E_{0.2\%}} + \left(\varepsilon_u - \varepsilon_{0.2\%} - \frac{\sigma_u - \sigma_{0.2\%}}{E_{0.2\%}} \right) \cdot \left(\frac{\sigma - \sigma_{0.2\%}}{\sigma_u - \sigma_{0.2\%}} \right)^m & \text{pour } \sigma > \sigma_{0.2\%} \end{cases} \quad (4.2)$$

This two-phase formulation builds on Hill's expression up to the 0.2% yield strain, after which the stress-strain curve is modified so that its origin shifts to the yield point. Whereas the FrpEN1993-1-14 (2025) prescribes a fixed hardening exponent for the first phase of the behavior depending on the steel grade, the exponent for the second phase is determined based on the f_y/f_u ratio in order to reach the ultimate stress state.

Accordingly, four theoretical material models are evaluated:

1. the bilinear elastic-perfectly plastic model, referred to as 'bilinear 1' (Figure 4.2),
2. the bilinear elastic-plastic model with linear strain-hardening, referred to as 'bilinear 2' (Figure 4.3),
3. the single-phase Ramberg-Osgood model, referred to as 'Ramberg-Osgood 1' (Figure 4.5),
4. the two-phase Ramberg-Osgood model, referred to as 'Ramberg-Osgood 2' (Figure 4.6).

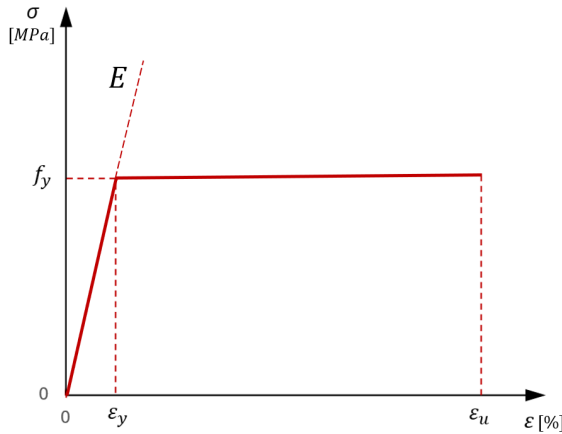


Figure 4.2: elastic-perfectly plastic

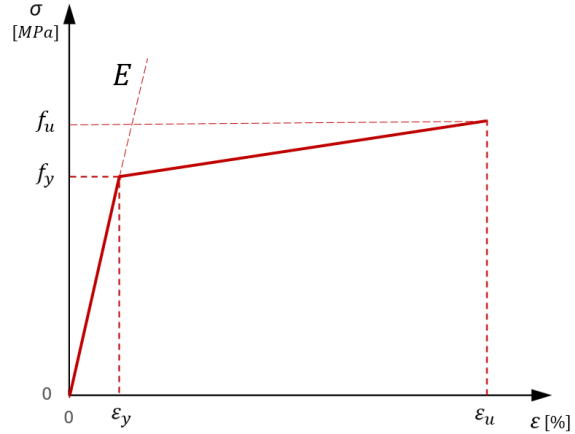


Figure 4.3: elastic-plastic with linear hardening

Figure 4.4: Bilinear behaviour laws

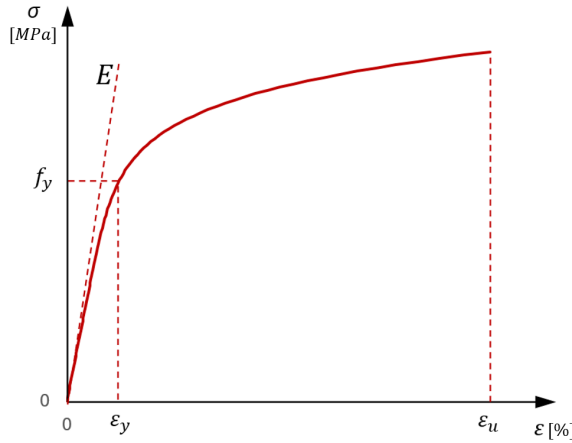


Figure 4.5: single-phase Ramberg-Osgood

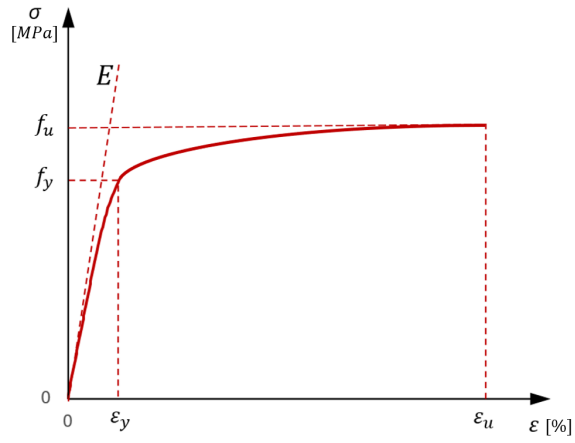


Figure 4.6: two-phase Ramberg-Osgood

Figure 4.7: Ramberg-Osgood behaviour laws

For each of these models, the values of f_y and f_u are defined based on the measurements obtained from the coupon tests under consideration. Similarly, the values of ϵ_u and E are taken directly from the coupon measurements where available. When such data is not available, these two parameters are defined in accordance with the recommendations of FrpEN1993-1-14 (2025). It is also important to note that the yield strength f_y is defined as the stress corresponding to a 0.2% plastic strain. In the case of SHS sections, the coupon curves and associated measurements correspond to the flat faces of the section. As a result, differences in mechanical properties between the flat faces and the corners, due to the higher strain hardening in the latter, are not taken into account. Moreover, in order to ensure the numerical stability of the simulations, the plastic plateau of the elastic-perfectly plastic model is assigned a small slope of $E/10000$.

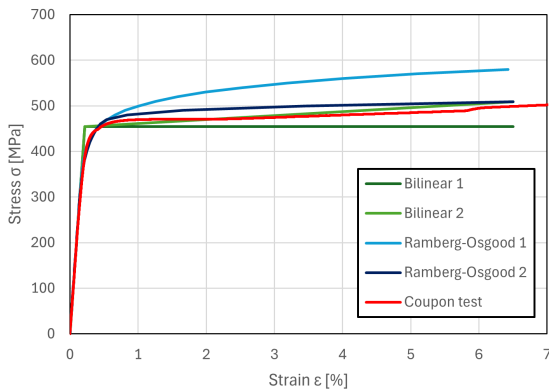


Figure 4.8: Theoretical material laws and coupon test from S275 SHS100x8 (Poursadrolah, D'Aniello, and Landolfo, 2022)

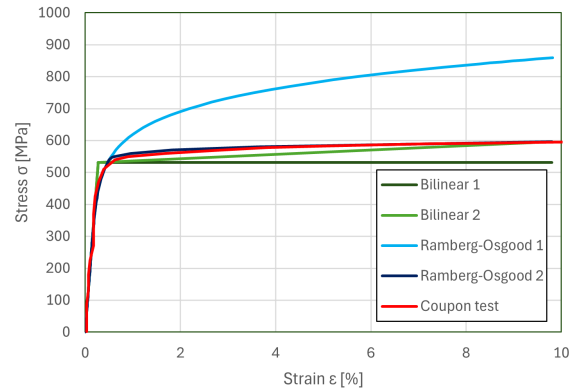


Figure 4.9: Theoretical material laws and coupon test from S355 SHS300x9 (Satou, 2015)

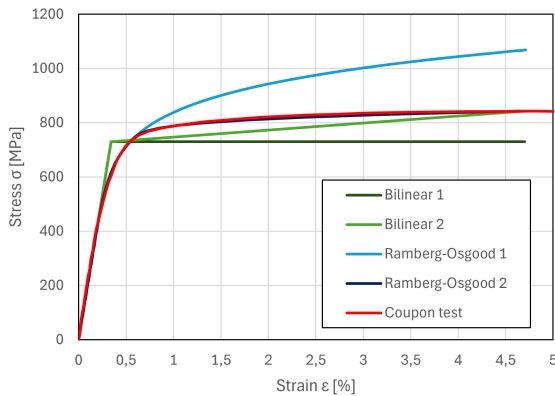


Figure 4.10: Theoretical material laws and coupon test from S700 CHS139.7x5 (Meng and Leroy Gardner, 2021)

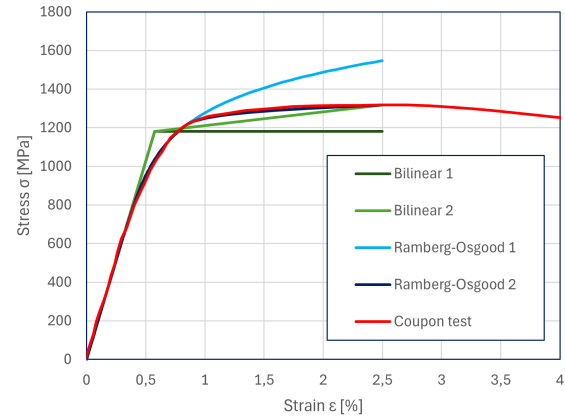


Figure 4.11: Theoretical material laws and coupon test from S1100 CHS89x4 (Ma, 2016)

Figure 4.12: Ramberg-Osgood behaviour laws

A preliminary visual comparison of these theoretical material models with the stress-strain curves available in the literature shows that the two-phase Ramberg-Osgood model best approximates the coupon test curves, as evidenced by its correlation with the S700 steel coupon curve measured by Meng and Gardner. However, in several cases, this model fails to fully replicate the shape of the experimental curve. In general, it appears to yield better results for high-strength steels than for standard grades. The latter typically exhibit a sharper transition at yielding, which the current definition of the Ramberg-Osgood model does not adequately capture. Furthermore, approximating the yield point using the 0.2% proof stress is not always representative of the actual onset of yielding in the material.

While the single-phase Ramberg-Osgood model provides a correlation as good as the two-phase model in the pre-yielding phase, it significantly overestimates the post-yield strength. Consequently, the two theoretical models that best fit the coupon curves are, first, the two-phase Ramberg-Osgood model, followed by the bilinear model with linear hardening.

However, it appears that defining the yield strength as the stress corresponding to a permanent plastic strain of 0.2% (0.2% proof stress) does not always provide an accurate estimate of the actual yield point in steels. This limitation is particularly evident in the coupon test of the S355-S420 SHS 100x8 series from the study by Meng and Gardner, where the steel strength is clearly underestimated.

It was also observed that the measured Young's modulus values for the various samples were slightly lower than the standard value of 210,000 MPa prescribed by Eurocode 3.

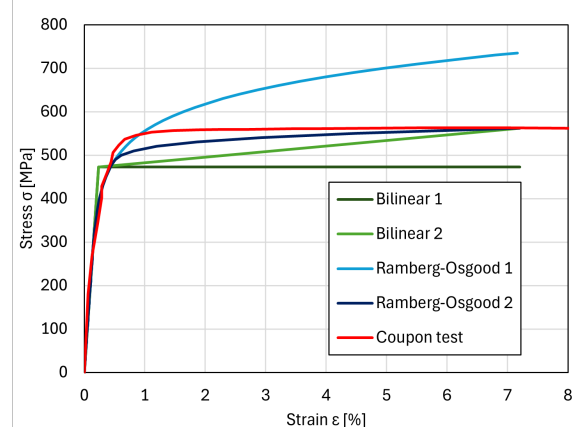


Figure 4.13: Theoretical material laws and coupon test from S355-S420 SHS100x8 (Meng, Whitfield, et al., 2024)

4.2 Numerical model meshing

Before any further discussion on the material laws, the discretisation of the columns using finite elements must be such that the mesh has no influence on the results, regardless of the stress-strain curve considered. The model used in this study is based on the one developed by Loris Saufnay in his doctoral thesis. The mesh sensitivity analysis conducted in that work to determine the optimal number of beam elements for modelling a column showed that ten finite elements were sufficient. Indeed, analysing the same column with 10 and 20 elements led to identical results within the relevant range of the simulated behaviour. Only the post-failure behaviour, which is numerically unstable, showed discrepancies. It can therefore be concluded that using 10 beam elements for the discretisation of the columns is sufficient to simulate the global buckling response of the elements studied.

4.3 Residual stresses

Residual stresses play a significant role in the buckling behaviour of columns (Li et al., 2009; M. Xiao et al., 2022). Indeed, the presence of residual stresses leads to premature yielding in parts of the material, which results in instabilities in compression members and causes a loss of strength.

These residual stresses are usually considered by applying idealised stress distributions. As such, Eurocode 3 defines the residual stresses in cold-formed hollow sections using a distribution proportional to the yield strength of the considered steel, as shown in Figure 4.14 below.

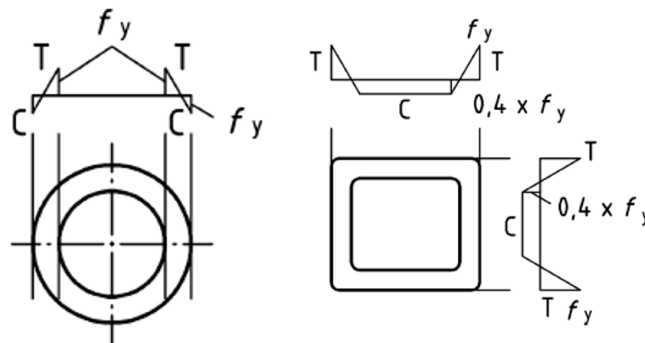


Figure 4.14: Residual stresses for CHS and RHS hot rolled-cold finished sections - (FrpEN1993-1-14, 2025)

For cold-formed sections, these models are based on limited laboratory measurements and are therefore complemented either by mechanical property specifications that distinguish between flat portions and corner regions, or by using the mechanical properties of the entire section obtained from tests on stub columns. These conventional approaches are highly empirical and do not provide an accurate description of the actual residual stresses or of the strain hardening induced by the manufacturing process.

Several studies have shown that the behaviour of HSS members, as well as that of cold-formed members, and therefore of cold-formed HSS differs, from that of conventional hot-rolled steel elements. The buckling response of compressed members is in fact influenced by the material properties as well as the ratio between the residual stress and the yield strength of the elements. These characteristics vary according to the steel grade and the forming method used (Key and Hancock, 1993; W. M. Quach, 2005; Li et al., 2009). Moreover, current models do not account for the cross-sectional geometry, even though several

previous test results have demonstrated that residual stresses are strongly dependent on the width-to-thickness ratio (b/t) of the cross section (Leroy Gardner and Yun, 2018; W. M. Quach, 2005). As a result, applying design rules developed for conventional hot-rolled steels to cold-formed HSS members can lead to inaccurate structural designs.

Indeed, the normalised strengths of cold-formed HSS columns have been shown to be higher than those of conventional hot-rolled steel columns. This has been particularly highlighted by the experimental and numerical studies conducted by Somodi and Kövesdi (2017) on the buckling behaviour of cold-formed square HSS tubular columns. This increase in normalised strength with higher steel grades can be attributed, among other factors, to the decreasing ratio of residual stress amplitude to yield strength.

In addition to their magnitude, the nature of residual stresses in cold-formed steels differs from those in hot-rolled steels. Previous studies have shown that the longitudinal residual stresses measured in cold-formed members can generally be considered as comprising two components (Key and Hancock, 1993; ECCS, 1976). The first is the membrane residual stress, which is primarily introduced during welding and is nearly uniform through the wall thickness. This component can be determined as the average of the values measured on both sides of the plate. The second is the bending residual stress, defined as the deviation between the extreme and average values. However, several measurements on thick-walled sections have shown that the residual stress distribution is not linear through the thickness (Key and Hancock, 1993). For this reason, some models introduce a third component, the through-thickness stratification stress, to account for the residual stresses in cold-formed elements. This non-linearity was more recently highlighted for cold-formed press-braked sections in the findings of W. M. Quach (2005), whose results showed a complex through-thickness variation in the corners, making the traditional assumption of linearity inappropriate.

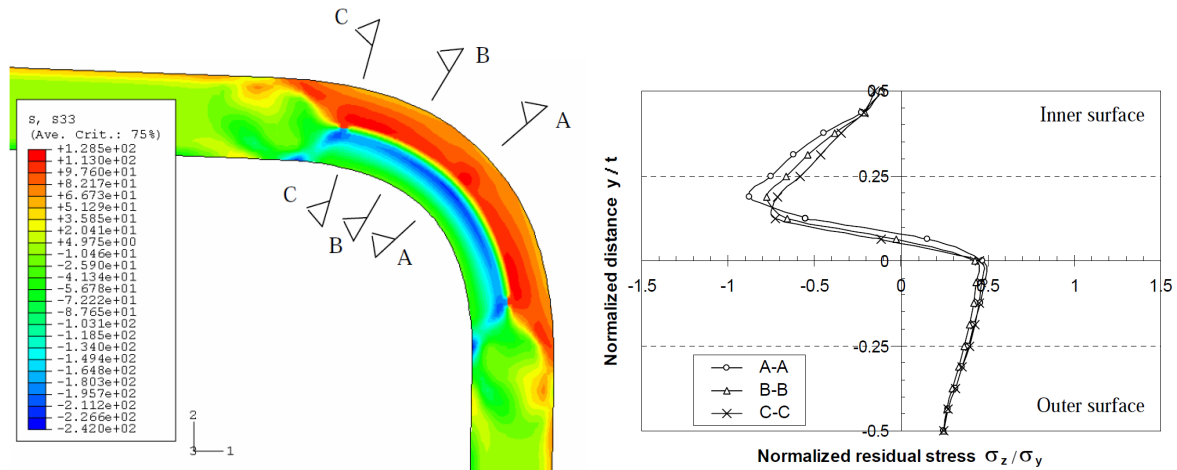


Figure 4.15: Longitudinal residual stresses in press-braked SHS sections (W. M. Quach, 2005)

Regardless of the residual stress models used, measurements of both membrane and bending residual stresses on cold-formed HSS tubular columns show that bending residual stresses are significantly larger than membrane residual stresses. This stress gradient leads to early yielding at the surface of cold-formed sections. In contrast, in hot-rolled steel members, residual stresses do not vary significantly through the thickness, and membrane residual stresses tend to dominate.

Furthermore, whereas the residual stresses in hot-rolled sections primarily result from thermal effects and uneven cooling of the cross-section, several previous studies on cold-formed sections have shown that the manufacturing process and the cold-forming history of the material have a significant influence on the distribution and magnitude of residual stresses.

As a result, theoretically predicting the distribution of residual stresses in cold-formed structures is quite difficult due to their complex manufacturing process. The residual stresses in cold-formed sections mainly stem from the coiling, uncoiling, and flattening of steel coils, as well as from the forming and welding of the section (W. M. Quach, 2005).

From the very uncoiling and flattening stage, the distribution of residual stresses is influenced by the diameter of the coil used for production. Consequently, residual stresses that should theoretically be identical for a given section type and manufacturing process can in fact differ simply because of a coil diameters variation, a parameter that is unknown to the designers using these sections. Furthermore, the amplitude and distribution of residual stresses are also affected by the various heating and cooling rates experienced by the coil, and later by the specific forming method, which further complicates the evaluation of the resulting stresses.

Following the coiling and uncoiling-flattening process ((a) and (b) on Figure 4.16) Cold-formed hollow sections may be shaped either by cold rolling or by press braking. The residual stresses generated by these two processes differ significantly in both amplitude and distribution. Moreover, the choice of manufacturing method depends on production volume, required tolerances, and cost. As a result, the same geometry can be produced using different cold-forming methods depending on the production context. Consequently, the distribution of residual stresses in a section may vary considerably between manufacturers.

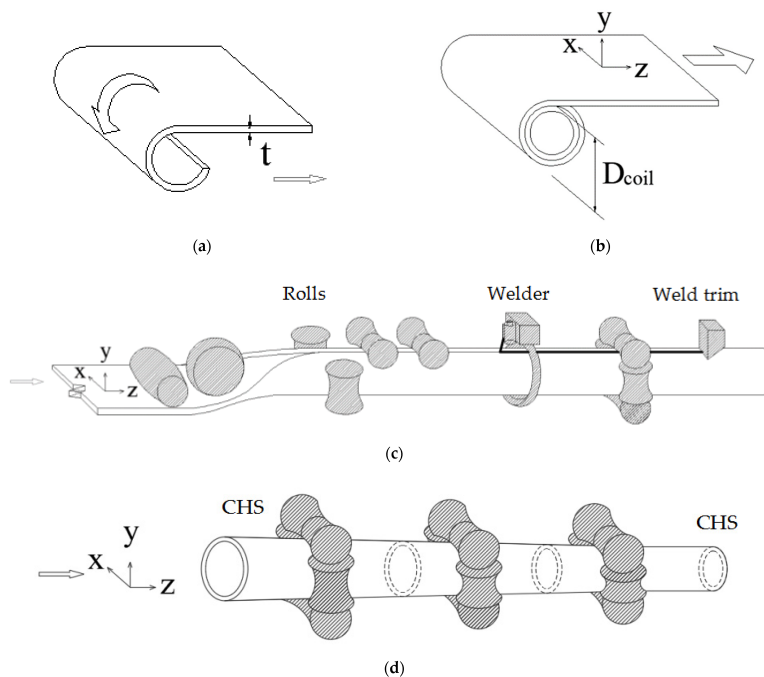


Figure 4.16: Indirect cold-rolling of CHS (W. M. Quach, 2005)

Cold-rolling is widely used when high production capacity is required. hollow sections with corners can be produced either by the direct or indirect forming method. As presented in Figure 4.16, in the case of indirect forming, the steel strip is first cold-rolled into a circular shape, which is then closed by longitudinal welding. The cross-section is then cold-rolled to obtain the desired final shape. In direct forming, the steel strip is immediately passed through a series of rollers to produce the final section geometry. After rolling, the open seam is closed by longitudinal welding.

In contrast, press-braking is commonly used for simple section shapes produced in small quantities as the process typically requires several successive press strokes to achieve the final section. Cold-formed hollow sections are manufactured by butt-welding two open sections that have been individually shaped through press-braking. Different punch and die sets may be used to form the same geometry (Figure 4.20). The selection of tooling depends on both the required tolerances and the desired geometry.

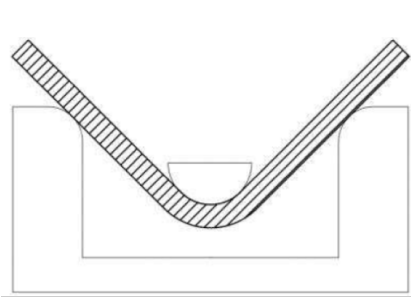


Figure 4.17: air bending

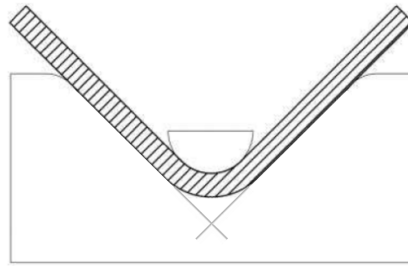


Figure 4.18: bottom bending

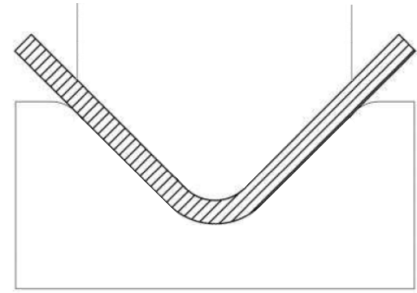


Figure 4.19: coining

Figure 4.20: Types of press and die for press-braking (Meng Xiao et al., 2022)

Accurately modelling residual stresses presents numerous challenges, including, among others, the lack of available data in the literature and the discretisation of residual stress measurements at the integration points of numerical models. As a result, residual stresses are often either neglected or their effects are approximated by modifying the material's stress-strain behaviour.

However, the coupon specimens extracted from cold-formed tubular members for material property testing exhibit an initial curvature. This curvature arises after cutting the coupons from the section and is due to the effect of bending-type residual stresses. Therefore, the initial stage of tensile coupon testing corresponds to the straightening of the specimen. This tensile testing thus exhibits progressive yielding starting from the inner side of the initial curvature, which leads to a progressive loss of stiffness. This results in the characteristic curved shape of the stress-strain curves obtained from tensile coupons of cold-formed steels. Consequently, dominant bending residual stresses are already inherently captured in the measured stress-strain relationships. This assumption has been validated in several numerical studies on tubular elements, including (Fang, T.-M. Chan, and Ben Young, 2018; Meng and Leroy Gardner, 2020; Meng and Leroy Gardner, 2021).

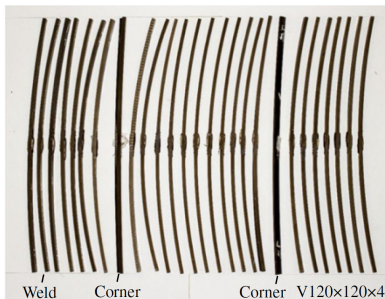


Figure 4.21: Deformed strips cut from SHS S900 (Ma, 2016)

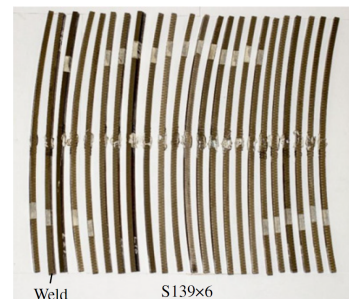


Figure 4.22: Deformed strips cut from CHS S1100 (Ma, 2016)

In contrast, membrane residual stresses, more prevalent in roll-formed elements than in press-braked ones, do not appear in the material behaviour curves obtained from coupon tests. Yet, they lead to a reduction in compressive strength. While it is common in cold-formed steel modelling to simply neglect membrane residual stresses due to their lower magnitude compared to bending residual stresses, the ECCS (1976) qualifies this assumption by noting that, although bending residual stresses are dominant in cold-formed sections, their influence on structural behaviour is proportionally less significant than that of membrane residual stresses. Thus, the lower amplitude of membrane residual stresses does not necessarily imply a negligible impact on global behaviour.

Experimental measurements, however, indicate that the most significant membrane residual stresses are primarily found in the corner regions due to more intense cold-working during forming. Offsetting this effect, the yield strength f_y , is also increased in the corner zones as a result of greater cold-work. Therefore, in cold-formed steel elements, residual stresses and the increase in yield strength resulting from the manufacturing process tend to counterbalance each other. Accordingly, applying the stress-strain relationship derived from flat zones to the corners of SHS sections, thus neglecting the increase in yield strength in those regions, provides a way to offset the omission of the membrane residual stress component. However, further studies are required to evaluate the extent to which these two effects cancel each other out.

Outside the regions with higher levels of cold work, the low amplitude of membrane residual stresses compared to that of bending residual stresses makes their effect on the strength of cold-formed columns rather limited. Moreover, membrane stresses outside the corner regions mainly result from the presence of welds. However, several studies on HSS sections have shown that the magnitude of residual stresses induced by welding is generally independent of the yield strength of the steel plates (Meng Xiao et al., 2022). Therefore, their effect becomes increasingly negligible as the yield strength increases.

The ability of finite element models, without explicit incorporation of residual stresses, to accurately reproduce the experimentally observed physical response of cold-formed tubular steel members has been confirmed by several numerical studies, such as those by Y. Huang and B. Young (2018), Toffolon and Taras (2019), and Meng and Leroy Gardner (2020).

Therefore, in the absence of a theoretical residual stress model capable of reflecting the diversity of residual stress distributions found in cold-formed sections, the validation of the numerical results presented below assumes, a priori, that the theoretical material laws approximate the coupon tests closely enough to implicitly account for the effect of bending residual stresses in the model, and that the use of a single material law across the entire section allows membrane residual stresses to be neglected. On this basis, the following simulations do not include an explicit modelling of residual stresses.

4.4 Numerical model validation

The validation of the developed finite element models is based on test results available in the literature, through load-deformation curves and buckling resistances. The buckling loads derived from the *FE* models, $N_{u,FE}$, are thus compared to the ultimate loads obtained from physical experiments, $N_{u,test}$. The stress-strain curves obtained from coupon tensile tests were used to define the material behaviour laws in the models. Given the modelling assumptions concerning residual stresses, it is essential that the material law accurately reflects the stress-strain behavior of the steel considered, in order to validate its use for modelling the global behaviour of the studied members.

Accordingly, as a reference for the numerical analysis of the buckling response of the different columns using theoretical material laws, a fifth stress-strain curve is considered through a multilinear law defined

by eight points extracted from the coupon test corresponding to the experimental buckling test in question.

Simulations are carried out using the measured section dimensions and global imperfection values from the experimental test, but without local geometric imperfections.

From the analysis of the numerical results, it generally emerges that the model is extremely sensitive to the material law. Even a very slight discrepancy between the theoretical material law and the measured stress-strain curve results in a notable difference between the real and simulated global behaviour of the column, even when using the two-phase Ramberg, Osgood law, even though it shows the best correlation with the coupon tests when compared to the other theoretical models. This sensitivity is particularly pronounced in the upper range of the investigated reduced slenderness domain (0.21; 1.33), which is strongly affected by differences in stiffness and deformation between the theoretical material law and the measured stress-strain curve.

This dependency on the accuracy of the stress-strain law becomes particularly evident when the numerical results are compared to the experimental curves of the SHS columns from the S355/S420 series in the study by Meng and Gardner. Indeed, it is for these tests that the two-phase Ramberg-Osgood model deviates the most from the measured coupon curve. Although the values of f_y , f_u , E , and ε_u used to define the theoretical material law are those measured during the experimental study, the two-phase Ramberg-Osgood model fails to accurately reproduce both the general curvature and the plastic behaviour of the coupon curve. These discrepancies stem directly from the imposed strain hardening exponent $n = 8$, as required by Eurocode 3 for cold-formed steels, and, in this case, from the inability of the 0.2% proof stress to accurately capture the true yield strength.

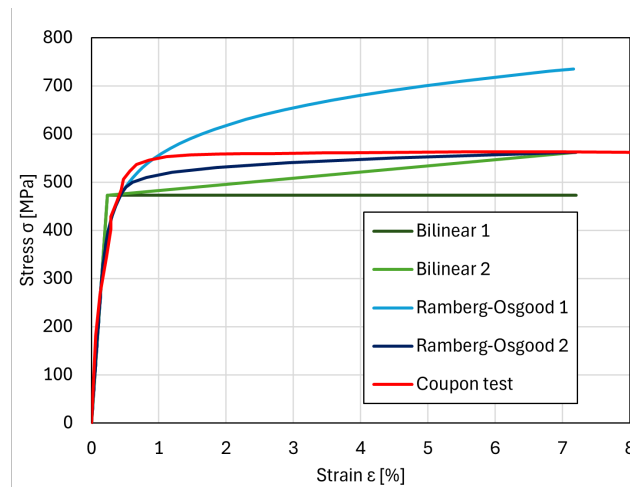


Figure 4.23: Coupon test and theoretical laws for S355/S420 serie from Meng, Whitfield, et al. (2024)

It should be noted that the steel grade used in the S355/S420 series by Meng and Gardner corresponds to a dual-certified S355/S420 steel, that is, it satisfies both the strength requirements of S420 steels and the ductility requirements of S355 steels. As such, this series uses a particular steel grade for which the standards are poorly suited. Consequently, in the first phase of the stress-strain behavior, the two-phase Ramberg-Osgood law slightly underestimates the material deformations. Conversely, around and beyond the plastic phase, it underestimates the steel strength, with local differences reaching up to 6% below the measured strength.

In terms of global behaviour, these discrepancies between the two-phase Ramberg-Osgood model and the coupon test result in both overestimations and underestimations of the column load-bearing capacity. Columns with low slenderness ratios exhibit buckling behaviour similar to stub columns, thus, their load-bearing capacity is governed by the yield strength. The underestimation of the actual yield strength by the 0.2% proof stress leads to an underestimation of the load capacity in the numerical simulations. This underestimation of load-bearing capacity reaches a maximum of 9% compared to the experimental measurements for the S420 series column with the lowest slenderness ratio, namely 0.26.

As the considered reduced slenderness increases, stiffness losses and increased deformations have a growing influence on the load-bearing capacity of the member. This effect is particularly evidenced by the decrease in the average stress at section failure. As a result, the underestimation of deformations and stiffness loss by the two-phase Ramberg-Osgood model in the pre-yield portion of the stress-strain response leads to a progressively larger overestimation of the load-bearing capacity as the reduced slenderness increases. Again, this discrepancy with the experimental load-bearing capacity reaches its maximum at the reduced slenderness where the underestimated parameter has the greatest influence. In the case of stiffness loss, this corresponds to the highest reduced slenderness considered in the S355/S420 series, namely 1.33, for which the ultimate load is overestimated by 18.5%.

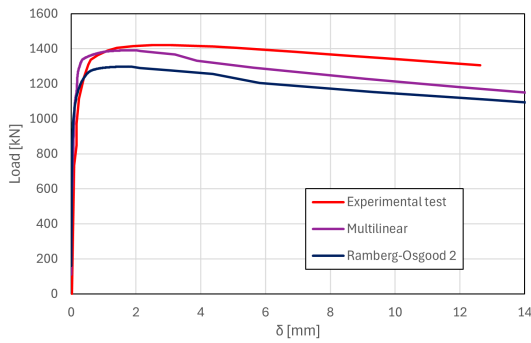


Figure 4.24: Load-deflection curves for S355-S420 SHS100x8 column with $\bar{\lambda} = 0.26$ (Meng, Whitfield, et al., 2024)

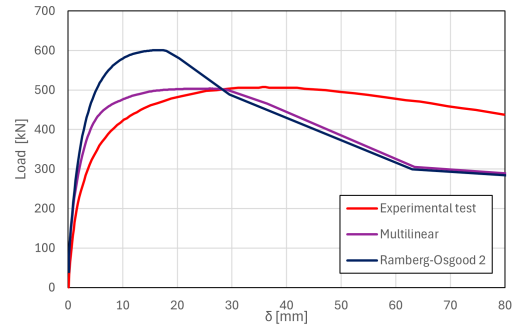


Figure 4.25: Load-deflection curves for S355-S420 SHS100x8 column with $\bar{\lambda} = 1.33$ (Meng, Whitfield, et al., 2024)

This significant overestimation stands in contrast with the relatively small underestimation of deformation by the theoretical law. Indeed, the maximum deformation discrepancy between the coupon test and the Ramberg-Osgood law in the pre-yield phase does not exceed 0.06%. This high sensitivity at higher reduced slenderness ratios underscores the importance of an accurate definition of the parameters constituting the material model.

Conversely, the use of the multilinear laws derived from the coupon tests enables a close approximation of the experimental results with relatively consistent accuracy across all elements considered. Once again, the sensitivity of the model to discrepancies between the numerical and actual material law is evident. The multilinear law consists of eight points selected from the coupon curve and connected linearly. As a result, the behaviour between these points overestimates the material deformations within each segment. Consequently, this slight overestimation of material deformation translates into a slight underestimation of the columns' load-bearing capacity. Models using the multilinear material law thus predict a load-bearing capacity equal to, on average, 96% of the ultimate load measured in laboratory tests.

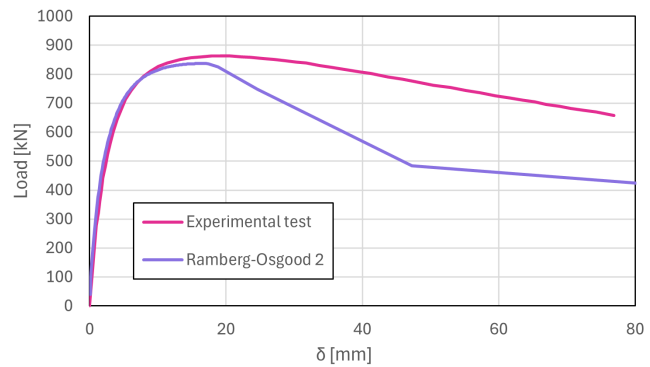
Reduced slenderness	Experimental $N_{u,Exp}$ [kN]	Ramberg-Osgood 2		Mutlilinear	
		N_u [kN]	$N_u/N_{u,Exp}$ [%]	N_u [kN]	$N_u/N_{u,Exp}$ [%]
$\bar{\lambda} = 1.33$	507.27	601.16	118.51	509.98	100.53
$\bar{\lambda} = 1.05$	720.44	779.72	108.23	678.30	94.15
$\bar{\lambda} = 0.79$	973.94	941.91	96.71	905.41	92.96
$\bar{\lambda} = 0.52$	1227.43	1121.56	91.37	1186.21	96.64
$\bar{\lambda} = 0.26$	1421.40	1297.79	91.30	1392.52	97.97

Figure 4.26: Ulitmates loads for S355-S420 SHS100x8 serie of Meng, Whitfield, et al. (2024)

These observations are confirmed across all other experimental tests evaluated, with the notable difference that the discrepancies between the experimental stress-strain curves and the Ramberg-Osgood law are much smaller, and consequently, so are the differences between the load-displacement curves. Once again, the particular nature of the dual-certified S355/S420 steel series exposes the limitations of the European recommendations concerning the 0.2% proof stress and the strain hardening exponent n . In contrast, for the other test series involving more conventional steels, the definition of the two-phase Ramberg-Osgood law provided by FrpEN1993-1-14 (2025) leads to a satisfactory approximation of the coupon curves from these tests. As mentioned in Section 4.1, the higher the steel grade considered, the more accurately the two-phase Ramberg-Osgood law fits the measured stress-strain curve. This trend arises from the more gradual yielding behaviour of higher-grade steels compared to standard grades which, although cold-formed, exhibit a sharper transition around their yield point. Lower-grade steels therefore require a strain-hardening exponent greater than 8 to better match the two-phase Ramberg-Osgood law with the experimental coupon curve.

Reduced slenderness	Experimental $N_{u,Exp}$ [kN]	Ramberg-Osgood 2	
		N_u [kN]	$N_u/N_{u,Exp}$ [%]
$\bar{\lambda} = 1.15$	862,48	837,09	97,06
$\bar{\lambda} = 1.00$	1015,06	970,81	95,64
$\bar{\lambda} = 0.84$	1141,53	1099,25	96,30
$\bar{\lambda} = 0.68$	1288,08	1232,83	95,71
$\bar{\lambda} = 0.53$	1424,59	1371,55	96,28
$\bar{\lambda} = 0.37$	1524,97	1452,64	95,26

Figure 4.27: Ultimate loads for S700 CHS139.7x5 column (Meng and Leroy Gardner, 2021)

Figure 4.28: Load-deflection curves for S700 CHS139.7x5 column with $\bar{\lambda} = 1.15$ (Meng and Leroy Gardner, 2021)

Accordingly, it is for the S700 series from the Meng and Gardner study that the numerical predictions of global buckling behaviour using the two-phase Ramberg-Osgood law most closely match the experimental results. Indeed, for this series, the two-phase Ramberg-Osgood law aligns almost perfectly with the coupon curve, although a very slight overestimation of deformations can be observed throughout. The predicted ultimate loads are therefore between 95% and 97% of the experimentally measured capacities across the six reduced slenderness values included in the series.

In light of these observations, it becomes clear that the other theoretical laws do not provide sufficiently accurate predictions of load-bearing capacity to be considered valid. In fact, visual comparisons of the bilinear theoretical curves and the single-phase Ramberg-Osgood law with the coupon curves revealed significant discrepancies.

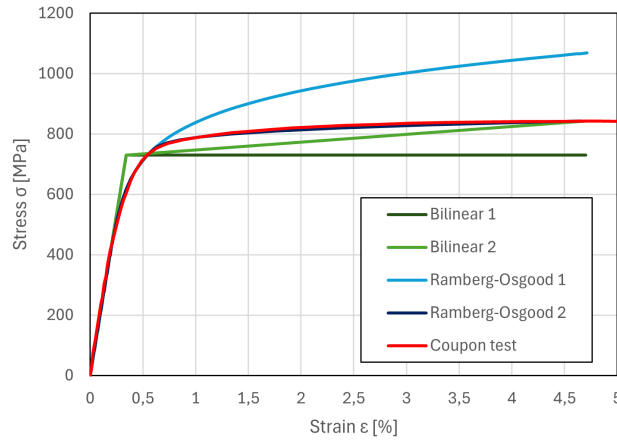


Figure 4.29: Theoretical material laws and coupon test from S700 CHS139.7x5 (Meng and Leroy Gardner, 2021)

Although the Ramberg-Osgood law shows very good agreement with coupon tests up to the onset of plasticity, the discrepancy it exhibits in the post-yield phase of the stress-strain response calls into question its ability to inherently account for flexural residual stresses in numerical models. However, several previous studies have shown that the global buckling behaviour of simply supported columns is primarily, if not exclusively, governed by the elastic phase of the steel's stress-strain behaviour. It is also worth noting that the single-phase Ramberg-Osgood law differs from the two-phase version only in its post-yield stress-strain behaviour. Numerical simulation results show that the single-phase Ramberg-Osgood law can predict the buckling resistance of slender columns with a similar level of accuracy as the two-phase law, but it systematically overestimates the resistance of stockier columns. Indeed, the single-phase Ramberg-Osgood law is identical to the two-phase version up to the yield point. Yet, it is precisely the accuracy of the theoretical model in capturing the deformation and stiffness loss of the material in this first phase that governs the quality of numerical predictions for slender column resistance. Conversely, the single-phase Ramberg-Osgood law significantly overestimates the material strength in the post-yield region of the stress-strain response. Since the behaviour of columns with low slenderness approaches that of stub columns, this overestimation of post-yield strength and ultimate stress leads to an overestimation of the column's buckling capacity. This overestimation, however, occurs within a relatively narrow slenderness range (from 0.2 to 0.6) and decreases rapidly as the reduced slenderness increases.

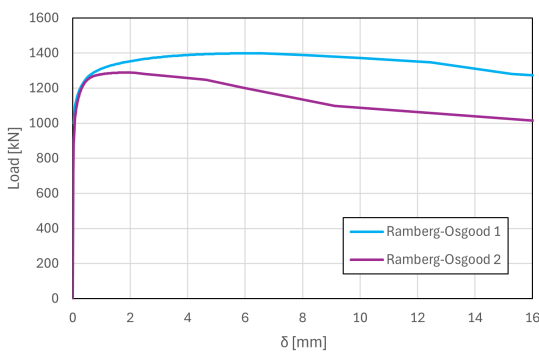


Figure 4.30: Load-deflection curves for S355-S420 SHS100x8 column with $\bar{\lambda} = 0.26$ (Meng, Whitfield, et al., 2024)

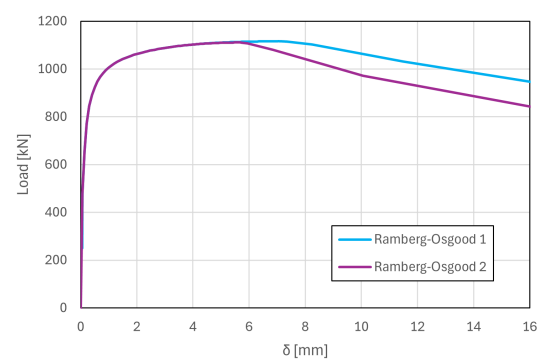


Figure 4.31: Load-deflection curves for S355-S420 SHS100x8 column with $\bar{\lambda} = 0.53$ (Meng, Whitfield, et al., 2024)

Concerning the two bilinear laws, elastic-perfectly plastic and elastic-plastic with linear hardening, nothing in their general shape justifies that they can implicitly account for the flexural residual stresses of the material. Indeed, both exhibit a sharply angular transition at yield, lacking the characteristic curvature seen in cold-formed steels. This invalidity of the residual stress assumption is clearly reflected in the results of numerical simulations that use these material models without explicitly modelling residual stresses. First, it should be noted that both bilinear models give the same results, whether or not linear hardening is included. In both cases, a sudden loss of stiffness occurs at yield, the Young's modulus drops from its initial elastic value to a negligible post-yield value. In the elastic-perfectly plastic law, the post-yield stiffness is $E/10000$. While the elastic-plastic law with linear hardening allows the material to retain some residual stiffness, this is limited to approximately 1% of the stiffness in the elastic range. This remaining stiffness is lower for standard steel grades than for higher grades, where strain-hardening is more pronounced. In both cases, the post-yield stiffness loss is too severe for the column to maintain its load-bearing capacity, and local section yielding leads to global failure of the simply supported column.

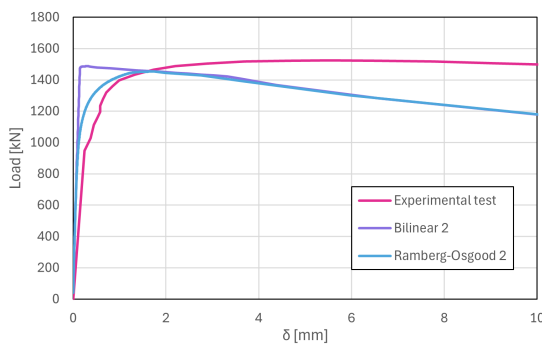


Figure 4.32: Load-deflection curves for S700 CHS139.7x5 column with $\bar{\lambda} = 0.37$ (Meng and Leroy Gardner, 2020)

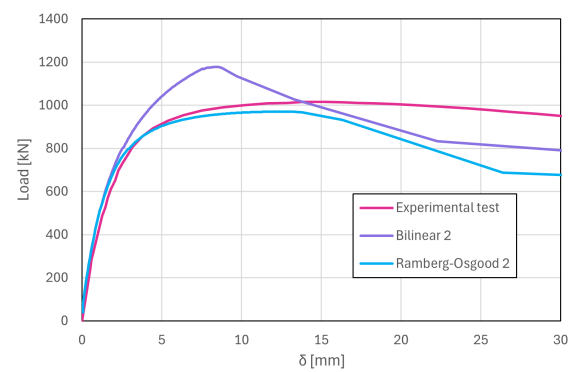


Figure 4.33: Load-deflection curves for S700 CHS139.7x5 column with $\bar{\lambda} = 1.00$ (Meng and Leroy Gardner, 2020)

As a result, for low slenderness ratios, the load-displacement curve exhibits a sharp peak at which the ultimate load is reached almost instantaneously before rapidly dropping due to failure of the member. Failure indeed occurs through the almost simultaneous yielding of the entire cross-section due to the absence of residual stresses that would otherwise lead to a more gradual yielding process. For higher slenderness ratios, buckling induces greater bending in the section, which then yields more progressively from the outer fibers toward the axis. However, the load-displacement curve associated with bilinear material laws still exhibits a more pronounced peak than those of other material models, again due to the absence of residual stresses that would allow for a more gradual yielding of the sections. Moreover, this peak leads to an overestimation of the load-bearing capacity, which becomes more significant as the considered column becomes more slender. Indeed, higher slenderness increases sensitivity to discrepancies in stiffness between the theoretical and actual material behaviour. This overestimation stems directly from the underestimation of strains at the yield point caused by the angular shape of these bilinear theoretical laws. For the column with a reduced slenderness of 1.00 in the S700 series of Meng and Gardner, the overestimation reaches 16

For comparison, a series of simulations is carried out for the S700 series from Meng and Gardner, considering the elastic-plastic law with linear strain hardening combined with the residual stress distributions defined by Eurocode 3. In this case, the shape of the load-displacement curve indeed reflects a progressive yielding of the section and the accompanying gradual loss of stiffness. However, the Eurocode's resid-

ual stress distribution is defined proportionally to the yield strength, which in this case is 729.7 MPa. This overestimation of the residual stresses leads to a significant underestimation of the load-bearing capacity for columns with higher slenderness. Since such columns are sensitive to stiffness losses, the overestimated residual stresses result in an early loss of stiffness and, consequently, premature failure of the column. For the column with a reduced slenderness of 1.15, where the influence of stiffness degradation is most pronounced, the underestimation of load-bearing capacity reaches 14%. Conversely, for very low slenderness ratios, where the Ramberg-Osgood models highlight post-yield behaviour, the inability of the linear model to reach stress levels beyond f_y leads to an underestimation of the load-bearing capacity.

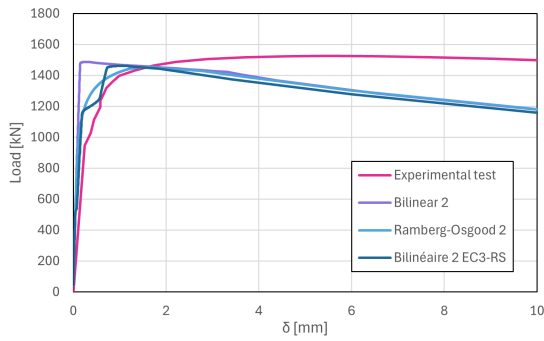


Figure 4.34: Load-deflection curves for S700 CHS139.7x5 column with $\bar{\lambda} = 0.37$ (Meng and Leroy Gardner, 2020)

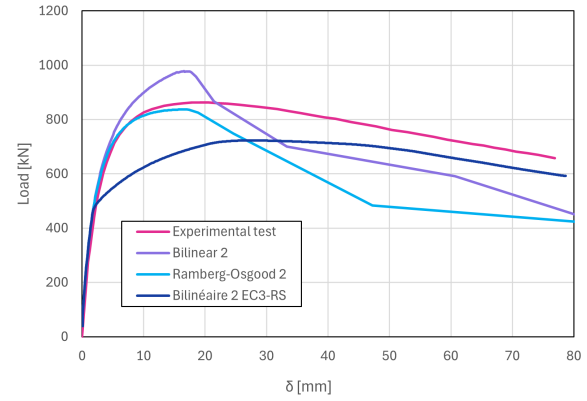


Figure 4.35: Load-deflection curves for S700 CHS139.7x5 column with $\bar{\lambda} = 1.15$ (Meng and Leroy Gardner, 2020)

It thus appears that the numerical model defined without explicit residual stresses and using the two-phase Ramberg-Osgood curve as the stress-strain law is capable of realistically simulating the buckling response of cold-formed tubular columns for various steel grades. However, the accuracy of the results produced by this model depends on an adequate and precise definition of the material's constitutive law. Indeed, current European standards that define the Ramberg-Osgood law do not offer it sufficient flexibility to adapt to the range of steel grades available in cold-formed sections. Several previous studies have already proposed and validated relationships that allow the Ramberg-Osgood law to be adapted to the specific steel grade under consideration. This topic is discussed in the following section

4.5 Discussion on Ramberg-Osgood law parameters

As described in the section 4.1, cold-formed steels are generally characterised by a rounded stress-strain response without a clearly defined yield point. Numerous publications have shown that the behavior of this material can be accurately described using a two-phase Ramberg-Osgood model, provided that the key input parameters can be precisely determined. The two-phase Ramberg-Osgood model is defined by four basic parameters: the Young's modulus E , the yield strength f_y (taken as the 0.2% proof stress), the ultimate strain ε_u , and the strain hardening exponent n .

Given the model's sensitivity to the constitutive law used, the definition of these parameters plays a crucial role in the model's ability to adequately simulate the buckling behaviour of cold-formed steel columns.

The predictive equation for the ultimate strain prescribed by standard FrpEN1993-1-14 (2025) originates from the expression proposed by Bock et al for ferritic stainless steel. The accuracy of this expression was evaluated and validated by Leroy Gardner and Yun (2018) for both hot-rolled and cold-formed steels, who subsequently applied a 0.6 reduction factor to Bock's expression.

$$\varepsilon_u = 0.6 \cdot \left(1 - \frac{f_y}{f_u}\right) \quad (4.3)$$

As shown in Figure 4.36, the experimental ultimate strains ε_u of cold-formed steels show good agreement with the predictions of Equation 4.3.

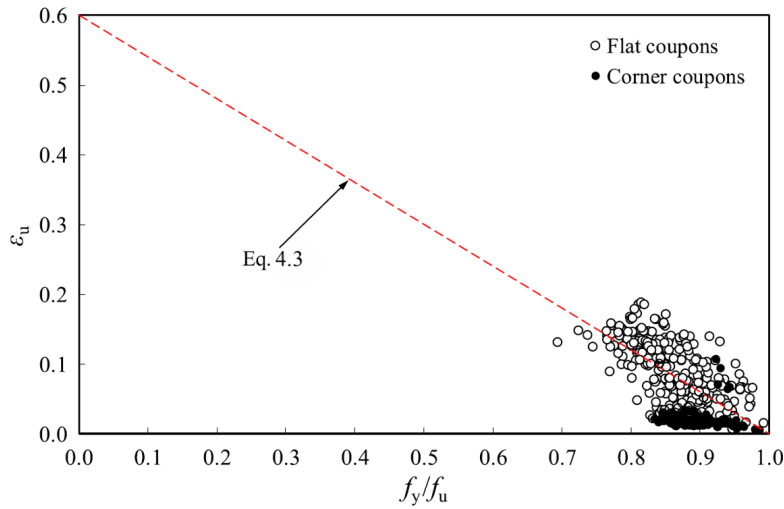


Figure 4.36: Assessment of ultimate strain ε_u for cold-formed steels (Leroy Gardner and Yun, 2018)

Similarly, for the parameter m , EC3 adopts the expression 4.4 introduced by Yun and Gardner, who adapted Rasmussen's linear predictive expression, originally developed for stainless steels and included in Annex C of EN1993-1-4:2007, to carbon steels. Observing a similar linear trend to that of stainless-steel in the data for cold-formed steel, Yun and Gardner established a linear relationship between m and the f_y/f_u ratio through linear regression.

$$m = 1 + 3.3 \frac{f_y}{f_u} \quad (4.4)$$

By plotting the test data m_{test} against the corresponding f_y/f_u ratios for flat coupons and corner coupons, it was observed that both sets of data follow a similar trend, as shown in Figure 4.38, although the corner coupons generally exhibit higher f_y/f_u ratios due to the greater degree of strain hardening they undergo.

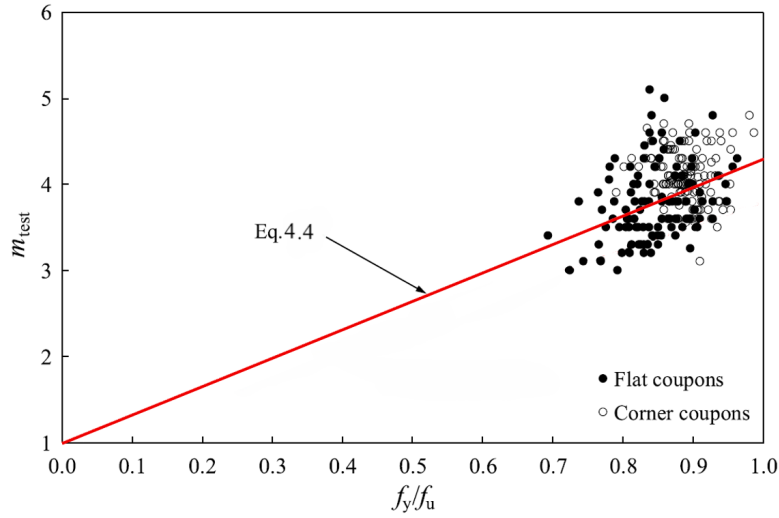


Figure 4.37: Evaluation of predictive expression for strain-hardening exponent m for cold-formed steels with measured f_y/f_u ratios (Leroy Gardner and Yun, 2018)

However, as discussed in the validation chapter, the current definition of the initial strain hardening exponent n in the two-phase Ramberg-Osgood model given in the FrpEN1993-1-14 (2025) standard leaves room for improvement. The fixed value of the strain hardening exponent n proposed by Eurocode 3 does not allow for a consistent level of accuracy in representing the stress-strain behaviour of different steel grades. Indeed, the curvature observed in coupon tests varies depending on the grade considered, it tends to be tighter for steels with lower yield strengths and becomes more gradual as the steel grade increases. Accordingly, a higher value of n would be more suitable for standard strength grades.

As with the parameters m and ϵ_u , the initial strain hardening exponent n can be calculated using the expression adopted in EN1993-1-4:2007 for modelling the stress-strain behaviour of stainless steels. This formulation, provided in Equation 4.5, was originally proposed by Ramberg and Osgood (1943). It defines n such that the analytical curve passes through the 0.01% and 0.2% proof stresses.

$$n = \frac{\ln(20)}{\ln(f_y/\sigma_{0.01\%})} \quad (4.5)$$

More recently, Rasmussen and Hancock (1993), Mirambell and Real (2000), Real et al (2014), and Arrayago and al (2015) have shown that using the 0.05% proof stress-given in Equation 4.5, instead of the 0.01% value results in more accurate predictions of n for stainless steels.

$$n = \frac{\ln(4)}{\ln(f_y/\sigma_{0.05\%})} \quad (4.6)$$

The evaluation of both expressions by Yun and Gardner (2018) for cold-formed carbon steels demonstrated that Equation 4.6 gives more accurate and consistent predictions of the test-based exponent n_{test} than Equation 4.5. They therefore recommend that the calculation of n for cold-formed steels be based on the 0.05% proof stress, and that this value be systematically measured and reported by researchers in future experimental programs.

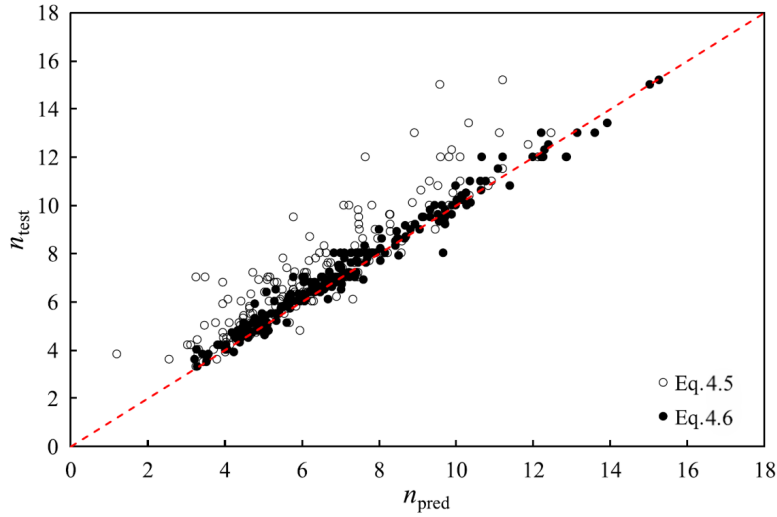


Figure 4.38: Evaluation for predictive expressions for strain hardening exponent n for cold-formed steels with measured $\sigma_{0.01\%}$ and $\sigma_{0.05\%}$ (Leroy Gardner and Yun, 2018)

However, this formulation of the parameter n was not adopted by the FrpEN1993-1-14 (2025) standard. Yet, the analysis of the numerical results in this study clearly highlights the relevance of such a formulation, which, if validated, would allow for a more accurate representation of the curvature observed in coupon tests and, consequently, the implicit consideration of residual bending stresses.

In parallel, the average Young's modulus calculated from the dataset of 700 stress-strain curves experimentally obtained and compiled by Yun and Gardner in their study on cold-formed steels was $203,000 \text{ [N/mm}^2\text{]}$. This value is slightly lower than the value of $210,000 \text{ [N/mm}^2\text{]}$ prescribed in FrpEN1993-1-1 (2022). Given the apparent sensitivity of slender columns to the stiffness of the material model, a revision of this value could be considered if this trend is confirmed through further studies.

Chapter 5

Parametric study and developments

In current European design recommendations, the beneficial effects of increasing the steel grade on the buckling behaviour of columns are neglected for cold-formed hollow sections. Therefore, the development of a modified imperfection factor, α^* , incorporating ε , would allow the influence of the yield strength on the buckling behaviour of columns to be accounted for in a consistent and continuous manner.

However, developing a modified formulation of the Eurocode 3 buckling curves first requires an assessment of the influence of steel grade on the buckling behaviour of columns. To this end, a parametric study is conducted based on experimental data from the literature and numerical results generated by the previously validated model.

5.1 Numerical parametric study

To supplement the experimental data available in the literature, a numerical study is conducted over a wide range of steel grades and slenderness ratios. This numerical simulation campaign is carried out for four distinct sections, namely the circular hollow sections (CHS) 177.8x10 and CHS 813x30, and the square hollow sections (SHS) 180x180x10 and SHS 350x350x16. The dimensions and cross-section classes of the different studied sections are presented in Figure ??.

In order to simulate a buckling curve for a given steel grade and cross-section, 13 simply supported columns of varying lengths, corresponding to 13 distinct non-dimensional slenderness values ranging from 0.2 to 2.6, are modeled. A total of 9 steel grades and 4 different cross-sections are considered, bringing the total number of simulations to 468. The length of the sample in each numerical simulation is defined according to the expression for the relative slenderness in the Eurocode, following the formulation 5.1 presented below.

$$L = L_{cr} = \frac{i \cdot \pi \cdot \bar{\lambda}}{\sqrt{\frac{f_y}{E}}} \quad (5.1)$$

The yield and ultimate strengths considered in the numerical study are those prescribed by the standard FrpEN1993-1-1 (2022) for the base material, thus neglecting the strengthening effect due to cold-forming. The initial global out-of-straightness is defined according to the first buckling mode, with an amplitude of $L/1000$ at mid-height.

The reduction factors for each column are obtained by evaluating the ratio between the ultimate load predicted by the numerical simulations and the plastic resistance of the corresponding section.

$$\chi_{FEM} = \frac{N_{u,FEM}}{A_{FEM} \cdot f_y} \quad (5.2)$$

5.2 Assessment of EC3 design rules

In a first step, the accuracy and safety level provided by the existing EC3 design rules for cold-formed columns are assessed using the results from the numerical study.

When comparing the EC3 design curve c to the numerical buckling curves obtained for steel grades S235, S460, and S690, it is clearly observed that, for the two higher-strength steels, the results follow a higher curves than that prescribed by the standards. This confirms the beneficial effect of the lower residual stress levels relative to the yield strength, as well as the reduced sensitivity to global geometric imperfections for a given relative slenderness λ , as previously reported in the literature. In addition, although the reduction factor χ shows a strong dependence on the yield strength, no significant influence of the section shape is observed.

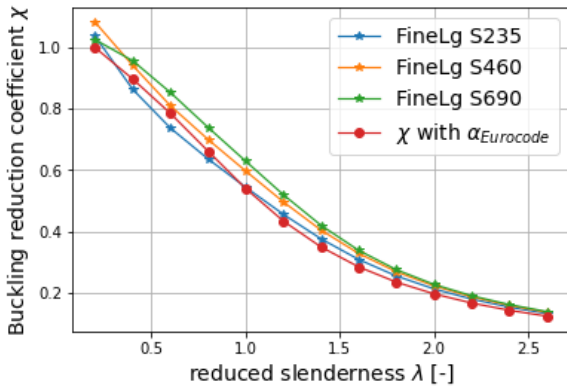


Figure 5.1: CHS 178x10 - Buckling curves for S235, S460 and S690

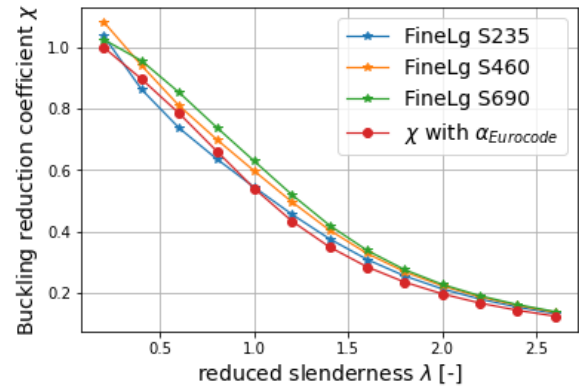


Figure 5.2: CHS 813x30 - Buckling curves for S235, S460 and S690

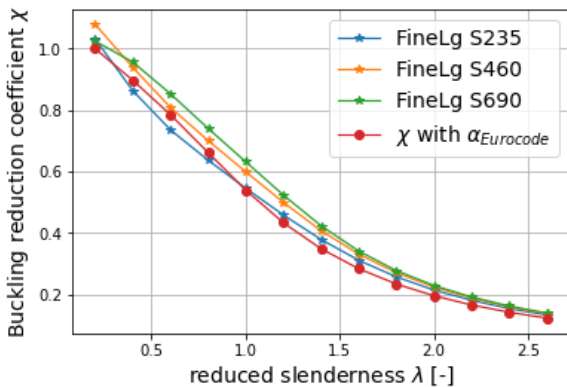


Figure 5.3: SHS 180x10 - Buckling curves for S235, S460 and S690

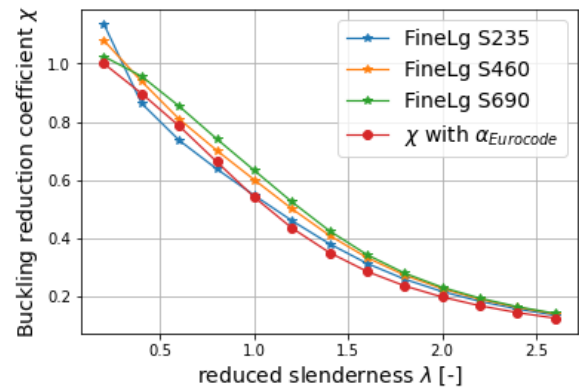


Figure 5.4: SHS 350x16 - Buckling curves for S235, S460 and S690

Moreover, regardless of the steel grade considered, the numerical model predicts a higher load-bearing capacity than that given by the EC3 analytical expression at a reduced slenderness of $\bar{\lambda} = 0.2$. This results from the fact that the maximum load-bearing capacity defined in the Eurocode is based on the

plastic resistance of the cross-section. However, the Ramberg-Osgood model allows the material to go beyond this plastic state while still retaining significant stiffness at early post-yield stages. This allows low-slenderness columns to support loads higher than their yielding resistance as highlighted in Section 4.4 through the comparison of single-phase and two-phase Ramberg-Osgood models.

Conversely, although EC3 predictions are generally on the conservative side, with an increasing margin of safety as the yield strength increases, a number of points along the analytical buckling curve are found to be non-conservative around $\bar{\lambda} = 0.7$. Indeed, As shown in Figure 5.2 for grades S235, S275, and S355, some values on the recommended curve c for cold-formed sections lie above the corresponding numerical predictions. In the case of S235, the use of $\alpha = 0.49$ leads to a maximum overestimation of the load-bearing capacity by 6% at $\lambda = 0.6$. More generally, the EC3 buckling curve c exhibits a local non-conservative region around $\lambda = 0.7$ compared to the numerical curve for the corresponding steel grade. This unsafe zone, however, diminishes with increasing steel strength and disappears entirely for grade S550. This phenomenon was already observed in the work of Somodi and Kövesdi (2017), as well as Meng and Leroy Gardner (2020), where a two-phase Ramberg-Osgood material model was used to derive modified European buckling curves for cold-formed tubular sections, accounting for the influence of the steel grade.

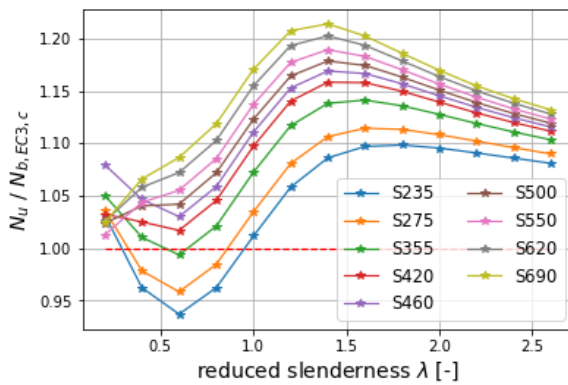


Figure 5.5: Comparisons of numerical data with unfactored EC3 resistance predictions for cold-formed tubular columns

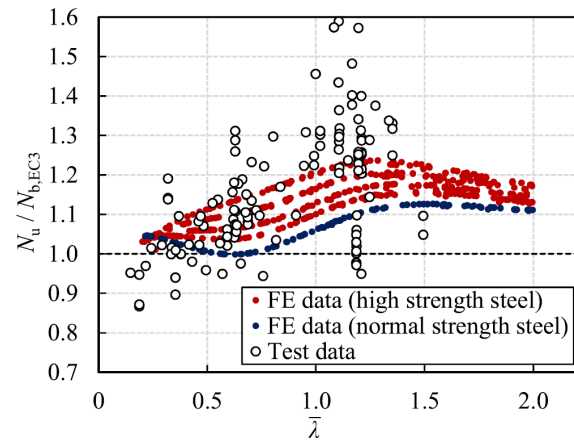


Figure 5.6: Comparisons of test and numerical data with unfactored EC3 resistance predictions for cold-formed CHS columns (Meng and Leroy Gardner, 2021)

Meng and Leroy Gardner (2020) highlight several experimental tests for which the EC3 standards are found to be unsafe. Their numerical study on steel grades ranging from S355 to S900 also shows a significantly reduced safety level for certain points of the S355 grade around a reduced slenderness of $\bar{\lambda} = 0.7$ (blue in Figure 5.6). They specify that this overestimation by EC3 mainly stems from the plateau imposed below the reduced slenderness of 0.2 in the expression of the generalised imperfection factor η . To address this issue, Xing Meng and Leroy Gardner propose shortening this plateau from 0.2 to 0.1 in their modified expression of the buckling curves for cold-formed SHS and RHS columns.

The parametric study by Somodi and Kövesdi (2017) on cold-formed tubular sections also highlights a smaller safety margin in the EC3 analytical buckling load prediction around $\bar{\lambda} = 0.7$. However, their numerical results for grade S235 showed a maximum overestimation of the bearing capacity by EC3 of about 2%. As a result, the modified expression of the imperfection factor they propose retains classical buckling curve c for S235 steel. It should be noted, however, that the Ramberg-Osgood law they use assumes a hardening exponent of $n = 14$, rather than $n = 8$, which significantly reduces the rounded shape of the

stress-strain curve near yielding and brings it closer to a bilinear material law. In fact, this value of $n = 14$ is the one defined for hot-formed steels with a more pronounced rounding in the FrpEN1993-1-14 (2025) standard, as compared to standard steels.

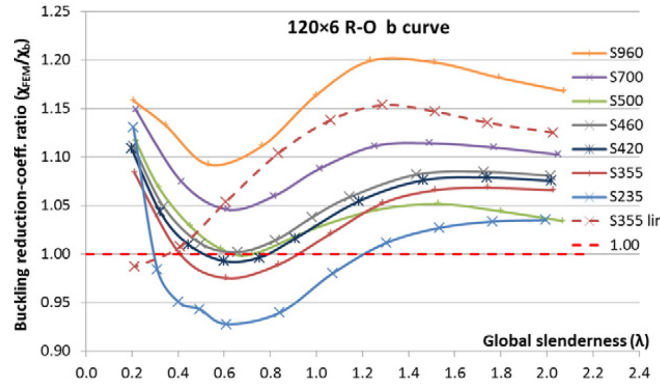


Figure 5.7: Comparison of simulation results to European buckling curve b for cold-formed SHS 120x120x6 (Somodi and Kövesdi, 2017)

The emergence of this less safe zone is linked to the difference in concavity between the buckling curve generated by the numerical model and the European buckling curve. Indeed, for lower-strength grades, the numerical curve is convex over the entire slenderness range, whereas EC3 curve c is slightly concave for reduced slenderness values below 1 and convex for higher values. This difference in concavity with curve c is not observed for hot-formed members, for which EC3 prescribes the use of this curve. It thus appears that the shape of the European curves is better suited to steels whose stress-strain behaviour approximates a bilinear material law. By comparing different material models, Somodi and Kövesdi (2017) demonstrated that this change in concavity is a consequence of the pronounced rounding in the stress-strain behaviour of cold-formed steels.

The numerical results from Somodi and Kosedí indeed showed that:

- The double-phase Ramberg-Osgood model results in higher strength at a reduced slenderness of 0.2 due to its post-yield behavior,
- However, as the slenderness increases, the two-phase Ramberg-Osgood model begins to predict lower strength than a linear hardening elastic-plastic law.

These are highlighted by comparing the numerical curves obtained using the bilinear elastic-plastic law with linear hardening and those obtained using the two-phase Ramberg-Osgood law in Figure 5.7.

This reduction in buckling resistance is due to the penalising effect of the larger deformation levels exhibited by the double Ramberg-Osgood law in the elastic range, which leads to greater global deformation of the column, thus increasing load eccentricity and bending moments within the member. However, as the slenderness exceeds $\lambda = 1.2$, buckling occurs increasingly early within the elastic range of the material behaviour, where the difference in deformation between the bilinear and Ramberg-Osgood laws becomes less significant. Consequently, the discrepancy in the predicted buckling capacities between the two models diminishes.

Therefore, the European buckling curves need to be re-evaluated to ensure safe design with cold-formed sections for low-strength grades across the entire range of reduced slenderness, while also optimising the design of high-strength steel grades. In this light, it is necessary to evaluate the value of α that should be considered for each steel grade so that the analytical load-bearing capacity obtained from the

European buckling curves ensures a sufficient safety level. To this end, various analytical buckling curves are generated by varying the imperfection factor from $\alpha_d = 0.76$ to $\alpha_a = 0.13$ with an increment of 0.001 for each steel grades. The resulting buckling curves are then compared to the numerical results. A buckling curve is considered adequate when it minimises the mean error over the entire slenderness range while limiting the maximum overestimation of the load-bearing capacity to 2%. The error for each slenderness value is calculated using the expression 5.3 where $N_{u,FEM}$ is numerical ultimate load of the column and $N_{u,EC3mod}$ is the load-bearing capacity predicted by the considered proposal of modified European standard.

$$\delta = \frac{N_{u,FEM} - N_{u,EC3mod}}{N_{u,FEM}} \cdot 100 [\%] \quad (5.3)$$

The condition on the maximum overestimation serves to limit the lack of safety observed in the reduced slenderness region around $\bar{\lambda} = 0.7$. Indeed, for all the numerically generated buckling curves, the progressive reduction of the imperfection factor from α_d consistently leads to the first instances of overestimation appearing in the critical zone around a reduced slenderness of 0.7. By further decreasing the value of α , the overestimation of the load-bearing capacity in this region reaches the upper limit of 2%, while the analytical buckling curve still underestimates the capacity over most of the reduced slenderness range. As a result, the optimised α values obtained for all steel grades lead to a positive mean error between 3% and 10%. Since lower-strength steels exhibit a much more pronounced unsafe zone than higher-strength steels, this mean error decreases as the yield strength of the steel increases. The choice of optimised α_{opt} values for a steel grade is therefore primarily driven by the critical zone around the reduced slenderness of 0.7.

The results of this optimisation of the imperfection factor according to the steel grade are presented in Figure 5.8 for the four sections of the parametric study.

Section type		Steel grade								
		S235	S275	S355	S420	S460	S500	S550	S620	S690
SHS 180x10	α_{opt}	0.606	0.548	0.458	0.402	0.373	0.347	0.323	0.299	0.279
	δ_{mean}	8.92 %	8.19%	6.93%	5.98%	5.97%	5.05%	4.59%	4.41%	4.14%
SHS 350x16	α_{opt}	0.606	0.547	0.457	0.402	0.373	0.346	0.323	0.299	0.279
	δ_{mean}	9.62 %	8.17%	6.92%	6.00%	5.98%	5.08%	4.61%	4.43%	4.16%
CHS 178x10	α_{opt}	0.601	0.543	0.454	0.398	0.368	0.345	0.325	0.302	0.281
	δ_{mean}	7.64 %	7.00%	5.90%	4.85%	4.72%	3.82%	4.48%	3.43%	3.17%
CHS 813x30	α_{opt}	0.601	0.543	0.454	0.399	0.369	0.345	0.325	0.302	0.281
	δ_{mean}	8.19 %	7.42%	6.21%	5.31%	5.30%	4.43%	4.05%	3.09%	3.06%

Figure 5.8: Optimised values of the imperfection factor α

The analysis of the buckling curves based on the numerical results did not reveal any significant influence of the cross-section type. This observation is confirmed here by the optimised values of the imperfection factor, which are all approximately identical across the different sections.

5.3 Assessment of modified EC3 design rules

As described in the Section 2.2, three general approaches exist for developing a modified expression of the imperfection factor in the European buckling curves, and each of them has been the subject of a proposal for cold-formed tubular columns.

Following the formulation initially introduced by Maquoi, Somodi and Kövesdi (2017) proposed to modify the imperfection factor according to expression 5.4.

$$\alpha^* = 0.49 \cdot \sqrt{\frac{235}{f_y}} \quad (5.4)$$

This proposal retains the classical buckling curve c for grade S235, as prescribed by the FrpEN1993-1-1 (2022), and is therefore unsafe due to the critical zone around the $\bar{\lambda} = 0.7$. However, as shown in Figure 5.11, the difference between the optimised imperfection factor and that proposed by Somodi and Kovesdi decreases as the steel strength increases, eventually disappearing beyond grade S550. This is explained by the progressive attenuation of the critical slenderness zone as the steel strength increases, until it vanishes entirely for grade S550, as mentioned in the previous section.

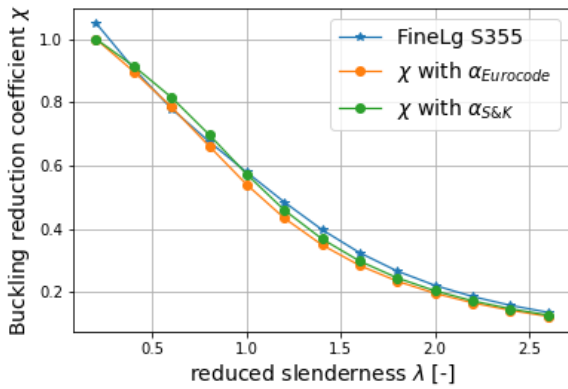


Figure 5.9: S355 numerical data with EC3 buckling curve c and Somodi and Kövesdi (2017) modified buckling curve

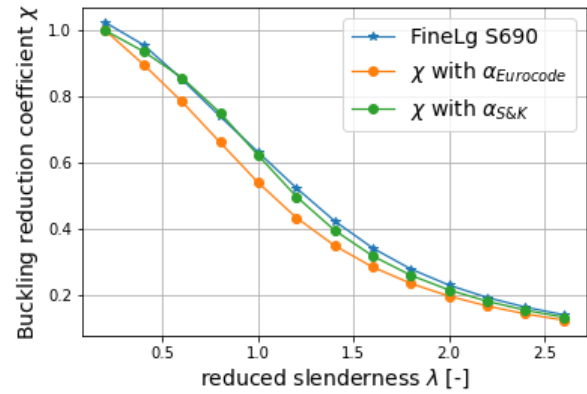


Figure 5.10: S690 numerical data with EC3 buckling curve c and Somodi and Kövesdi (2017) modified buckling curve

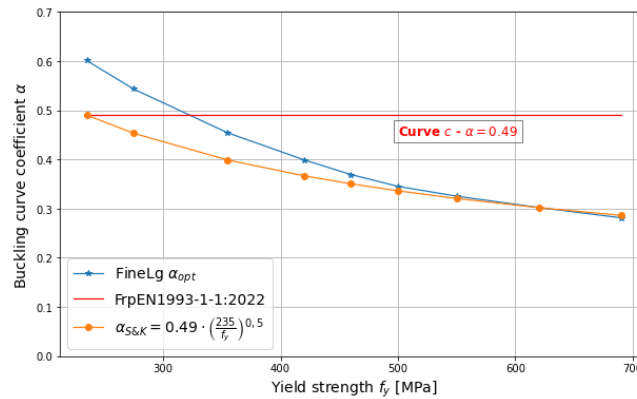


Figure 5.11: Comparison of Somodi and Kövesdi (2017) modified imperfection factor $\alpha_{S\&K}$ and the numerical α_{opt}

The more optimistic predictions of the imperfection factor proposed by Somodi and Kovesdi for standard-grade steels result from the use of a hardening exponent $n = 14$, which produces a sharper curvature in the corresponding Ramberg-Osgood law. The critical zone at low slenderness values is indeed caused by the curvature of the stress-strain relationship, and it becomes more pronounced as the steel grade decreases. Therefore, using an exponent n higher than the value recommended by FprEN 1993-1-14 mitigates the critical zone around the reduced slenderness of 0.7 and allows for lower values of the imperfection factor α to be considered for low-grade steels.

In parallel, Han Fang and his team proposed using Jonsson's formulation for cold-formed tubular columns, based on numerical simulations employing a two-phase Ramberg-Osgood model. Again, the value $\alpha = 0.49$ is retained for grade S235, leading to unsafe predictions of the load-carrying capacity for low-grade steels.

$$\eta^* = \alpha \cdot (\varepsilon \cdot \bar{\lambda} - 0.2)$$

However, unlike the proposal of Somodi and Kovesdi, the overestimation of the bearing capacity in the critical zone around a slenderness of 0.7 tends to slightly increase with rising steel grade. Compared with the numerical results of the present study, the generalised modified imperfection factor proposed by Han Fang proves to be unsafe for reduced slenderness values ranging from 0.4 to 1 across all steel grades. This is due to the parameter ε , which extends the plastic plateau with increasing steel strength, resulting in a better correlation of the buckling curve with the results for reduced slenderness values greater than 1. However, this extension counteracts the attenuation of the unsafe zone around 0.7 as the steel strength increases, leading to a systematic overestimation of the bearing capacity for the affected slenderness range, regardless of the steel grade. The maximum overestimation of the load-carrying capacity thus occurs for all steel grades around 7%, corresponding to slenderness values between 0.6 and 0.8.

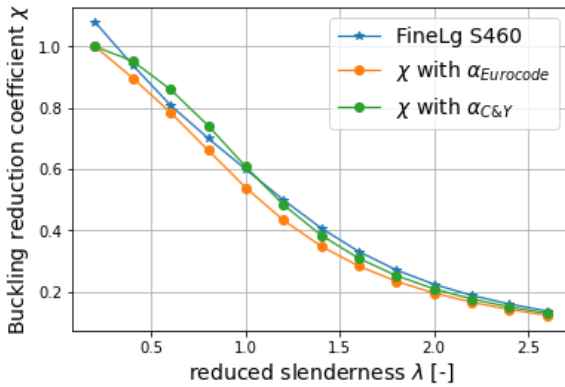


Figure 5.12: S460 numerical data with EC3 buckling curve c and Fang, T.-M. Chan, and Ben Young (2018) modified buckling curve

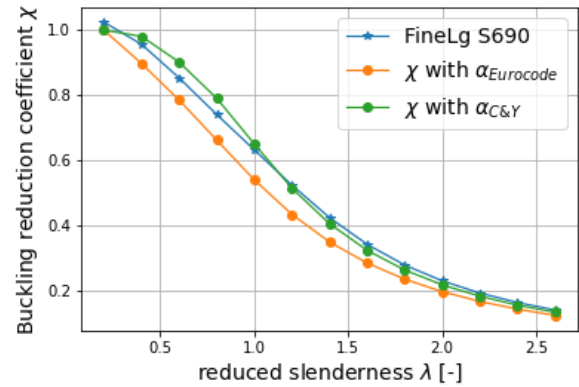


Figure 5.13: S690 numerical data with EC3 buckling curve c and Fang, T.-M. Chan, and Ben Young (2018) modified buckling curve

By adapting the Eurocode formulation according to the expression proposed by Fang and Hang, the optimisation of the imperfection factor α yields a value that is consistently greater than 0.6 and approaches 0.7 for grade S690.

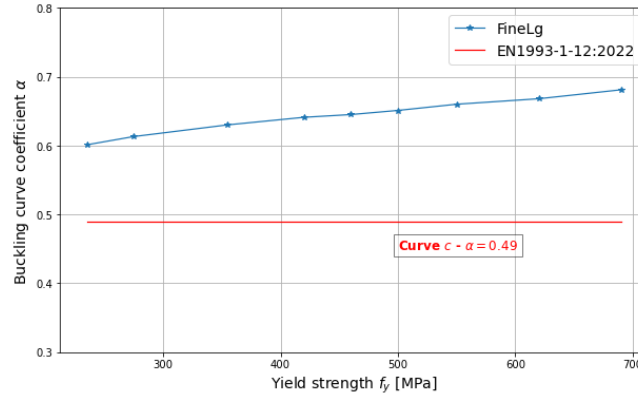


Figure 5.14: Optimised imperfection factor α_{opt} for the modified generalised imperfection factor η as proposed by Fang, T.-M. Chan, and Ben Young (2018)

Only the proposal by Meng and Leroy Gardner (2020) enables a safe prediction of the load-bearing capacity of cold-formed tubular columns across the full range of considered steel grades. They propose reducing the length of the plastic plateau from a reduced slenderness of 0.2 to 0.1. This adjustment allows the analytical buckling curve to better match the shape of the numerical results curve and thereby reduces the unsafe margin around the slenderness of 0.7. The beneficial effect of increasing steel strength on buckling performance is accounted for here by moving away from the historical discretisation of European buckling curves.

The imperfection factor is redefined specifically for cold-formed tubular sections through a linear function of ε .

$$\eta = \alpha^* \cdot (\bar{\lambda} - 0.1) \quad \text{with} \quad \alpha^* = 0.56 \cdot \varepsilon$$

As the critical slenderness zone attenuates with increasing steel strength, the shape of the analytical curve increasingly resembles that of the numerical reference curve. However, the modified curve proposed by Meng and Gardner tends to slightly underestimate the load-bearing capacity predicted by the numerical model, resulting in a safety margin that becomes slightly more conservative as the steel strength increases.

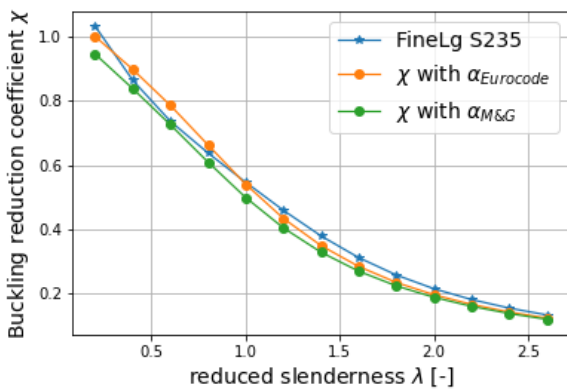


Figure 5.15: S235 numerical data with EC3 buckling curve c and Meng and Leroy Gardner (2020) modified buckling curve

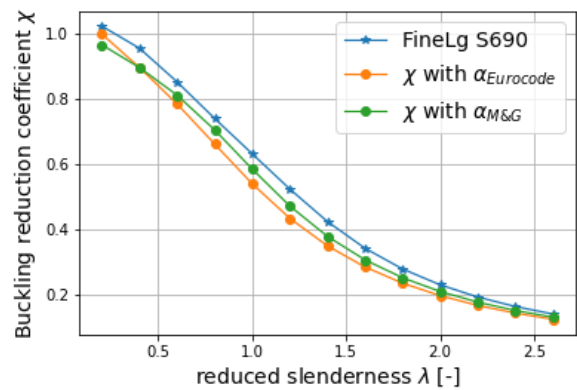


Figure 5.16: S690 numerical data with EC3 buckling curve c and Meng and Leroy Gardner (2020) modified buckling curve

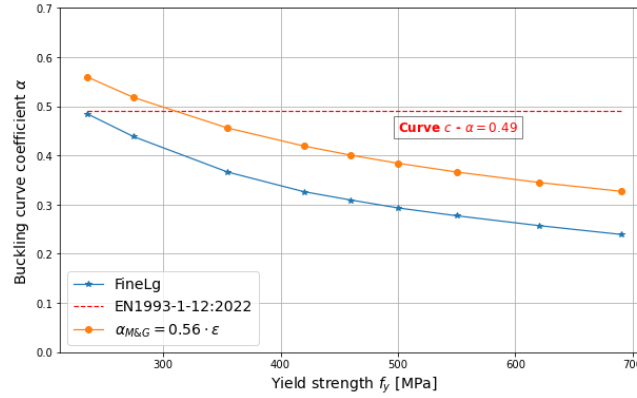


Figure 5.17: Comparison of Meng and Leroy Gardner (2020) modified imperfection factor $\alpha_{Gardner}$ and the numerical α_{opt} with the modified plateau $\bar{\lambda} = 0.1$ of η

5.4 Developement of a modified imperfection factor

In light of the observations drawn from examining existing proposals to modify the imperfection factor of the European buckling curves, the approach followed in this work builds on the expression originally put forward by Maquoi (1982) but shortens the plastic plateau from a reduced slenderness of 0,2 to 0.1.

Meng and Gardner demonstrated that reducing the length of the plastic plateau offers a closer match between analytical buckling curves and numerical results. An optimisation of the imperfection factor α with this shortened plateau, however, showed that the imperfection factor associated with curve c can be retained.

Moreover, when the modified imperfection factor η expression introduced by Meng and Gardner is rewritten in a form analogous to Maquoi's, it applies an exponent $n = 0.5$ to the ratio $235/f_y$. The optimisation study revealed that the decay of the optimal imperfection factor α_{opt} is faster than what an exponent $n = 0.5$ allows. Testing higher values of n indicates that $n = 0.68$ offers the best agreement with the α_{opt} extracted from the numerical results. This value is very close to the exponent $n = 0.7$ proposed by Saufnay (2025) for hot-finished tubular sections, which likewise matches the numerical data well.

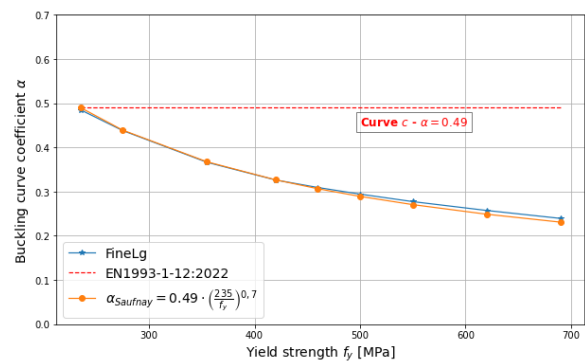
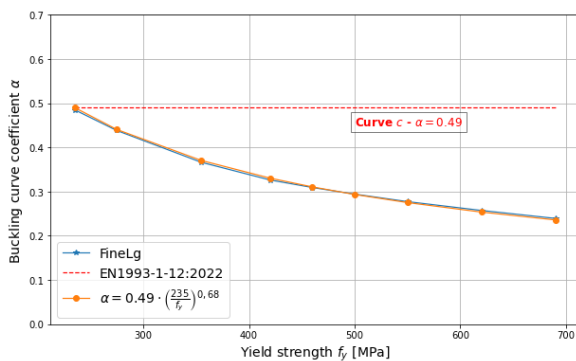


Figure 5.18: Correlation between the optimised imperfection factor α_{opt} and the formulations by Maquoi, considering $n = 0.68$ (left) and $n = 0.7$ (right) with the 0.1 plateau introduced by Meng and Leroy Gardner (2020)

The analytical curves for each steel grade are safe across the entire reduced-slenderness range, except for a narrow region near $\bar{\lambda} = 0.7$. Adopting the same exponent n as Saufnay's would foster coherence between the design rules for cold-formed and hot-finished hollow sections, since they would then differ only in the length of the plastic plateau in the generalised imperfection-factor expression.

Determining the precise value of n and incorporating this proposal into the standards will require a Monte Carlo statistical study to verify that it delivers the partial safety factor $\gamma_{M0} = 1.0$ currently recommended. That analysis, however, lies beyond the scope of the present work.

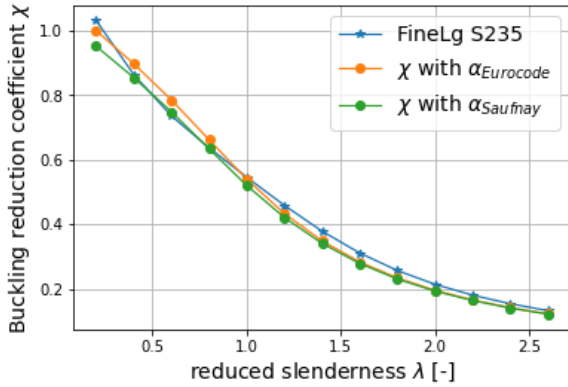


Figure 5.19: S235 numerical data with EC3 buckling curve c and the modified buckling curve with 0.1 plateau for η and Saufnay (2025) modified α^*

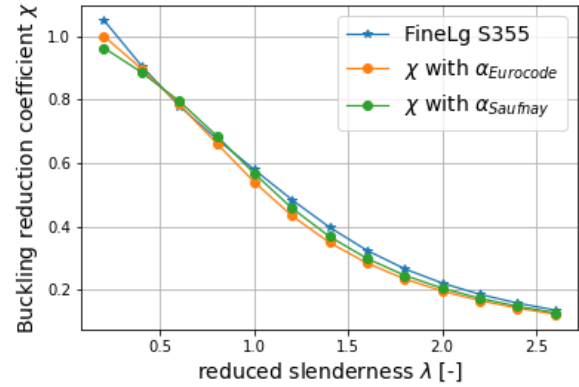


Figure 5.20: S355 numerical data with EC3 buckling curve c and the modified buckling curve with 0.1 plateau for η and Saufnay (2025) modified α^*

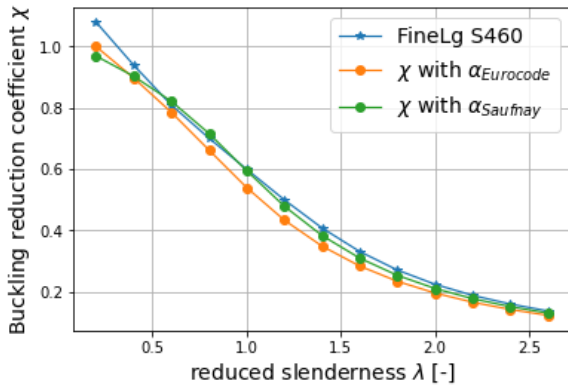


Figure 5.21: S460 numerical data with EC3 buckling curve c and the modified buckling curve with 0.1 plateau for η and Saufnay (2025) modified α^*

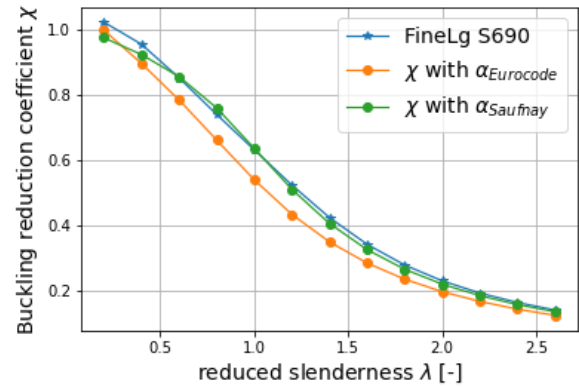


Figure 5.22: S690 numerical data with EC3 buckling curve c and the modified buckling curve with 0.1 plateau for η and Saufnay (2025) modified α^*

Chapter 6

Conclusions and perspectives

This master's thesis addressed the development of a modified expression of the generalised imperfection factor defined by the FrpEN1993-1-1 (2022) standard for the buckling design of cold-formed tubular columns.

The aim was to improve existing design standards by accounting for the normalised enhancement in buckling resistance associated with increasing steel grades. The methodology followed a classical scientific approach based on experimental tests from the literature, used for the development and validation of a numerical model capable of reproducing test results, in order to conduct a parametric study over different steel grades and non-dimensional slenderness values of the columns.

The first part of this study therefore focused on evaluating the various modelling assumptions found in the literature regarding the material law and residual stresses that characterise cold-formed sections.

It was shown that the two-phase Ramberg-Osgood law as defined by FrpEN1993-1-14 (2025) provided the best match with experimental coupon test results, though there is potential to improve the accuracy of this law. Conversely, the residual stress distribution in cold-formed sections was found to vary significantly from one profile to another, due to its dependence on the specific manufacturing methods. The dominant component of residual stresses corresponds to bending stress, which was shown to be implicitly captured in experimental coupon tests, thus making explicit modelling unnecessary. Similarly, membrane residual stresses were found to be counterbalanced by increased material strength in strain-hardened areas, allowing them to be neglected when ignoring the strengthening of the most strain-hardened regions.

The validation of the established model showed good agreement with experimental load-displacement curves. However, an accurate correlation between the material law and the true stress-strain behavior of cold-formed steels proved essential to ensure the quality of these results. Possible improvements to the definition of the parameters governing this law are presented based on proposals from the literature.

With regard to the research questions posed at the outset, this first part provides answers to the first two:

- 1 : The two-phase Ramberg-Osgood law offers the best agreement with experimental measurements of the stress-strain behavior of cold-formed steels. It accurately captures the smooth transition between elastic and plastic behavior. However, the current FrpEN1993-1-14 (2025) definition, which fixes the strain-hardening exponent n at 8, does not provide consistent accuracy across all steel grades. A higher value of n may be more suitable for standard grades due to their sharper curvature. Several proposals to improve the definition of the Ramberg-Osgood parameters already exist in the literature.

- 2 : Various studies have shown that the residual stress distribution in cold-formed sections is determined by the manufacturing method used, and that its magnitude decreases relative to the yield strength when higher-grade steels are considered. Experimental residual stress measurements reveal a dominant bending component along with a membrane component. Given the wide variety of cold-forming methods and resulting residual stress distributions, many residual stress models exist in the literature, though their large-scale validation is still needed. It has been shown, however, that the dominant bending stresses are implicitly included in coupon tension test measurements. The curvature these stresses induce during specimen cutting is incorporated into the stress-strain curve through coupon straightening during loading, resulting in a pronounced rounding of the measured curve. By defining a material law whose curvature reflects that of the experimental measurements, a numerical model can inherently account for the dominant residual stresses in cold-formed sections. Although membrane residual stresses are released during specimen cutting, they are considered to be counterbalanced by increased material strength in highly strain-hardened regions. It is therefore possible to neglect this component as well, by using a uniform material law defined from the least strain-hardened region. Conversely, if the strengthening of more hardened regions is to be modelled explicitly, then a proper distribution of membrane residual stresses adapted to the specific manufacturing method must be included.

In the second part of the study, and based on the validated numerical model, the parametric study generated over 400 column buckling resistance data points for four different SHS and CHS sections, covering a wide range of lengths and steel grades. The numerical results, combined with experimental data from the literature, highlighted the positive influence of increasing steel strength on column buckling resistance.

The parametric results were then used to assess the safety margins offered by current Eurocode design rules and by EC3-based proposals from the literature for cold-formed SHS and CHS sections. This analysis revealed that the European buckling curve *c* leads to unsafe predictions for some low slenderness ratios using standard steel grades, and that there is room for improvement for higher-grade steels. A review of improvement proposals showed that the imperfection factor α could be expressed as a function of steel strength and that reducing the plateau length in the generalised imperfection factor η expression offers better correlation between analytical buckling curves and numerical results. Based on these two considerations, an improved buckling design approach for cold-formed tubular columns is proposed, which yields better resistance predictions than current Eurocode recommendations.

The developments presented in the second part of the work provide answers to the last two research questions:

- 3 : The European buckling curve *c* recommended for the design of cold-formed hollow sections is globally conservative and shows increasing conservatism with higher steel strength. However, the high deformation levels exhibited by the stress-strain curve of cold-formed steels near yielding lead to a critical safety margin at slenderness values between plastic and elastic buckling. This critical range, centered around $\bar{\lambda} = 0.7$, results in unsafe capacity predictions when using curve *c* for grades S235 to S355. For higher grades, the increasing conservatism of EC3 compensates for the safety risk in this critical range.
- 4 : Improving the Eurocode recommendations for the buckling design of cold-formed tubular columns requires, on one hand, accounting for the normalised improvement in buckling resistance with increasing steel grades, and on the other hand, ensuring better alignment between analytical buckling curves and numerical data. These two aspects can be respectively addressed by redefining the imperfection factor as a decreasing function of steel strength and by reducing the plateau length in the generalised imperfection factor expression.

Appendices

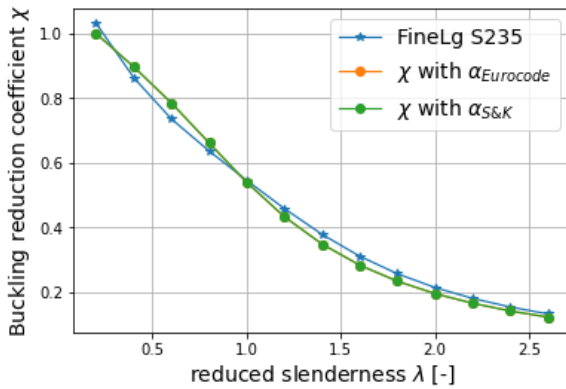


Figure 6.1: S235 numerical data with EC3 buckling curve c and Somodi and Kövesdi (2017) modified buckling curve

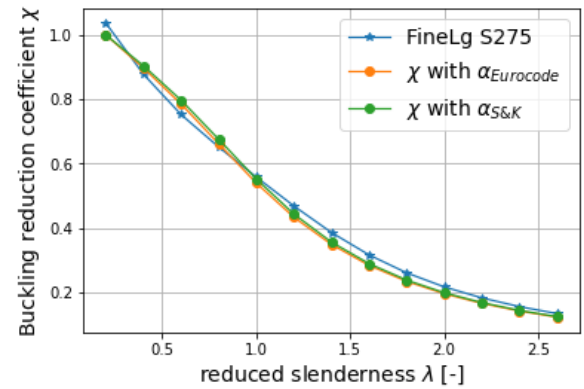


Figure 6.2: S275 numerical data with EC3 buckling curve c and Somodi and Kövesdi (2017) modified buckling curve

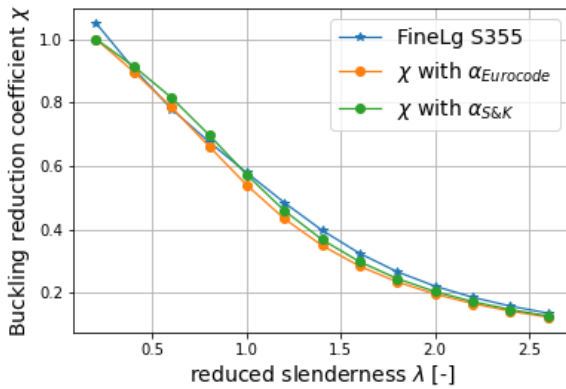


Figure 6.3: S355 numerical data with EC3 buckling curve c and Somodi and Kövesdi (2017) modified buckling curve

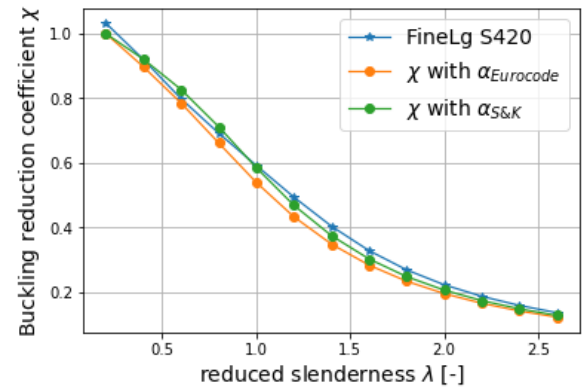


Figure 6.4: S420 numerical data with EC3 buckling curve c and Somodi and Kövesdi (2017) modified buckling curve

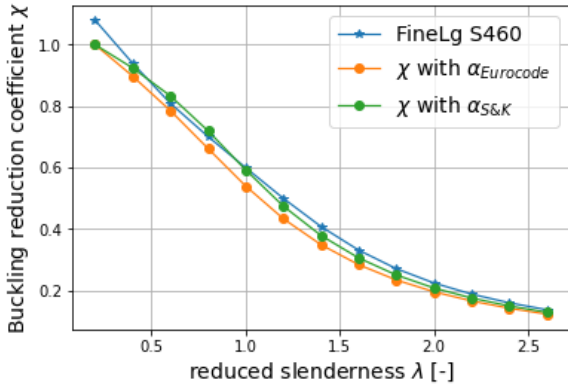


Figure 6.5: S460 numerical data with EC3 buckling curve c and Somodi and Kövesdi (2017) modified buckling curve

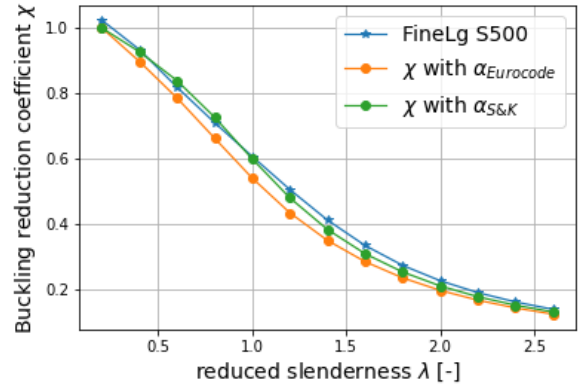


Figure 6.6: S500 numerical data with EC3 buckling curve c and Somodi and Kövesdi (2017) modified buckling curve

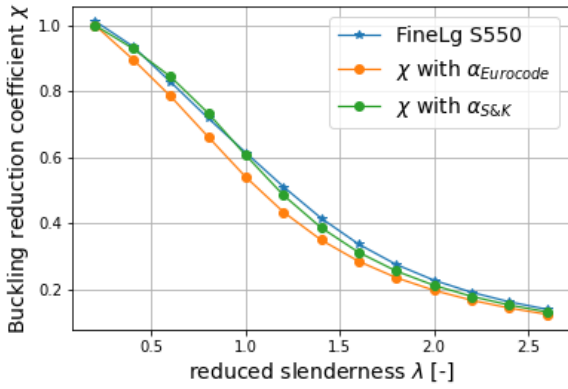


Figure 6.7: S550 numerical data with EC3 buckling curve c and Somodi and Kövesdi (2017) modified buckling curve

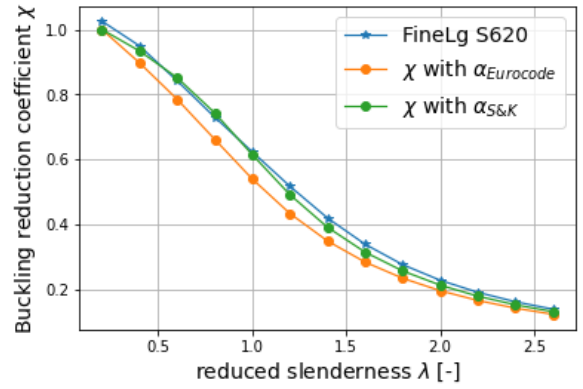


Figure 6.8: S620 numerical data with EC3 buckling curve c and Somodi and Kövesdi (2017) modified buckling curve

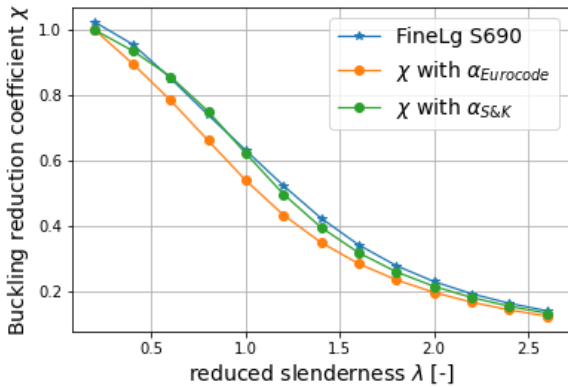


Figure 6.9: S690 numerical data with EC3 buckling curve c and Somodi and Kövesdi (2017) modified buckling curve

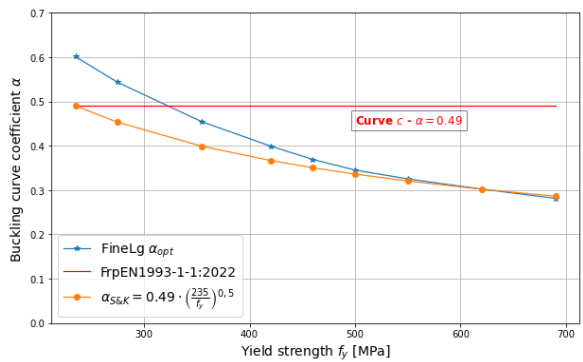


Figure 6.10: Comparison of Somodi and Kövesdi (2017) modified imperfection factor $\alpha_{S\&K}$ and the numerical α_{opt}

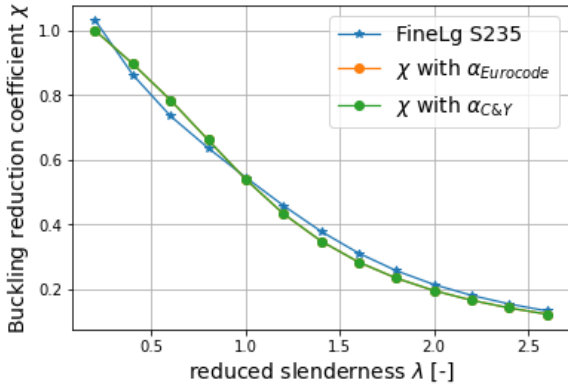


Figure 6.11: S235 numerical data with EC3 buckling curve c and Fang, T.-M. Chan, and Ben Young (2018) modified buckling curve

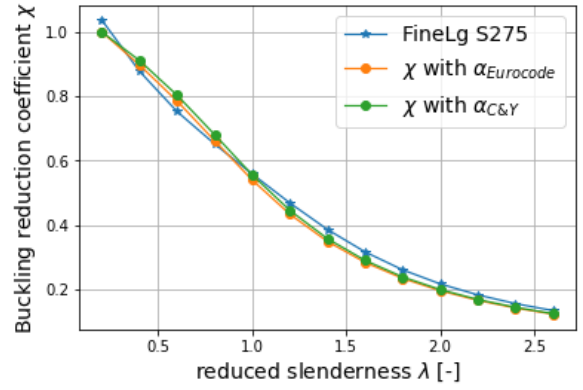


Figure 6.12: S275 numerical data with EC3 buckling curve c and Fang, T.-M. Chan, and Ben Young (2018) modified buckling curve

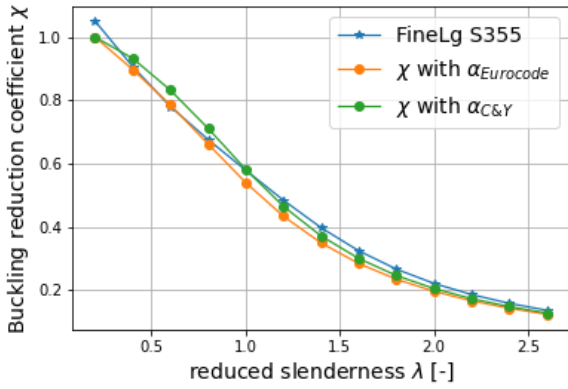


Figure 6.13: S355 numerical data with EC3 buckling curve c and Fang, T.-M. Chan, and Ben Young (2018) modified buckling curve

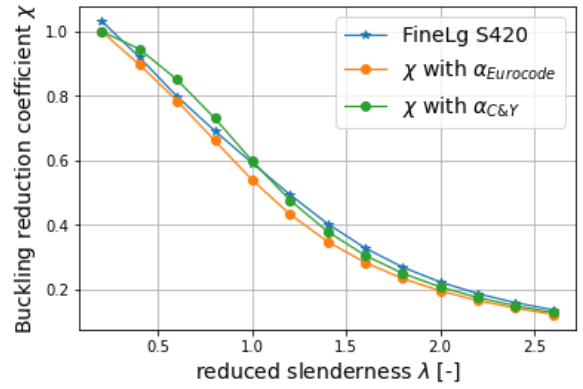


Figure 6.14: S420 numerical data with EC3 buckling curve c and Fang, T.-M. Chan, and Ben Young (2018) modified buckling curve

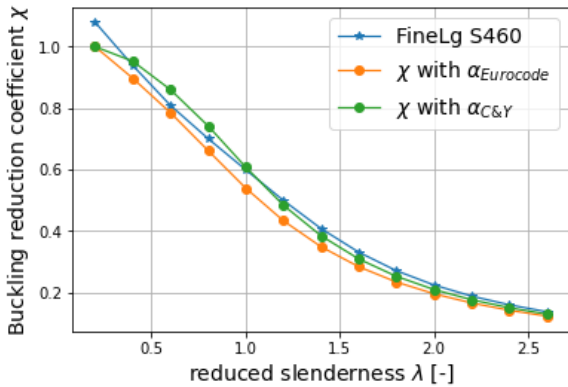


Figure 6.15: S460 numerical data with EC3 buckling curve c and Fang, T.-M. Chan, and Ben Young (2018) modified buckling curve

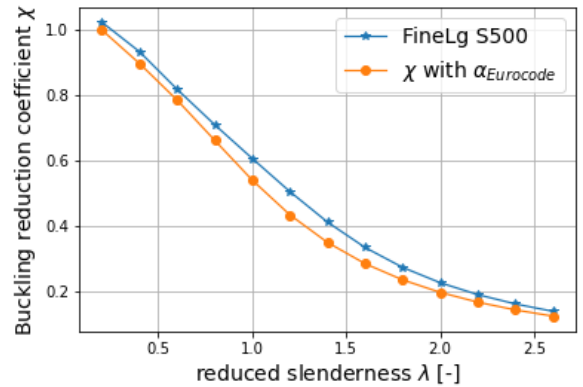


Figure 6.16: S500 numerical data with EC3 buckling curve c and Fang, T.-M. Chan, and Ben Young (2018) modified buckling curve

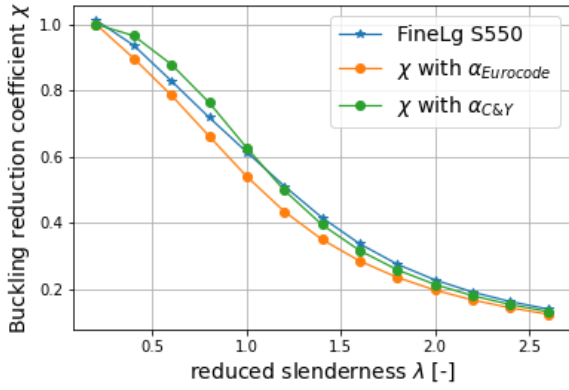


Figure 6.17: S550 numerical data with EC3 buckling curve c and Fang, T.-M. Chan, and Ben Young (2018) modified buckling curve

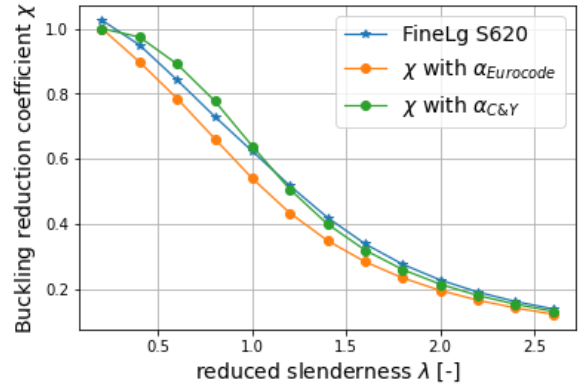


Figure 6.18: S620 numerical data with EC3 buckling curve c and Fang, T.-M. Chan, and Ben Young (2018) modified buckling curve

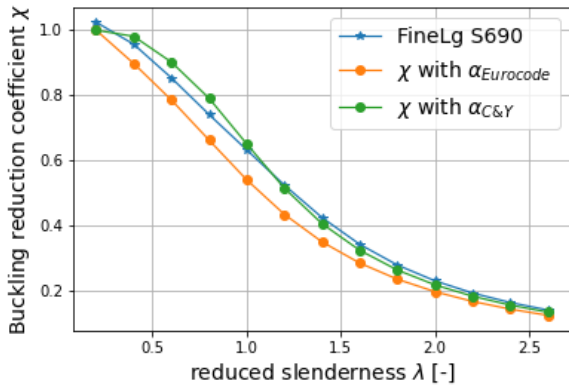


Figure 6.19: S690 numerical data with EC3 buckling curve c and Fang, T.-M. Chan, and Ben Young (2018) modified buckling curve

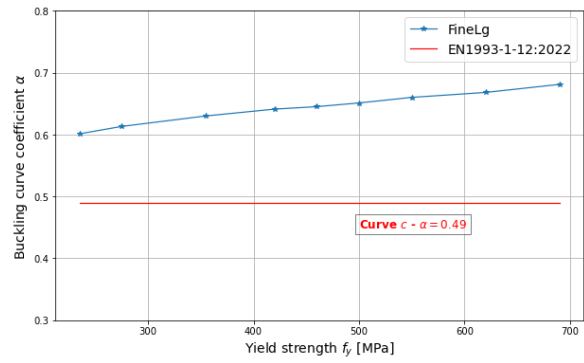


Figure 6.20: Optimised imperfection factor α_{opt} for the modified generalised imperfection factor η as proposed by Fang, T.-M. Chan, and Ben Young (2018)

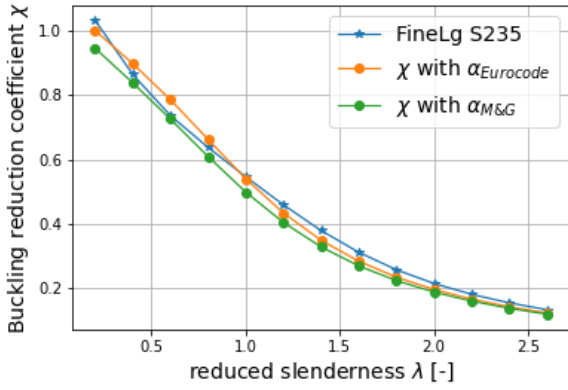


Figure 6.21: S235 numerical data with EC3 buckling curve c and Meng and Leroy Gardner (2020) modified buckling curve

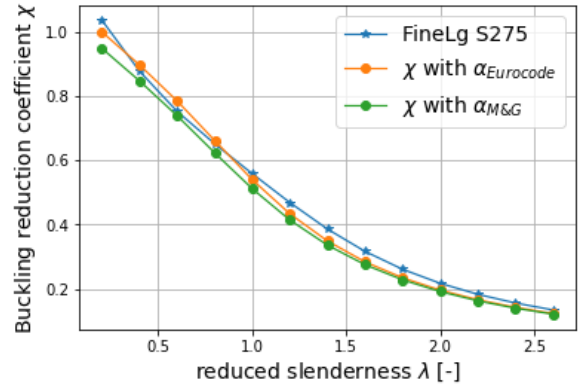


Figure 6.22: S275 numerical data with EC3 buckling curve c and Meng and Leroy Gardner (2020) modified buckling curve

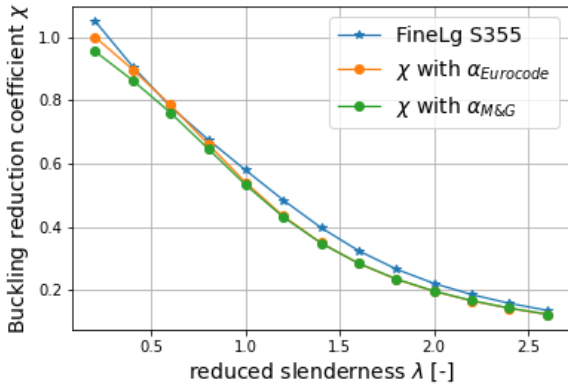


Figure 6.23: S355 numerical data with EC3 buckling curve c and Meng and Leroy Gardner (2020) modified buckling curve

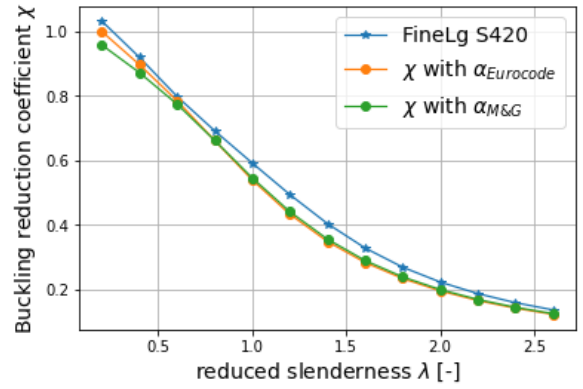


Figure 6.24: S420 numerical data with EC3 buckling curve c and Meng and Leroy Gardner (2020) modified buckling curve

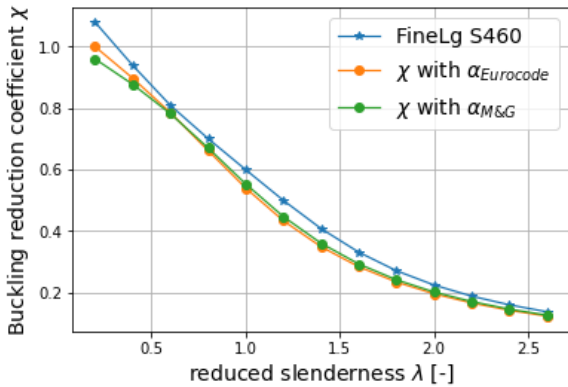


Figure 6.25: S460 numerical data with EC3 buckling curve c and Meng and Leroy Gardner (2020) modified buckling curve

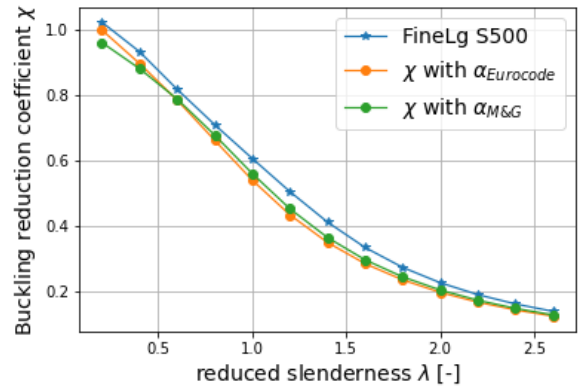


Figure 6.26: S500 numerical data with EC3 buckling curve c and Meng and Leroy Gardner (2020) modified buckling curve

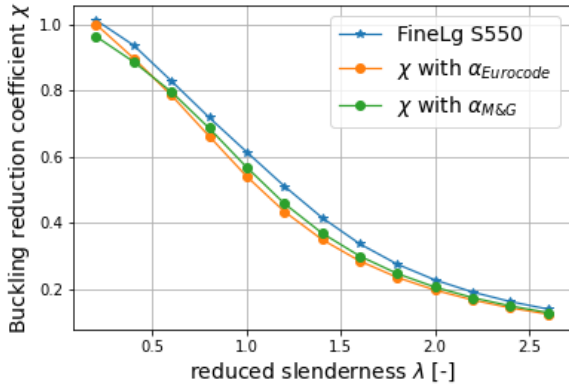


Figure 6.27: S550 numerical data with EC3 buckling curve c and Meng and Leroy Gardner (2020) modified buckling curve

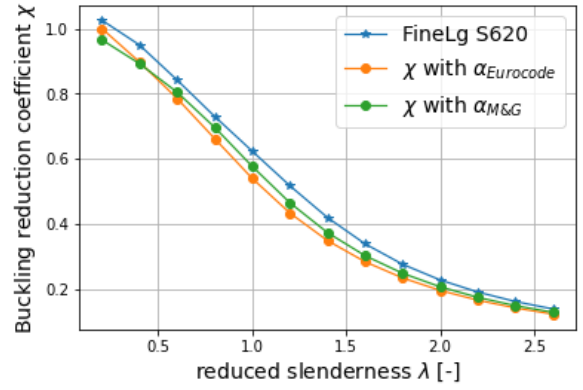


Figure 6.28: S620 numerical data with EC3 buckling curve c and Meng and Leroy Gardner (2020) modified buckling curve

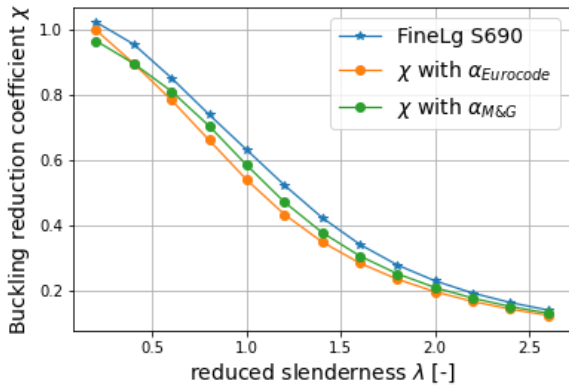


Figure 6.29: S690 numerical data with EC3 buckling curve c and Meng and Leroy Gardner (2020) modified buckling curve

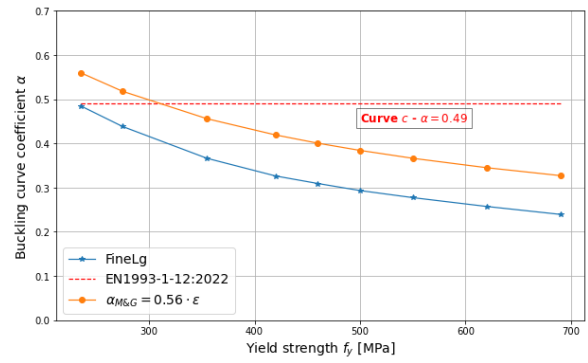


Figure 6.30: Comparison of Meng and Leroy Gardner (2020) modified imperfection factor $\alpha_{Gardner}$ and the numerical α_{opt} with the modified plateau $\bar{\lambda} = 0.1$ of η

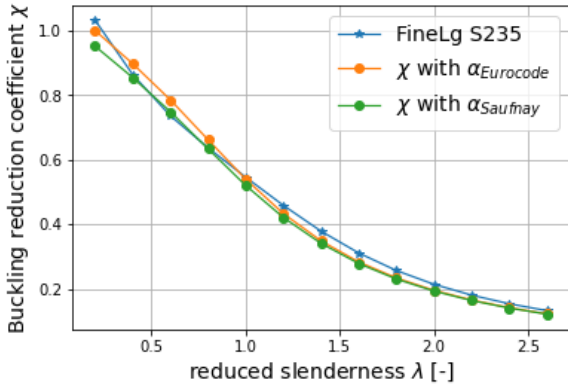


Figure 6.31: S235 numerical data with EC3 buckling curve c and the modified buckling curve with 0.1 plateau for η and Saufnay (2025) modified α^*

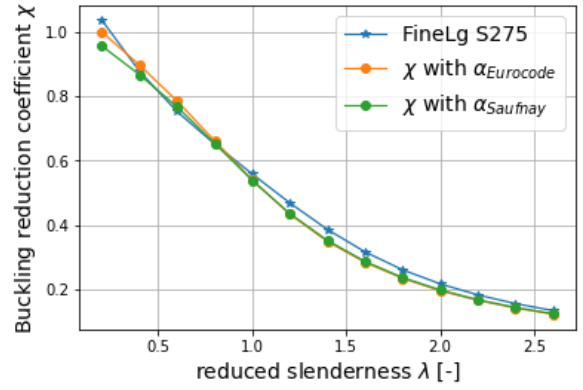


Figure 6.32: S275 numerical data with EC3 buckling curve c and the modified buckling curve with 0.1 plateau for η and Saufnay (2025) modified α^*

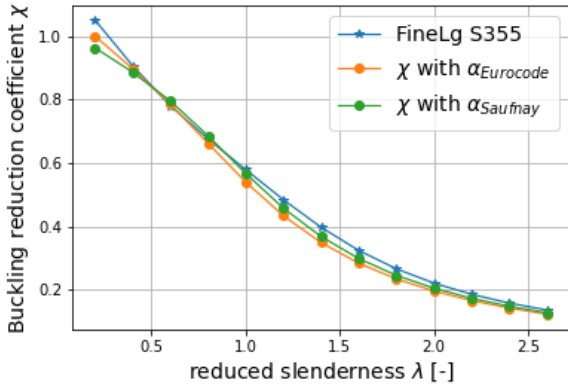


Figure 6.33: S355 numerical data with EC3 buckling curve c and the modified buckling curve with 0.1 plateau for η and Saufnay (2025) modified α^*

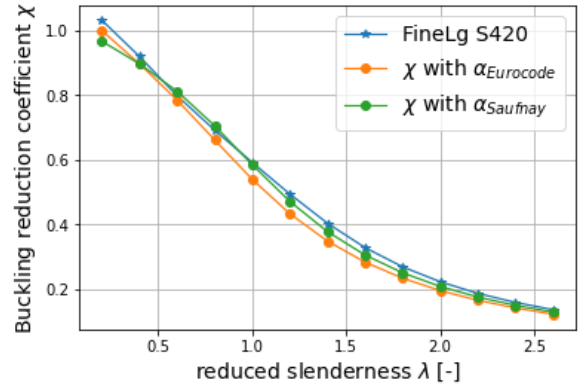


Figure 6.34: S420 numerical data with EC3 buckling curve c and the modified buckling curve with 0.1 plateau for η and Saufnay (2025) modified α^*

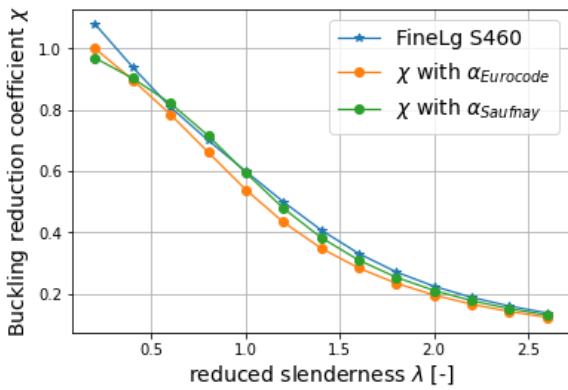


Figure 6.35: S460 numerical data with EC3 buckling curve c and the modified buckling curve with 0.1 plateau for η and Saufnay (2025) modified α^*

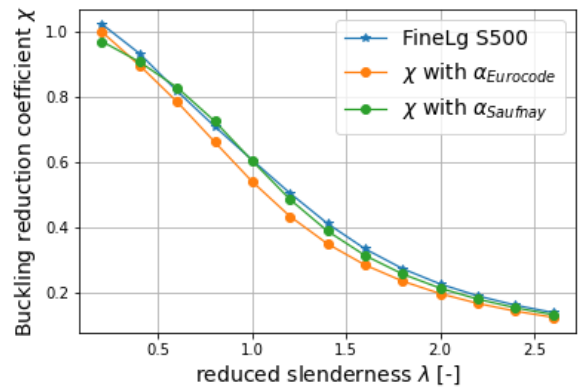


Figure 6.36: S500 numerical data with EC3 buckling curve c and the modified buckling curve with 0.1 plateau for η and Saufnay (2025) modified α^*

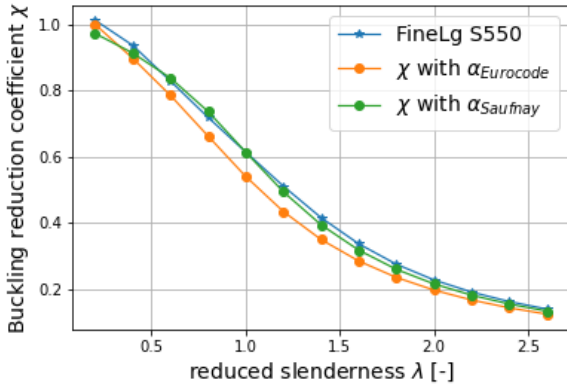


Figure 6.37: S550 numerical data with EC3 buckling curve c and the modified buckling curve with 0.1 plateau for η and Saufnay (2025) modified α^*

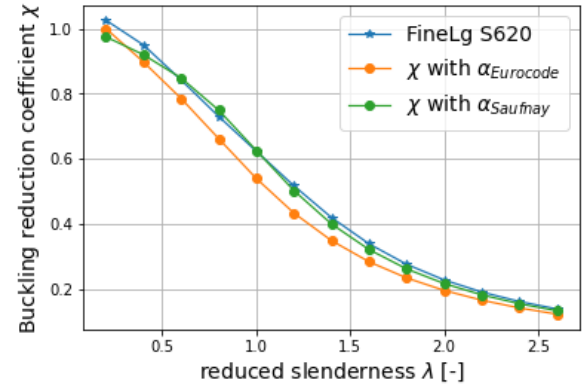


Figure 6.38: S620 numerical data with EC3 buckling curve c and the modified buckling curve with 0.1 plateau for η and Saufnay (2025) modified α^*

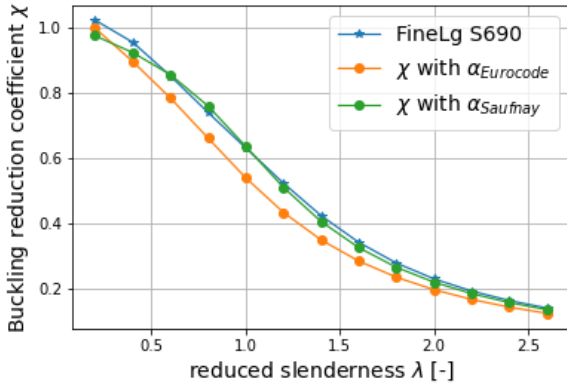


Figure 6.39: S690 numerical data with EC3 buckling curve c and the modified buckling curve with 0.1 plateau for η and Saufnay (2025) modified α^*

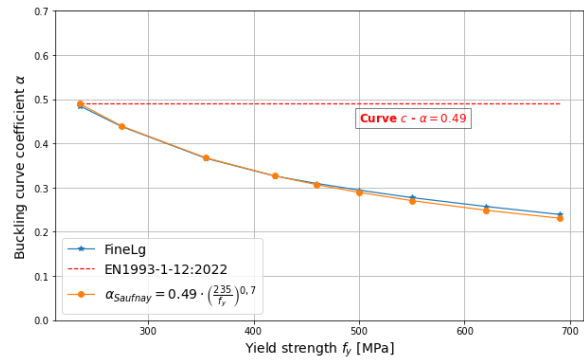


Figure 6.40: Comparison of Saufnay (2025) modified imperfection factor $\alpha_{Saufnay}$ and the numerical α_{opt} with the modified plateau $\bar{\lambda} = 0.1$ of η

Bibliography

- Abdel-Rahman, N. and K. S. Sivakumaran (1997). "Material properties models for analysis of cold-formed steel members". In: *Journal of Structural Engineering* 123.9, pp. 1135–1143. doi: 10.1061/(ASCE)0733-9445(1997)123:9(1135). url: [https://ascelibrary.org/doi/10.1061/\(ASCE\)0733-9445\(1997\)123:9\(1135\)](https://ascelibrary.org/doi/10.1061/(ASCE)0733-9445(1997)123:9(1135)).
- American Iron and Steel Institute (AISI) (1946). *Specification for the Design of Light Gage Steel Structural Members*. Design Specification. Washington, D.C., USA: American Iron and Steel Institute. url: <https://scholarsmine.mst.edu/ccfss-aisi-spec/1/>.
- Baddoo, Nancy and Anqi Chen (2020). *High Strength Steel Design and Execution Guide*. 1st ed. SCI Publication P432. Prepared under the guidance of the SCI Project Steering Committee. Silwood Park, Ascot, Berkshire, UK: Steel Construction Institute. isbn: 978-1-85942-248-9. url: <https://www.steel-sci.com>.
- Batista, E. M. and F. C. Rodrigues (1992). "Residual stress measurements on cold-formed profiles". In: *Experimental Techniques* 16.5, pp. 25–29.
- Bjorhovde, Reidar (1977). *Strength and behavior of cold-formed HSS columns*. Tech. rep. SER 65. Department of Civil Engineering, University of Alberta. doi: 10.7939/R3C824F46. url: <https://era.library.ualberta.ca/items/81264c69-da68-4aa6-bdab-8a0356ab62f2>.
- Braham, M., J. P. Grimault, and J. Rondal (1979). *Flambement des profils creux à parois minces, cas des profils rectangulaires chargés axialement*. French. Research Report 2H 79/19. Altendorf, Switzerland: Committee for International Development and Education on Construction of Tubular Structures (CIDECT).
- Dawson Shanahan (2021). *Cold Forming Process – What Is Cold Forming?* url: https://dawson-shanahan.co.uk/services/cold-forming/?gad_source=1&gad_campaignid=21414994518&gbraid=OAAAAADhovq1yOwoU-f2ML-t0km_l_23Xi&gclid=EAiaIQobChMI2uiByY7ijQMVSZCDBx0rqDP2EAAYASAAED_BwE.
- ECCS (1976). *Manual on Stability of Steel Structures*. Technical Manual Publication No. 22. Brussels, Belgium: European Convention for Constructional Steelwork (ECCS).
- Fang, Han, Tak-Ming Chan, and Ben Young (2018). "Structural Performance of Cold-Formed High Strength Steel Tubular Columns". In: *Engineering Structures* 177, pp. 473–488. doi: 10.1016/j.engstruct.2018.09.082. url: <https://doi.org/10.1016/j.engstruct.2018.09.082>.
- FprEN1993-1-1 (2022). *Eurocode 3: Design of Steel Structures – Part 1-1: General Rules and Rules for Buildings*. Draft European Standard FprEN 1993-1-1:2022. Brussels, Belgium: European Committee for Standardization (CEN).
- FprEN1993-1-14 (2025). *Eurocode 3: Design of Steel Structures – Part 1-14: Design Assisted by Finite Element Analysis*. Draft European Standard FprEN 1993-1-14:2025. Brussels: European Committee for Standardization (CEN).
- Gardner, L. and D. A. Nethercot (2004). "Experiments on stainless steel hollow sections Part 1: Material and cross-sectional behaviour". In: *Journal of Constructional Steel Research* 60.9, pp. 1291–1318. issn: 0143-974X. doi: 10.1016/j.jcsr.2004.03.005. url: <https://www.sciencedirect.com/science/article/pii/S0143974X04000475>.

- Gardner, Leroy and Xiang Yun (2018). "Description of stress-strain curves for cold-formed steels". In: *Construction and Building Materials* 189, pp. 527–538. doi: 10.1016/j.conbuildmat.2018.08.195. url: <https://doi.org/10.1016/j.conbuildmat.2018.08.195>.
- Guiaux, P. (1972). *Essais de flambement sur profils creux formés à froid, carrés et circulaires*. French. Research Report 72/28/F. Altendorf, Switzerland: Committee for International Development and Education on Construction of Tubular Structures (CIDECT).
- Hill, H. N. (1944). *Determination of Stress-Strain Relations from "Offset" Yield Strength Values*. Tech. rep. TN 927. Washington, D.C., USA: National Advisory Committee for Aeronautics. url: <https://ntrs.nasa.gov/citations/19930081673>.
- Huang, Y. and B. Young (May 2018). "Design of cold-formed stainless steel circular hollow section columns using direct strength method". In: *Engineering Structures* 163, pp. 177–183. doi: 10.1016/j.engstruct.2018.02.012. url: <https://doi.org/10.1016/j.engstruct.2018.02.012>.
- Intergovernmental Panel on Climate Change (IPCC) (2023). *Climate Change 2023: Synthesis Report. Contribution of Working Groups I, II and III to the Sixth Assessment Report of the Intergovernmental Panel on Climate Change*. Tech. rep. Core Writing Team: H. Lee & J. Romero (eds.) Geneva, Switzerland: IPCC. doi: 10.59327/IPCC/AR6-9789291691647. url: <https://www.ipcc.ch/report/ar6/syr/>.
- Johansson, Bernt (2005). "Buckling Resistance of Structures of High Strength Steel". In: *Use and Application of High-Performance Steels for Steel Structures*. Ed. by Hans-Peter Günther. Zurich, Switzerland: International Association for Bridge and Structural Engineering (IABSE), pp. 120–128. isbn: 3-85748-113-7.
- Jönsson, Jeppe and Tudor-Cristian Stan (2017). "European Column Buckling Curves and Finite Element Modelling Including High Strength Steels". In: *Journal of Constructional Steel Research* 128, pp. 136–151. doi: 10.1016/j.jcsr.2016.08.013. url: <https://doi.org/10.1016/j.jcsr.2016.08.013>.
- Kato, Masahiro et al. (1984). "Structural properties of high strength structural steel tubes". In: *Transactions of the Iron and Steel Institute of Japan* 24.2, pp. 147–155. doi: 10.2355/isijinternational1966.24.147. url: https://www.jstage.jst.go.jp/article/isijinternational1966/24/2/24_2_147/_article/-char/en.
- Key, P. W. and G. J. Hancock (1993). "A theoretical investigation of the column behaviour of cold-formed square hollow sections". In: *Thin-Walled Structures* 16.1–4, pp. 31–64. doi: 10.1016/0263-8231(93)90040-H. url: <https://www.sciencedirect.com/science/article/pii/026382319390040H>.
- Key, P. W., S. W. Hasan, and G. J. Hancock (1988). "Column behavior of cold-formed hollow sections". In: *Journal of Structural Engineering* 114.2, pp. 390–407. doi: 10.1061/(ASCE)0733-9445(1988)114:2(390). url: [https://ascelibrary.org/doi/10.1061/\(ASCE\)0733-9445\(1988\)114:2\(390\)](https://ascelibrary.org/doi/10.1061/(ASCE)0733-9445(1988)114:2(390)).
- Kwon, Y. B. and G. J. Hancock (1992). "Tests of cold-formed channels with local and distortional buckling". In: *Journal of Structural Engineering* 118.7, pp. 1786–1803. doi: 10.1061/(ASCE)0733-9445(1992)118:7(1786). url: [https://ascelibrary.org/doi/10.1061/\(ASCE\)0733-9445\(1992\)118:7\(1786\)](https://ascelibrary.org/doi/10.1061/(ASCE)0733-9445(1992)118:7(1786)).
- Li, S. H. et al. (2009). "Residual stresses in roll-formed square hollow sections". In: *Thin-Walled Structures* 47.5, pp. 505–513. doi: 10.1016/j.tws.2008.10.015. url: <https://doi.org/10.1016/j.tws.2008.10.015>.
- Ma, Jia Lin (2016). "Behaviour and design of cold-formed high strength steel tubular members". Ph.D. Thesis. Pokfulam, Hong Kong SAR: The University of Hong Kong. url: <https://hub.hku.hk/handle/10722/235900>.
- Ma, Jia Lin, Tak Ming Chan, and Ben Young (2021). "Cold-formed high strength steel tubular beam-columns". In: *Engineering Structures* 230, p. 111618. doi: 10.1016/j.engstruct.2020.111618. url: <https://doi.org/10.1016/j.engstruct.2020.111618>.
- Maquoi, René (1982). "Some Improvements to the Buckling Design of Centrally Loaded Columns". In: *Proceedings of the Annual Technical Session and Meeting*. Structural Stability Research Council, pp. 1–

15. url: <https://www.aisc.org/globalassets/continuing-education/ssrc-proceedings/1976-2010/1982-annual-technical-session-and-meeting.pdf>.
- Meng, Xin and Leroy Gardner (2020). "Behavior and Design of Normal- and High-Strength Steel SHS and RHS Columns". In: *Journal of Structural Engineering* 146.11, p. 04020227. doi: 10.1061/(ASCE)ST.1943-541X.0002728. url: [https://doi.org/10.1061/\(ASCE\)ST.1943-541X.0002728](https://doi.org/10.1061/(ASCE)ST.1943-541X.0002728).
- (2021). "Flexural buckling of normal and high strength steel CHS columns". In: *Structures* 34, pp. 4364–4375. doi: 10.1016/j.istruc.2021.09.106. url: <https://www.sciencedirect.com/science/article/pii/S235201242100953X>.
- Meng, Xin, Steve Whitfield, et al. (Oct. 2024). "Stability of hot-finished and cold-formed steel hollow section columns: A comparative study". In: *Structures* 68, p. 107192. issn: 2352-0124. doi: 10.1016/j.istruc.2024.107192. url: <https://www.sciencedirect.com/science/article/pii/S2352012424013444>.
- Mirambell, Enrique and Esther Real (2000). "On the Calculation of Deflections in Structural Stainless Steel Beams: An Experimental and Numerical Investigation". In: *Journal of Constructional Steel Research* 54.1, pp. 109–133. doi: 10.1016/S0143-974X(99)00051-6. url: <https://www.sciencedirect.com/science/article/abs/pii/S0143974X99000516>.
- Nishino, Fumio and Lambert Tall (1970). *Experimental Investigation of the Strength of T-1 Steel Columns*. Technical Report Report No. 290.9. Bethlehem, Pennsylvania, USA: Fritz Engineering Laboratory, Department of Civil Engineering, Lehigh University. url: https://preserve.lehigh.edu/_flysystem/fedora/2024-01/320037.pdf.
- Nishino, Fumio, Yukio Ueda, and Lambert Tall (1966). *Experimental Investigation of the Buckling of Plates with Residual Stresses*. Technical Report Report No. 290.3. Bethlehem, Pennsylvania, USA: Fritz Engineering Laboratory, Department of Civil Engineering, Lehigh University. url: https://preserve.lehigh.edu/_flysystem/fedora/2024-01/321451.pdf.
- Pavlovčič, Luka et al. (2012). "Finite element simulation of slender thin-walled box columns by implementing real initial conditions". In: *Advances in Engineering Software* 44.1, pp. 63–74. doi: 10.1016/j.advengsoft.2011.05.036. url: <https://doi.org/10.1016/j.advengsoft.2011.05.036>.
- Poursadrollah, Arash, Mario D’Aniello, and Raffaele Landolfo (2022). "Experimental and Numerical Tests of Cold-Formed Square and Rectangular Hollow Columns". In: *Engineering Structures* 273, p. 115095. doi: 10.1016/j.engstruct.2022.115095. url: <https://www.sciencedirect.com/science/article/pii/S0141029622006871>.
- Quach, W.M. and J.F. Huang (2011). "Stress-strain models for light gauge steels". In: *Procedia Engineering* 14, pp. 288–296. issn: 1877-7058. doi: 10.1016/j.proeng.2011.07.035. url: <https://www.sciencedirect.com/science/article/pii/S187770581101112X>.
- Quach, Wai Meng (2005). "Residual Stresses in Cold-Formed Steel Sections and Their Effect on Column Behaviour". Ph.D. Thesis. Hong Kong: The Hong Kong Polytechnic University. url: <https://theses.lib.polyu.edu.hk/handle/200/2574>.
- Raksha Sharma, V. Chandola (2021). *Global Cold Formers Market Report, Forecast from 2025 to 2033*. <https://dataintelo.com/report/global-cold-formers-market>.
- Ramberg, W. and W. R. Osgood (1943). *Description of Stress-Strain Curves by Three Parameters*. Technical Note Technical Note No. 902. Washington, D.C., USA: National Advisory Committee for Aeronautics (NACA). url: <https://ntrs.nasa.gov/api/citations/19930081614/downloads/19930081614.pdf>.
- Rasmussen, K. J. R. (2003). "Full-range stress-strain curves for stainless steel alloys". In: *Journal of Constructional Steel Research* 59.1, pp. 47–61. issn: 0143-974X. doi: 10.1016/S0143-974X(02)00018-4. url: <https://www.sciencedirect.com/science/article/pii/S0143974X02000184>.
- Rondal, Jean (1984). "Contribution à l'étude de la stabilité des profils creux à parois minces". French. Ph.D. thesis. Université de Liège, Faculté des sciences appliquées.
- Salvarinas, J. J., J. D. Barber, and P. C. Birkemoe (1978). *An Experimental Investigation of the Column Behaviour of Cold-Formed Stress-Relieved Hollow Structural Steel Sections*. Research Report 2F-78/10.

- Altendorf, Switzerland: Committee for International Development and Education on Construction of Tubular Structures (CIDECT).
- Satou, Atsushi (2015). *Survey of Rational Design Procedure for Steel Columns that are Supporting the Living Spaces*. Research Report. Technical report in Japanese with experimental results on STKR400 and BCR295 square steel tubes under axial and bending loads. Nagoya Institute of Technology.
- Saufnay, Loris (2025). "High-strength steels and innovative design approaches for sustainable steel structures". Available via ORBi repository. PhD thesis. University of Liège. url: <https://hdl.handle.net/2268/323818>.
- Saufnay, Loris, Jean-Pierre Jaspart, and Jean-François Demonceau (2024). "Improvement of the prediction of the flexural buckling resistance of hot-rolled mild and high-strength steel members". In: *Engineering Structures* 315, p. 118460. doi: 10.1016/j.engstruct.2024.118460. url: <https://hdl.handle.net/2268/320235>.
- Sedlacek, G., B. Kuhn, et al. (1999). *Buckling Behaviour of Hot-Formed SHS in High Strength Steel Grade E-460*. Research Report 2T-2/99. Altendorf, Switzerland: Committee for International Development and Education on Construction of Tubular Structures (CIDECT).
- Sedlacek, G., J. Rondal, et al. (1996). *Buckling Behaviour of a New Generation of Cold-Formed Hollow Sections*. Research Report 2R-2-96. Altendorf, Switzerland: Committee for International Development and Education on Construction of Tubular Structures (CIDECT).
- Somodi, Balázs and Balázs Kövesdi (2017). "Flexural buckling resistance of cold-formed HSS hollow section members". In: *Journal of Constructional Steel Research* 128, pp. 179–192. doi: 10.1016/j.jcsr.2016.08.014. url: <https://doi.org/10.1016/j.jcsr.2016.08.014>.
- SSAB (2014). *Axial resistance of double grade (S355, S420) hollow sections manufactured by SSAB: Statistical evaluation based on tests*. Tech. rep. Helsinki, Finland: SSAB. url: <https://websitecdn.ssab.com/-/media/Files/EN/Hollow-sections/Technical-articles/Technical-article-Design-guide-for-cold-formed-S500MH-and-S700MH-structural-hollow-sections.pdf>.
- Sully, R. M. and G. J. Hancock (1996). "Behavior of cold-formed SHS beam-columns". In: *Journal of Structural Engineering* 122.3, pp. 326–336. doi: 10.1061/(ASCE)0733-9445(1996)122:3(326). url: [https://ascelibrary.org/doi/10.1061/\(ASCE\)0733-9445\(1996\)122:3\(326\)](https://ascelibrary.org/doi/10.1061/(ASCE)0733-9445(1996)122:3(326)).
- Toffolon, A. and A. Taras (Nov. 2019). "Development of an OIC-Type local buckling design approach for cold-formed unstiffened and groovestiffened hollow sections". In: *Thin-Walled Structures* 144, p. 106266. doi: 10.1016/j.tws.2019.106266. url: <https://doi.org/10.1016/j.tws.2019.106266>.
- UN Environment Programme (UNEP) and Global Alliance for Buildings and Construction (GlobalABC) (Mar. 2025). *Global Status Report for Buildings and Construction 2024/2025*. Tech. rep. Préparé sous la direction de Prof. Ian Hamilton et Dr. Shih-Che Hsu. Nairobi, Kenya / Paris, France: UN Environment Programme (UNEP) and Global Alliance for Buildings and Construction (GlobalABC). url: <https://www.unep.org/resources/report/global-status-report-buildings-and-construction-20242025>.
- Wang, Jing and Leroy Gardner (2017). "Flexural buckling of hot-finished high-strength steel SHS and RHS columns". In: *Journal of Structural Engineering* 143.6, p. 04017028. doi: 10.1061/(ASCE)ST.1943-541X.0001763. url: [https://doi.org/10.1061/\(ASCE\)ST.1943-541X.0001763](https://doi.org/10.1061/(ASCE)ST.1943-541X.0001763).
- Weng, C. C. and T. Peköz (1990). "Residual stresses in cold-formed steel members". In: *Journal of Structural Engineering* 116.6, pp. 1611–1625. doi: 10.1061/(ASCE)0733-9445(1990)116:6(1611). url: [https://ascelibrary.org/doi/10.1061/\(ASCE\)0733-9445\(1990\)116:6\(1611\)](https://ascelibrary.org/doi/10.1061/(ASCE)0733-9445(1990)116:6(1611)).
- Xiao, M. et al. (2022). "Prediction of residual stresses in high-strength S690 cold-formed square hollow sections using integrated numerical simulations". In: *Engineering Structures* 253, p. 113682. issn: 0141-0296. doi: 10.1016/j.engstruct.2021.113682. url: <https://www.sciencedirect.com/science/article/pii/S0141029621017685>.
- Xiao, Meng et al. (2022). "Compression Tests on Stocky and Slender Columns of High Strength S690 Cold-Formed Square Tubes". In: *Engineering Structures* 273, p. 115012. doi: 10.1016/j.engstruct.2022.115012. url: <https://doi.org/10.1016/j.engstruct.2022.115012>.

- Young, B. and K. J. R. Rasmussen (1995). *Compression Tests of Fixed-Ended and Pin-Ended Cold-Formed Lipped Channels*. Research Report R715. School of Civil and Mining Engineering, University of Sydney. url: <https://ntrl.ntis.gov/NTRL/dashboard/searchResults/titleDetail/PB97104426.xhtml>.
- Zhao, Xiao-Ling (2000). "Section capacity of very high strength (VHS) circular tubes under compression". In: *Thin-Walled Structures* 37.3, pp. 223–240. doi: 10.1016/S0263-8231(00)00017-3. url: [https://doi.org/10.1016/S0263-8231\(00\)00017-3](https://doi.org/10.1016/S0263-8231(00)00017-3).
- Zhao, Xiao-Ling et al. (2004). "Stub column tests of fabricated square and triangular sections utilizing very high strength steel tubes". In: *Journal of Constructional Steel Research* 60.11, pp. 1637–1661. doi: 10.1016/j.jcsr.2004.04.003. url: <https://doi.org/10.1016/j.jcsr.2004.04.003>.